MASS. INST. OF TECHNOLOGY
WITHDRAWN
MAR 1967
FROM
MIT LIBRARIES

THE DYNAMICS OF CUMULUS CONVECTION IN THE TRADES - A COMBINED OBSERVATIONAL AND THEORETICAL STUDY

by

Joseph Levine

A.B., Harvard College
(1939)
S.M., Massachusetts Institute of Technology
(1941)
M.S., University of New Mexico
(1956)

MASS. INST. TECH.
LIBRARY
LINDGREN

Submitted in Partial Fulfillment of the Requirements
for the Degree of Doctor of Philosophy
at the
Massachusetts Institute of Technology
2 July, 1965

Signature of Author _____
Department of Meteorology, 2 July, 1965

Certified by _____
Thesis Supervisor

Accepted by _____
Chairman, Departmental Committee on Graduate Students

PREFACE

The following study of cumulus convection has been divided into three parts: (1) concerning the liquid water content instruments, (2) on the theory of cloud dynamics, and (3) about the observations and their interpretation. Although in the work described here the liquid water instruments were only a means to the end of acquiring cloud observations, the details of the author's instrument development and calibration work are given here in Part I, because well-calibrated aircraft instruments for recording cloud liquid water are not at present commercially available. The writer wishes to emphasize that aircraft instrumentation is not at all a highly developed technology like that of the digital computer, which has been favored economically by its well-nigh universal applicability. Hence there has been a tendency to take whatever is available in aircraft instruments without looking too closely at their performance characteristics. Also the information explosion has created a gulf separating theory from observation and observation from instrumentation. The author for several years has been and is still trying to bridge the gulf. The work described here represents the writer's effort devoted to achieving a balanced synthesis of instrumentation, observation, and theory in the study of cumulus dynamics.

The proliferation of cumulus models and numerical experiments over the last few years has induced a need for more definitive observa-

tions to establish the relative merits of the various theoretical approaches. Adequate instrumentation is important in the measurement of physical quantities such as cloud liquid water and temperature anomaly, which are associated with buoyancy, and turbulent vertical velocity, which is an important indication of kinetic energy developed by buoyancy forces. In addition the form that cumulus convection assumes must be inferred from probing of clouds along a line by aircraft and in two dimensions by radar.

The scope of the thesis is so broad that some statement concerning motivation may be helpful to the reader. The initial impetus to the author's work was supplied by the desire of Dr. J. Simpson to record cloud liquid water, along with temperature and turbulent vertical velocity in work on trade wind cumulus clouds. During an August 1956 field trip under her supervision, the writer used the paper tape instrument built and supplied by Warner and Newnham (1952) and a lithium chloride instrument built and supplied by aufm Kampe, Weickman and Kelly (1956).

The shortcomings of these cloud liquid water instruments became apparent in field and wind tunnel use. The former was extremely non-linear in its response. Its tape tended to wet excessively and tear during exposure to clouds of high liquid water content. The latter was extremely fragile and tended to short out after a short period of use.

The difficulties experienced with these instruments supplied the motivation for developing a simpler,more accurate instrument.

The hot wire instrument as developed by Neel (1955) appeared to offer the most promise and was therefore adopted. The dependence on drop size of this instrument's response was a disadvantage, which the writer turned into an advantage by developing a companion hot wire instrument consisting of wire wound on a ceramic cone. The two instruments together were calibrated to yield liquid water content and an approximate indication of volume median drop size.

In Part II a comparative analysis of the bubble and steady state jet models is made and related to the tank experiments of Scorer et al. The essential unity of the various models is stressed here. The bubble model is also adapted to cumulus convection.

A statistical summary of all the available cloud observations made in the Caribbean area by the writer and his collaborators is presented in Part III. Comparison of this data with bubble model computations suggests that the value of .75 for the entrainment parameter inferred from tank experiments may also be valid in cumulus clouds. The detrainment parameter, on the other hand, appears to be negligible. Autocorrelation and cross correlation analyses of six cloud passes through two cloud lines are given as a preliminary to possible spectral analyses of better data in the future. The autocorrelation analyses indicate a larger dominant turbulence scale in cloud than in the sub-cloud layer. Cross correlations of liquid water content, temperature, and vertical velocity are positive except

for the cloud top pass along a cloud line, in which the temperature-cloud correlation is negative. The negative cross correlation may be due either to inertial overshoot or mixing with the dry environment air.

References

Aufm Kampe, H.J., H.K.Weickmann, and J.J.Kelly, 1956: A continuously recording water-content meter. J.Meteor., 13, 64-66.

Neel, C.B., 1955: A heated-wire liquid-water-content instrument and results of initial flight tests in icing conditions. NACA RM A54123, 33 pp.

Warner, J. and T.D.Newnham, 1952: A new method of measuring cloud-water content. Quart.J.R.Met.Soc., 78, 46-52.

PART I

An Aircraft Hot Wire Instrument System for Measuring Cloud Liquid Water Content

"In a sense, the present trend toward handsome, beautifully streamlined commercial instruments with engraved scales and direct-reading charts is a highly dangerous one. It seems almost like lèse-majesté to doubt for a moment the accuracy of calibration of any thing so beautiful and expensive, whereas the usually junky-looking homemade instrument simply cries aloud that it needs calibration." E.Bright Wilson, Jr. (1952).

1. Introduction

A basic requirement of an aircraft instrument system for cloud study is a simple method of measuring cloud liquid-water content and drop size. A hot wire instrument consisting of a wire loop developed by Neel and Steinmetz (1952) and Neel (1955) appeared to satisfy the requirement for simplicity; but for such an instrument to be useful it had to be adequately calibrated.

Neel and Steinmetz used a paint spray nozzle to supply the liquid water in a wind tunnel in which their hot wire instrument was mounted. The liquid water content was established by exposing absorbent blotting paper cylinders in the tunnel ahead of the instrument. The writer tried this method and found the results to be unreproducible. The writer finally chose to meter the water flow of a nozzle array spraying into the tunnel in such a way that water was not lost to the sides.

Drop-size distribution is a problem in calibration, because the hot wire tends to slice through drops comparable in size to the

wire diameter. A shadowgraph technique with a fast spark source was used to photograph the drops in the test section to establish drop size distribution for various water flow rates and atomizing air pressures.

It is desirable to have a theoretical analysis of the instrument response for comparison with the empirical calibration curves. Neel made a heat balance calculation for the hot wire based on the assumption of uniform wire temperature. The author has found the end effects to be appreciable but not important for clear air heat transfer computation. Solution of the dry wire boundary value problem as indicated by Carslaw and Jaeger (1959, p.152), based on the heat transfer coefficient given by McAdams (1942, pp.217-221), gave reasonable results. For the wet wire Neel assumed all the water impinging on the wire would evaporate. Comparison of theoretical with empirical calibration curves indicate that Neel's assumption is not correct. Furthermore the wire center was observed to become red hot ($\sim 1000^{o}C$) for high liquid water contents. At a temperature of $250^{o}C$ or above, drops tend to roll along the surface on a cushion of steam without much evaporation. Therefore the central region of the wire is not appreciably cooled by the impingement of water, and practically all of the cooling takes place near the ends where the wire is at a temperature less than $250^{o}C$. The net effect is a considerably larger effective range of response and less sensitivity than that computed from Neel's heat balance equation.

The writer has developed a companion hot wire instrument in addition to the simple loop consisting of wire wound on a ceramic cone which favors interception of the large drops. The responses of the two instruments overlap at a volume median drop diameter of about 100 microns. The ceramic cone (precipitation instrument) response tends to level off at a volume median diameter above 170 microns, whereas the wire loop (cloud instrument) levels off at a diameter less than 42 microns. The two instruments together give cloud liquid water content and approximate volume median diameter.

2. Description of the hot wire instrument system

The cloud instrument consists of a loop of nickel iron wire (4.1 cm long and .05 cm thick) (Figure 1), which is part of a very unconventional Wheatstone bridge circuit (Figure 2). This instrument was designed to work from a 2-volt storage battery. By putting 14 to 16 wires of the above length in series, a cloud instrument which would operate from the 28-volt supply of the aircraft was made.

The precipitation instrument consisted of 93 inches of the same nickel iron wire wound on a grooved ceramic cone about 3 inches long and about 2 inches in diameter (Figure 1). The wire was divided in half, both sections of which were connected in parallel in a Wheatstone bridge circuit (Figure 3). The power for this circuit was supplied by the 28-volt aircraft supply.

The instruments were first mounted on an 18-inch mast on top of the cabin, left of the central axis and just a little back of the

windshield of the Woods Hole C47 (Figure 4). According to Singleton and Smith (1960) this position was poor. They sampled clouds with coated glass slides from two aircraft. In one aircraft the slides were exposed in a position just aft of the windshield on the cabin roof, whereas in the other they were exposed nearer the nose. Samples taken by both aircraft, flying one behind the other, in the same cloud indicated twice as much water on the roof-mounted slide as found on the nose-mounted slide. To compare nose and cabin exposures of the hot wire instruments a duplicate pair of instruments were mounted on a boom projecting 3 feet from the nose of the C47 (Figure 4).

During a field trip towards the end of May, 1962, the two exposures were compared by operating the two sets of instruments simultaneously. Comparison of simultaneous deflections obtained by the two sets of instruments, after allowance for differences in galvanometer sensitivity, led to average deflection ratios (cabin to nose) of 1.64 for the cloud and 1.48 for the precipitation instrument. The difference in response can perhaps be accounted for either by transport of water from the aircraft surface to instrument level by eddies separating from the windshield or by concentration of the drops due to inertia effects. Data from the cabin installation obtained before May, 1962, were corrected with the above factors.

3. Procedure for wind tunnel calibration of liquid water instruments.

The two instruments were quite simple to build, but their calibration was difficult. Inasmuch as no well-established procedures for liquid water content instrument calibration exist, the writer was forced to develop them. Experimentation with a small tunnel of circular cross section 3¼" in diameter built by the writer at Woods Hole gave him the necessary experience, which is briefly summarized as follows:

A single spray gun produced a strong liquid water concentration near the center, a characteristic of nozzles using compressed air to atomize the spray. Attempts to smooth out the water distribution by a mixing chamber in front of the bell mouth resulted in unpredictable and unmeasurable losses to the tunnel walls. The expedient of metering the water flow and injecting the water spray so that none was lost to the tunnel walls was finally adopted.

There was still the problem of having a reasonably flat spray distribution across the tunnel cross section. Ideally the distribution should have a rectangular or top-hat profile, but obviously this ideal can only be roughly approximated. A fairly flat but irregular distribution was finally achieved with a circular array of commercially available nozzles, which required compressed air to atomize the spray. These were mounted just in front of the tunnel bell mouth. The air pressure applied to the nozzles was used to control the drop size.

Since the responses of both instruments were dependent on drop

size, a shadowgraph technique of photographing the drops in the tunnel was developed to estimate the drop size distribution. Earlier use of the above technique by McCullough and Perkins (1951) for photographing cloud drops from aircraft had been complicated by the relatively long light pulse duration of spark sources then available. Very high-speed spark sources have recently become commercially available so that the technical problem of shadowgraphing drops moving at aircraft speeds is greatly simplified. A simple box camera was built, and a commercial high-speed spark source was modified somewhat to shadowgraph droplets in the tunnel.

The final calibration of the instruments was done at a tunnel belonging to the Air Force Cambridge Research Laboratory at Hanscom Field. It had a square cross section of 6x6 inches. This cross section - larger than the author's three-inch tunnel - was considered better with respect to tunnel wall interference and spray plume size. The circular array of nozzles was placed just outside the bell mouth, centered at the tunnel axis and pointing slightly inward. The arrangement of the instruments in the tunnel is shown in Figure 5 and the shadowgraph equipment is shown in Figure 6.

The technique of calibration consisted of exposing the instruments to systematically varied combinations of water flow rate and air pressure. Shadowgraph pictures (Figure 7) were taken of the spray at various flow rates and air pressures, corresponding to the exposure conditions of the instruments, but not simultaneously. Also the two

instruments were not exposed simultaneously. The exposures had to be separated, because the test section was too small to accomodate both the instruments and the shadowgraph apparatus.

The spray density varied with position in the tunnel cross section but was confined to the inner 5x5 square inch cross section. The cloud instrument readings were therefore taken at each of 25 points in a square array as illustrated in Figure 8. The average liquid water content in gm/m^3 then was computed on the basis of the water flow rate, the grid cross section area (25 square inches), and the air speed.

The precipitation instrument was exposed only at the tunnel center because of its larger size. The liquid water concentration in the cross-sectional area covered by the precipitation instrument head was assumed equal to the total liquid water multiplied by the ratio of the average cloud instrument reading taken at 5 grid points grouped about the tunnel center to the average reading at all 25 points.

The storage batteries which supplied the electric current to the instruments were connected in parallel with a DC power supply. The power supply output could be adjusted so as to maintain a particular voltage across the instruments independent of the current drain. When the instruments were exposed to the spray, the fluctuations in spray density caused slight voltage fluctuations of less than 0.1 volt. Systematic errors due to voltage drops at high current drains were thereby eliminated.

4. Volume median drop diameter and liquid water content as established from shadowgraph pictures.

A total of about 400 photographs were taken to obtain adequate samples of the drop population at each combination of water-flow rate and air pressure. A total of 48 different combinations of flow rate and air pressure were used so that on the average about 8 pictures were taken for each spray condition. Three different camera lenses were used to vary the magnification (3.5, 5.1, and 10.1 times) according to dominant drop size. The problem of sizing and counting the drop images was so considerable that the author was motivated to find a convenient technique for doing the job.

This technique was centered around a commercially available image-splitting microscope eyepiece. Since only a rather low magnification was needed to look at the films, the image splitter was mounted on one end of an optical bench lined up with the film at the other end. A negative lens mounted between them formed a Galilean-type telescope with the image-splitter eyepiece. The field of view and magnification were regulated by moving the negative lens and film. The best compromise between field of view and magnification was obtained by viewing the film a quadrant at a time. A rectangular grid was superimposed so that the eye would not get lost while counting drops.

Instead of measuring every drop to establish the drop size distribution, a less laborious,but somewhat less exact method was

adopted. The set of pictures for a given spray condition was inspected to determine the maximum drop size. The image-splitter micrometer was used to measure this maximum drop diameter and set at half the maximum size. The double drop images in the field of view could then be counted in two groups, greater than or equal to and less than half the maximum drop diameter, by noting whether or not the images overlapped.

The volume median drop size was computed on the basis of a simple model of the drop size distribution (see Figure 9). Let N_2 and N_1 represent the numbers of drops larger than or equal to and less than half the maximum drop diameter, respectively. In the assumed model distribution, the frequency distribution function n is given in terms of the drop radius a. a_{max} is the maximum drop radius, for which n is zero. The actual distribution function, which was probably a skewed bell-shaped curve, is represented by a bent line consisting of two straight-line segments as shown in Figure 9. The equations for the straight lines are

$$n = n_1 = 4(N_1 - N_2)/a_{max} + 8(2N_2 - N_1)a/a_{max}^2, \text{ for } 0 \leq a \leq \tfrac{1}{2} a_{max} \qquad (1)$$

and

$$n = n_2 = 8N_2(a_{max} - a)/a_{max}^2, \text{ for } \tfrac{1}{2} a_{max} < a < a_{max} \qquad (2)$$

Multiplication of equations (1) and (2) by $\frac{4}{3}\pi\rho a^3 da$ and integration from 0 to a_{max} leads to the equation for total liquid water content

$$\rho_a \ell = \frac{4\pi\rho a_{max}^3}{3V}(.0125N_1 + .362N_2) \qquad (3)$$

where ρ is the density of water, ρ_a that of air, V is the volume photographed, and ℓ is the liquid water mixing ratio.

The volume median radius is denoted by a_m and is such that half the total liquid water content is contained on either side of a_m. Evaluation of the integrals of $\frac{4}{3}\pi\rho a^3 n da$ from 0 to a_m and from a_m to a_{max}, which equal $\frac{1}{2}\rho_a \ell$ lead to the following relation between N_1/N_2 and a_m/a_{max}:

$$\frac{N_1}{N_2} = 320\left[\frac{7}{64} - \left(\frac{a_m}{a_{max}}\right)^4\left(1 - \frac{4}{5}\frac{a_m}{a_{max}}\right)\right], \text{ for } .5 < \frac{a_m}{a_{max}} < .7 \qquad (4)$$

and

$$\frac{N_1}{N_2} = \left[2\left(\frac{a_m}{a_{max}}\right)^4\left(3.20\frac{a_m}{a_{max}} - 1\right) - .362\right] \Big/ \left[.0125 - 2\left(\frac{a_m}{a_{max}}\right)^4\left(1 - 1.60\frac{a_m}{a_{max}}\right)\right], \text{ for } .5 > \frac{a_m}{a_{max}} > .308 \qquad (5)$$

N_1/N_2 was evaluated for various assumed values of a_m/a_{max}, the results of which are graphed in Figure 10. Four different straight lines are given in Figure 9 for a $\frac{1}{2}a_{max}$, where cases I, II, and III represent the model distributions for N_1 , = , and N_2, respectively, and case IV represents $N_1 = 0$. Equations (4) and (5) take care of cases I and II with $\frac{N_1}{N_2}$ ranging from 1 to ∞ , and $\frac{a_m}{a_{max}}$ ranging from .7 to .308, respectively. For $N_1 = 0$, $\frac{a_m}{a_{max}}$ is .725. It is not necessary to compute case III, since the points corresponding to $\frac{N_1}{N_2} = 1$ and $\frac{N_1}{N_2} = 0$ are so close together.

The droplet count data derived from the shadowgraphs may be used to evaluate liquid water content with the aid of equation (3). To do this the volume V must be found by multiplying the depth of focus by the area photographed.

To evaluate the depth of focus a drawing of several parallel lines of graded thickness were photographed and transferred, reduced in size, to a photographic plate. This plate inclined at an angle of 45^{o} to the focal plane plate, was shadowgraphed with its center in the center of the drop camera's field of view so that the lines on the plate cut diagonally across the focal depth. The focal depth of each lens was evaluated from the measured lengths of the sharp parts of the line images. Then the volume of sharp focus was computed for each lens to be $.77 \pm .08$, $.25 \pm .03$, and $.17 \pm .02$ cm^3 for the 127, 90 and 50 mm lenses, respectively. The cloud instrument, because of its one-second response time, averaged over a volume of approximately $(1.9 \pm .4) \times 10^3 cm^3$.

The results of computations with equation (3) are summarized in Figure 11, where the liquid water contents computed are plotted against values of the average liquid water derived from the flow meter readings. The latter were corrected for non-uniform distribution of liquid water across the section by using the cloud instrument responses (as illustrated in Figure 8) to estimate the liquid water present in the volume photographed. There appears to be a systematic dependence of variance on the lens used, which may be due to the combined effect of a bias toward counting the large drops in an effectively

larger volume and the tendency to lose the small drops by smearing out of the image because of the drop motion. The liquid water contents derived from the photographs are well-correlated with the values derived from the water flow rates, but the scatter from the line of equality is about 6 and .06 times the flow rate values. The largest part of the variance is probably due to sampling errors resulting from small-scale fluctuations in space and time of the liquid water concentration.

5. Graphical analysis of data to obtain calibrations.

The maximum and volume median diameters (the latter read from Figure 10) were plotted against water flow rate for each value of air pressure. Empirical equations were fitted to the data in such a way that extreme values were generally enveloped by the resultant straight lines for each nozzle air pressure. The results are summarized in Figures 12 and 13. The empirical equations fitted the data reasonably well except for the lowest pressure of 5 lb/sq.in. The anomalous behavior of the data at 5 lb/sq.in. probably was caused by settling out of the larger drops on the bottom bell mouth wall, which was observed to be badly wetted by the spray. At higher air pressures the wetting of the wall was negligible.

Then Figures 12 and 13 were used to obtain the maximum and volume median drop diameters contained in Table 1. The data in Table 1 were grouped in 4 sizes and averaged as indicated by the zig-zag lines. This grouping made the wind tunnel data more manageable in the graphi-

cal construction of calibrations. The average galvanometer current for each average liquid water content (determined from the flow rate) and drop-size group were evaluated and plotted (Figures 14 and 15) to give calibration graphs for the cloud and precipitation instruments. Inasmuch as there was no systematic non-linear behavior apparent within the accuracy of the data, straight lines through the origin were drawn for each drop-size group. These lines are of the form

$$i = S' w \tag{6}$$

where i is the current (in microamps), w is the liquid water (gm per cubic meter) and S is a function of drop-size, different for each of the two instruments. As shown on Figures 15 and 16 S decreases with drop size for the cloud instrument and increases for the precipitation instrument. From these lines the volume median drop diameter as a function of cloud to precipitation instrument current ratio was found and is given in Figure 16. With either of the calibrations and Figure 16, volume median drop diameter and cloud liquid water may be found from the two instrument readings. First the volume median drop diameter is evaluated from the ratio of the instrument responses. Then the liquid water content is found from either one of the calibrations by the line on the graph corresponding to the volume median diameter.

Empirical and theoretical instrument response efficiencies are shown in Figure 17. The former are defined by the ratio of the drop-size function S in equation (6) to its maximum value.

Theoretical collection efficiency curves are also plotted for the cloud instrument and a prolate ellipsoid close in size to the precipitation instrument. These curves are based on the computations by Brun and Mergler (1953) and Dorsch, Brun and Gregg (1954). The theoretical collection efficiency of the cloud instrument is shown only for drop diameters less than 30 microns, because drops larger than 30 microns tend as their size increases to be less efficient in cooling the wire because of incomplete evaporation. For example, drops 500μ or more in diameter are larger than the wire and may be sliced through with very little cooling effect per unit mass of water. On the other hand, the theoretical collection efficiency of the prolate ellipsoid is remarkably close to the response curve of the precipitation instrument, since the slicing effect has been eliminated by the ceramic backing.

6. Solution of the boundary value problem of the cloud instrument in dry air.

The solution of the steady-state boundary value problem of a wire heated by an electric current is given by Carslaw and Jaeger (1959). The wire temperature gradient is assumed to be only along the wire because of its thinness. The differential equation of the heated wire is

$$y'' - \lambda^2 y + C = 0, \tag{7}$$

where y is the difference of wire and air temperature and the

primes represent derivatives with respect to X , the distance along the wire. The constants are

$$C = \frac{.239\, I^2 r_{wo}}{\omega^2 K}$$

and

$$\lambda^2 = \frac{2h}{K a_w} - \alpha C$$

where I is the current in amperes, r_{wo} the specific resistivity of the wire in ohm cm at air temperature, ω the wire cross section area in cm^2, α the temperature coefficient of resistance in $^oC^{-1}$, h the turbulent heat transfer coefficient in cal $cm^{-2}sec^{-1}\ ^oC^{-1}$, K the conductivity of the wire in cal $sec^{-1}\ ^oC^{-1}cm^{-1}$, and a_w the wire radius in cm. λ^2 is positive in the computations of interest.

The solution of equation (7) which satisfies the boundary conditions $y = 0,\ X = 0$ or L is

$$y = \frac{C}{\lambda^2}\left[1 - \frac{\cosh \lambda\left(\frac{L}{2} - X\right)}{\cosh \lambda \frac{L}{2}}\right] , \tag{8}$$

where L is the wire length.

The equation for the potential gradient along the wire is

$$\frac{dE}{dX} = \frac{I r_{wo}}{\omega}\left\{1 + \frac{\alpha C}{\lambda^2}\left[1 - \frac{\cosh \lambda\left(\frac{L}{2} - X\right)}{\cosh \lambda \frac{L}{2}}\right]\right\} \tag{9}$$

and its solution

$$\Delta E = \frac{I r_{wo}}{\omega}\left[\left(1 + \frac{\alpha C}{\lambda^2}\right)L - \frac{2\alpha C}{\lambda^3}\tanh \frac{\lambda L}{2}\right] \tag{10}$$

Computations based on equation (8) and values of h derived from empirical data given by McAdams (1942) are summarized in Figure 18. Table 2 contains values of h as a function of y and air speed. For approximate computations both h and α were assumed constant. When y approached a value of 600°C, the constant α was taken as zero, and an appropriate value of the resistivity r_w substituted for r_{wo} in equations (7) to (10). The numerical values of the parameters contained in equations (7) to (10) are summarized in Table 3.

Figure 19 gives a comparison of the computed curves of current as a function of voltage with measured values. This comparison makes the wire temperature profiles given in Figure 18 more credible. Note that the wire temperature gradients in Figure 18 are mostly confined to regions on the ends, 0.6 cm in length.

Therefore, in the case of the dry wire, the assumption by Neel of a uniform temperature was quite reasonable. In the case of the wet wire, however, as evident from the redness observed in a small region near the center of the wire, the assumption of uniform temperature is not justified. Nevertheless, for purposes of comparison with the empirical tunnel calibrations, computations based on Neel's heat balance equation have been carried out for both instruments.

7. Results of heat balance computations.

The equation for liquid water content as a function of current, voltage, and wire temperature is given by Neel:

$$\rho_w = \frac{.239IE}{VA_pH} - \frac{hA_sy}{VA_pH} \qquad (11)$$

where I is the current in amperes, E the voltage, V the air speed in cm/sec, A_p the projected area of the instrument on a plane normal to the air flow in cm^2, H the enthalpy of water at air temperature in cal/gm, and A_s the surface area of the wire in cm^2. Equation (11) is based on the assumption that all the water that impinges on the instrument evaporates. From wind-tunnel measurements of I and E for zero liquid water and appropriate values of the constants, the values of h were computed by the writer to be .027 and .034 cal $(cm^2\ ^oC\ sec)^{-1}$ at air speeds of 50 and 90 m/sec, respectively, which agree with Table 2 well within the 20% accuracy specified by McAdams for his empirical curve on p. 221. The constants for both instruments are given in Table 4.

The liquid water contents corresponding to various values of instrument current and the operating voltages (1.65 volts for the cloud and 28 volts for the precipitation instrument) were computed. From the resistances E/I the values of y were established by reference to a resistance-temperature curve. Since the dependence of h on temperature is rather weak, the dry air values already computed were used.

The results of the above computations are superimposed on the calibrations given in Figures 14 and 15. The evidence indicates very definitely that all the water impinging on the instruments is not

evaporated, since the observed readings are less than the heat balance computations predict. This is especially true for the precipitation instrument. The computed heat balance curves are quite linear, which agrees with the behavior of the tunnel data within their accuracy; but they are strongly dependent on air speed. However, an examination of the tunnel data (not shown) did not confirm such a dependence. Therefore the evaporation efficiency of the instruments must vary in such a way as to nullify the air speed dependence. Such an effect is physically quite plausible inasmuch as the water residence time on the instruments varies inversely as the air speed.

8. A slight digression.

The development of a red hot spot in the middle of the cloud instrument wire when exposed to liquid water has already been mentioned. Similarly the precipitation instrument has also been observed to develop irregularly placed red hot spots mostly towards the rear of the cone when exposed to very large liquid water contents (the extremes used in the calibration). The hot spots have already been related to the tendency for water drops to ride on a cushion of steam over a hot enough surface. An experiment has been performed with a heated plate which indicates that the transition temperature from boiling with intimate contact to compact spherical shape without contact of a water drop on a hot plate is about 250 to 300°C.

The way in which the wire can be heated to red heat (about 900°C) at its center and still average cooler than the dry wire is

illustrated in Figure 20. The wire near the center, which is above 275°C, is not cooled by evaporation. As the liquid water is increased from zero the wire center begins to gradually glow dull red. Then as the water flow increases the center glows brighter and is more concentrated. At the extreme water flow used, the wire sometimes was cooled so much that the red spot was quenched.

The quenching of the red spot was first noticed when some calibration readings ran off scale. Sometimes during a measurement the reading appeared on scale at first but then fluctuations forced the galvanometer off scale. Apparently at extreme liquid water contents the wire was in a metastable state which could be triggered by the liquid water density fluctuations normally occurring in the tunnel. After quenching the wire could be returned to the high temperature regime only by drastically reducing the liquid water.

The wire at high liquid water contents was found inadvertently to constitute a simple physical system which is a climatological analogue. The two states of the wire may be looked upon as analogous to an ice age and a warm age. The finite amplitude fluctuations of liquid water content which trigger the system from one state to the other are analogous to hypothetical fluctuations which possibly trigger the earth's atmosphere from one climatological state to the other.

9. Accuracy and response times of the instruments.

In the calibration curves of Figures 14 and 15, the errors are practically confined to fluctuations of liquid water content in space and time. The error due to fluctuation of tunnel air speed is at most $\pm$ 1 μamp. Therefore all calibration curves must go through the origin. Some of the error may be the result of neglecting the possible non-linearity and dependence on air speed of the instruments' performance, but as already mentioned these factors were not apparent in the data. Therefore the error analysis was based on the standard deviations of the individual points from the lines as drawn. The average standard deviations are 18% and 30% for the cloud and precipitation instruments, respectively. The corresponding probable errors are 12% and 20%.

On the basis of the above probable errors, the probable error of the ratio of cloud to precipitation instrument response and hence the probable error of volume median diameter can be determined. The probable error of the ratio is approximately the sum of the errors of the two instruments, which is 32%. By taking extremes of the ratio based on its estimated error, an estimate of the probable error of volume median drop diameter was established to be 29%.

The response times of the two instruments have been made amply evident both from wind tunnel work and aircraft use. The cloud instrument response time was found to be 1 sec (the time required to reach 63% of its full-scale value in response to a sharp change in liquid

water) and is entirely a function of wire diameter. The response time of the precipitation instrument is more complicated in nature, since its response is conditioned by the ceramic cone as well as the wire size, and was evaluated to be 3 sec. This response time may appear short for a large mass such as the ceramic cone, which is quite apparent in the warm-up time of the instrument (considerably larger than 3 sec); but actually the wire and the ceramic surface immediately under it are most influential in establishing the response time to changes in liquid water content.

References

Brun, R.J. and H.W.Mergler, 1953: Impingement of water droplets on a cylinder in an incompressible flow field and evaluation of rotating multicylinder method for measurement of droplet-size distribution, volume-median droplet size, and liquid-water content in clouds. NACA TN 2904, 71 pp.

Carslaw, H.S. and J.C.Jaeger, 1959: Conduction of heat in solids. Oxford University Press, London, 509 pp.

Dorsch, R.G., R.J.Brun, and J.L.Gregg, 1954: Impingement of water droplets on an ellipsoid with fineness ratio 5 in axisymmetric flow. NACA TN 3099, 50 pp.

McAdams, W.H., 1942: Heat Transmission. McGraw-Hill, New York, 459 pp.

McCullough, S. and P.J.Perkins, 1951: Flight camera for photographing cloud droplets in natural suspension in the atmosphere. NACA RM E50K0/a.

Neel, C.B., 1955: A heated-wire liquid-water-content instrument and results of initial flight tests in icing conditions. NACA RM A54123, 33 pp.

Neel, C.B. and C.P.Steinmetz, 1952: The calculated and measured performance characteristics of a heated-wire liquid-water-content meter for measuring icing severity. NACA TN 2615, 59 pp.

Singleton, F. and D.J.Smith, 1960: Some observations of drop-size distributions in low layer clouds. Quart.J.Roy.Meteor.Soc. 86, 454-467.

Wilson, E.B.Jr., 1952: An introduction to scientific research. McGraw-Hill, New York, 375 pp.

Table 1

Maximum and volume median drop sizes for various spray conditions. (Broken lines represent grouping boundaries).

Flow cc/min. \ Pressure lb/sq.in.		5	10	15	20	30	40	60	80
117	Max	230μ	204	160	135	104	85	65	50
	Med	120	100	80	68	54	44	34	28
174	Max	245	220	174	145	110	95	70	55
	Med	138	122	97	82	66	56	43	36
230	Max	260	230	185	155	120	100	75	60
	Med	151	136	108	92	74	62	48	40
287	Max	277	245	195	165	130	105	80	65
	Med	164	150	120	102	82	70	54	46
414	Max	310	280	220	185	145	123	95	75
	Med	192	184	147	126	102	86	68	58
545	Max	348	310	250	210	165	140	108	88
	Med	220	218	174	150	120	102	82	70
		Group 1		Group 2			Group 3		Group 4
	Avg	Max 283		Max 195			Max 110		Max 64
		Med 173		Med 120			Med 70		Med 42

Table 2

h in cal/cm^2 ^{o}C sec as a function of airspeed and wire temperature.

y/air speed	48 m/sec	90 m/sec
0^{o}C	.025	.035
200	.027	.037
400	.029	.041
600	.031	.043
800	.033	.046
1000	.034	.049

Table 3

Values of constants used in equations (7) to (10).

h = .027 (air speed 48 m/sec)

h = .037 (air speed 90) cal/cm^2 ^{o}C sec

K = .067 cal/sec cm ^{o}C

L = 4.1 cm

α = 7.0 x 10^{-3}

a_w = .0255 cm

r_{ow} = 2.06 x 10^{-5} ohm cm

ω = 2.06 x 10^{-3} cm^2

r_w = 5.3 x 10^{-5} ohm cm ($\alpha = 0$)

Table 4

Constants used in equation (11)

H = 580 cal/gm

V = 5.0 x 10^3 and 9.0 x 10^3 cm/sec

	Cloud instrument	Precipitation instrument
A_s =	.659 cm^2	34.4 cm^2
A_p =	.209 cm^2	20.2 cm^2
h =	.027 (air speed 50 m/sec)	.011 cal/cm^2 ^{o}C sec
" =	.034 (" " 90 ")	.016 " " "



Figure 1. From left to right are shown the 28 volt precipitation instrument and the 2 and 28 volt cloud instruments.

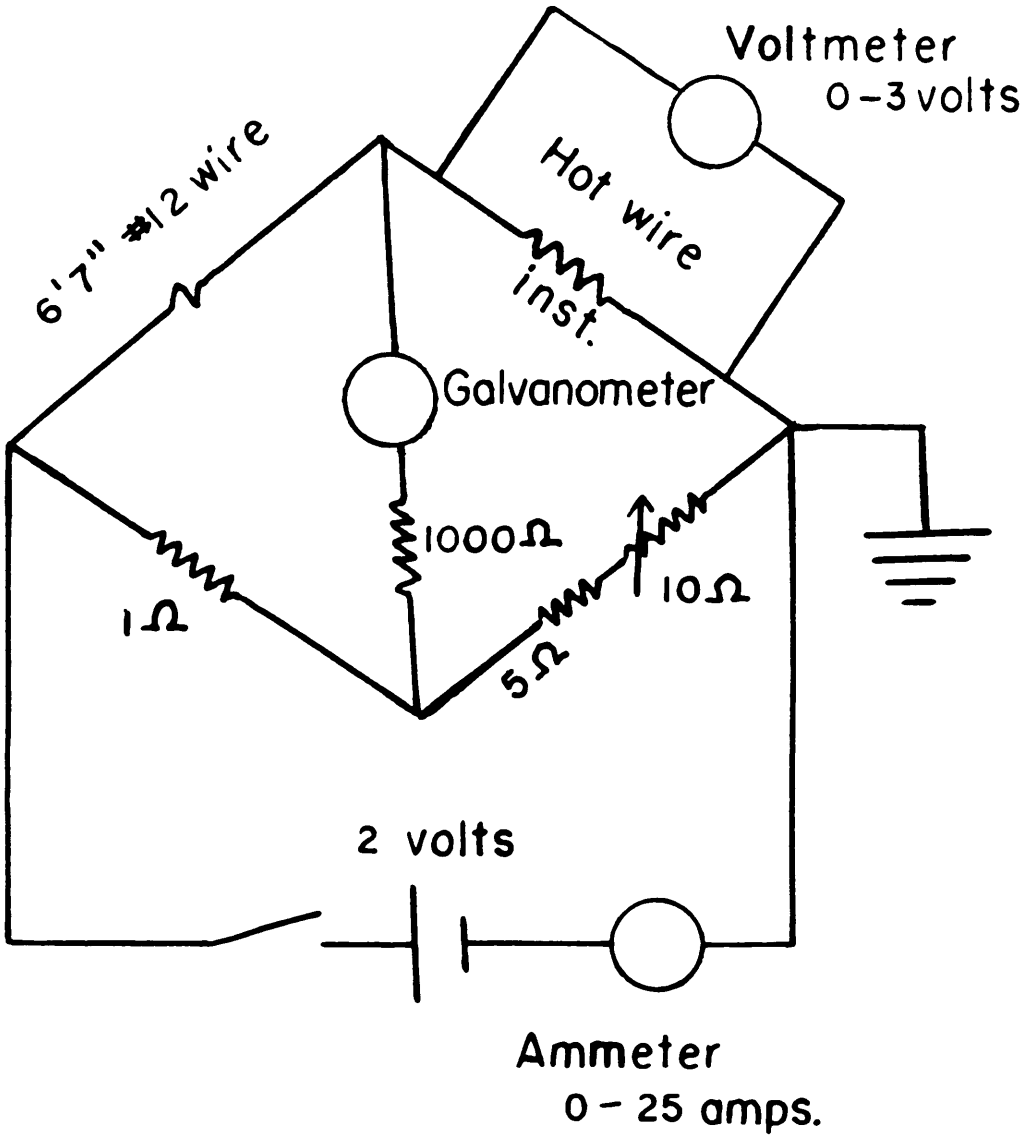


Figure 2. Cloud instrument bridge circuit.

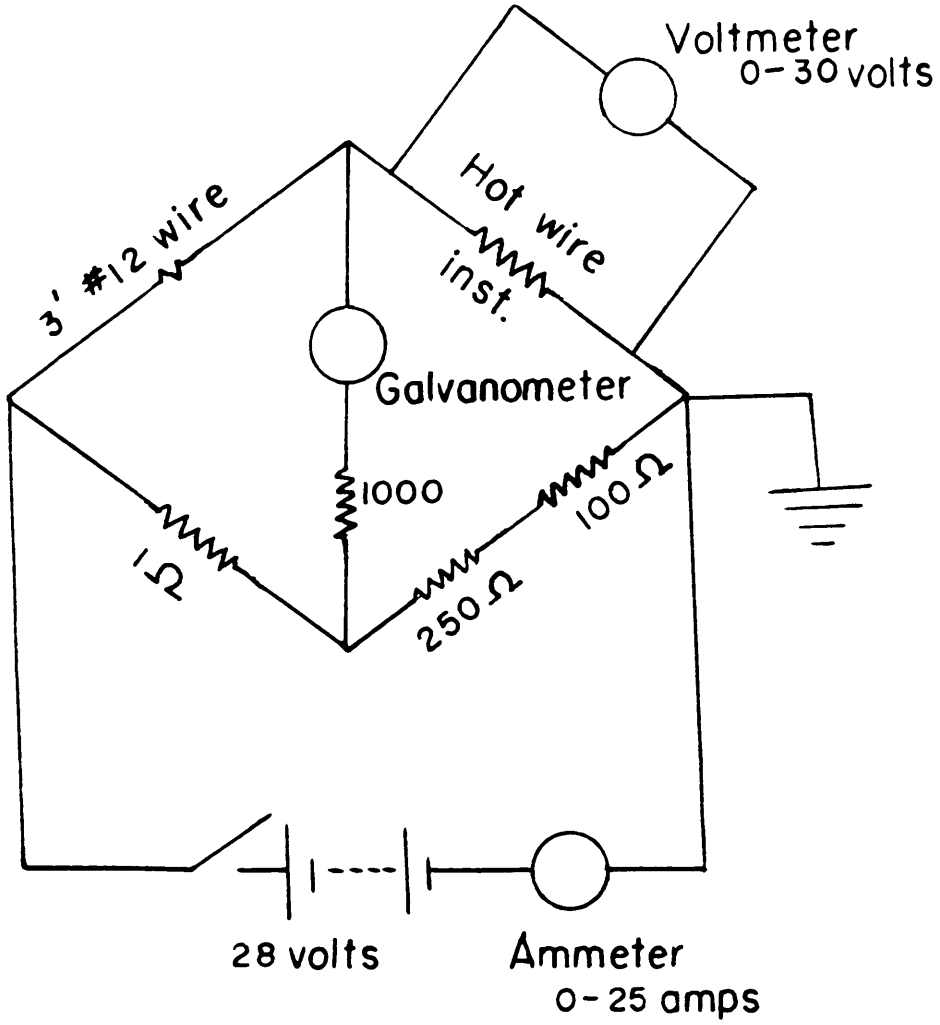


Figure 3. Precipitation instrument bridge circuit.



Figure 4. Duplicate nose and cabin installations of liquid water content instruments on Woods Hole C47 aircraft.

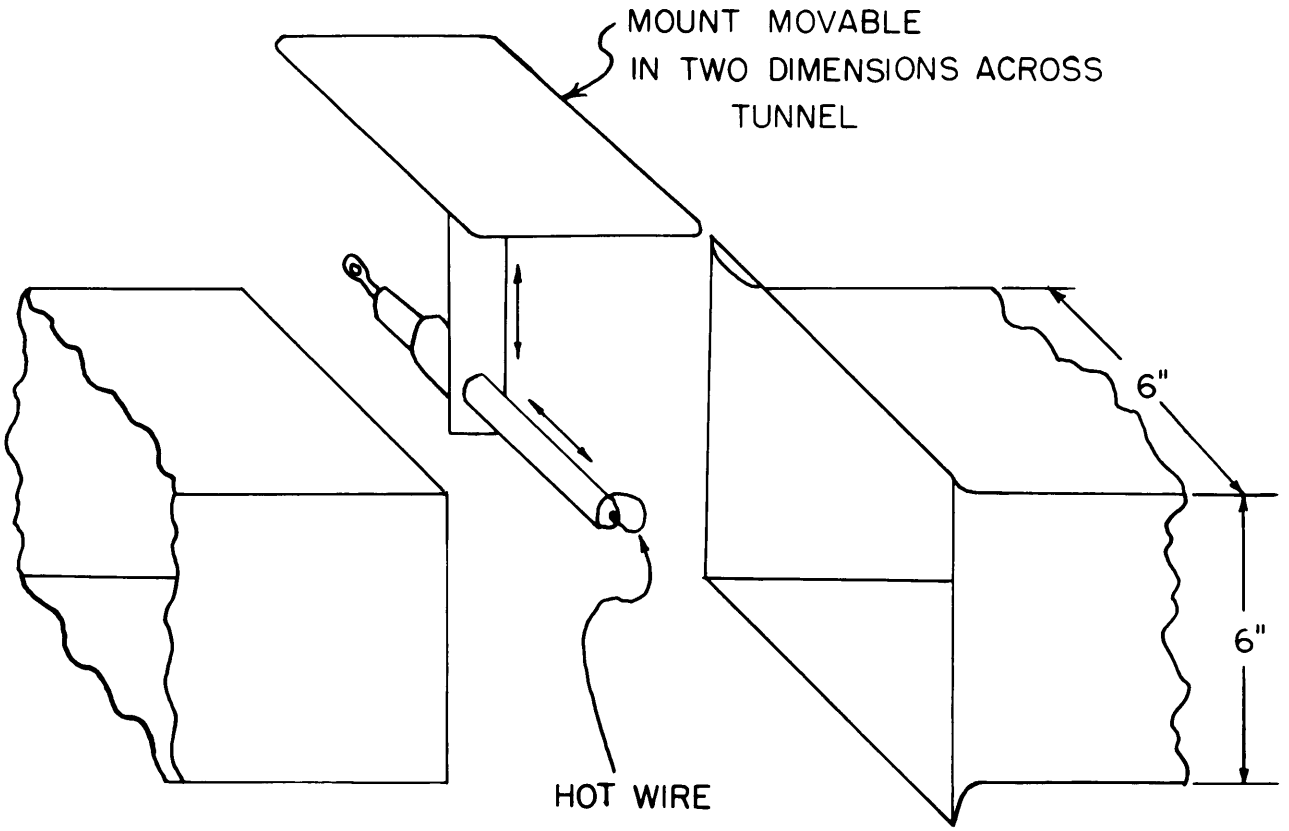


Figure 5. Cloud instrument mounted in tunnel test section.

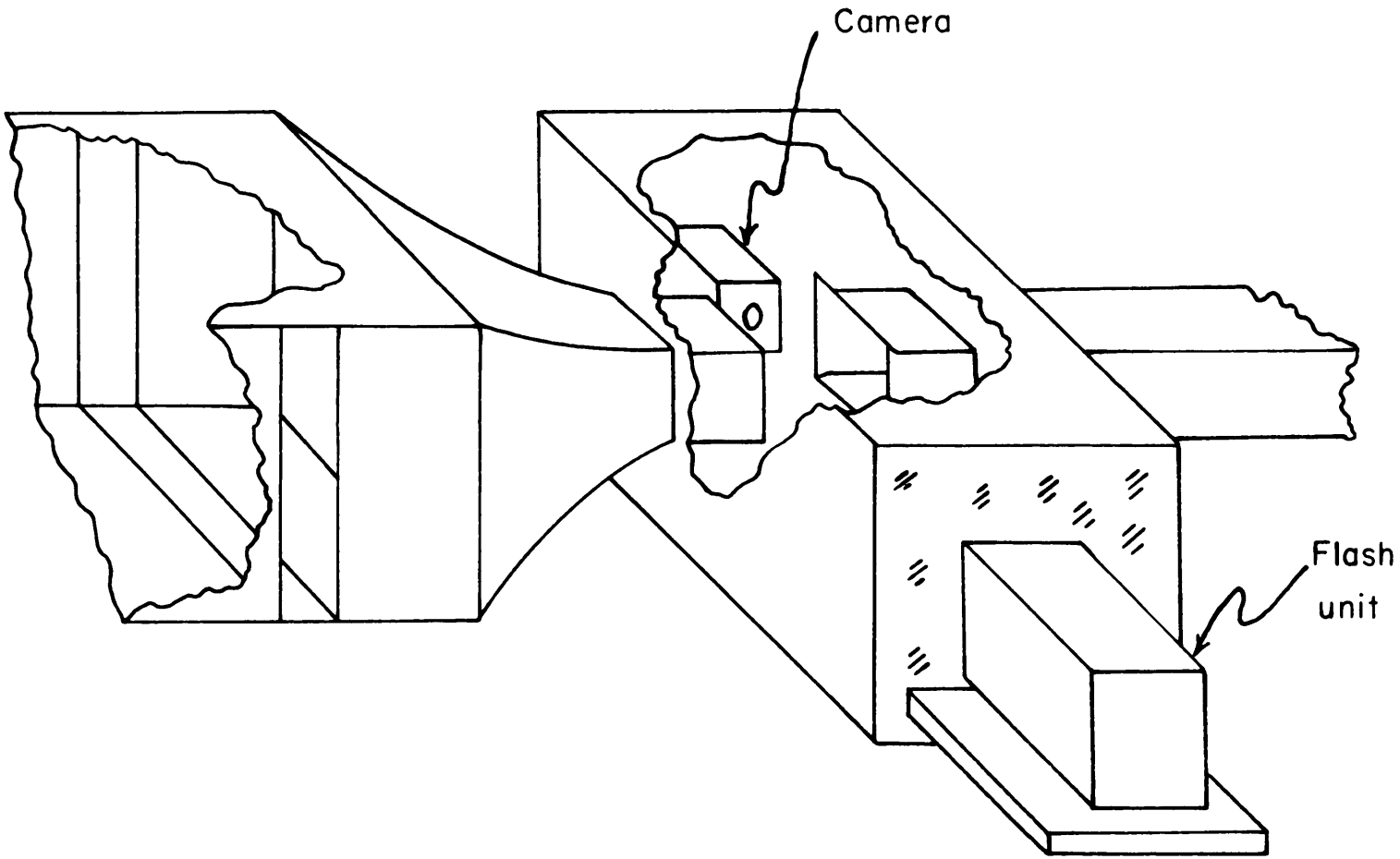


Figure 6. Shadowgraph equipment mounted to photograph spray drops in tunnel.

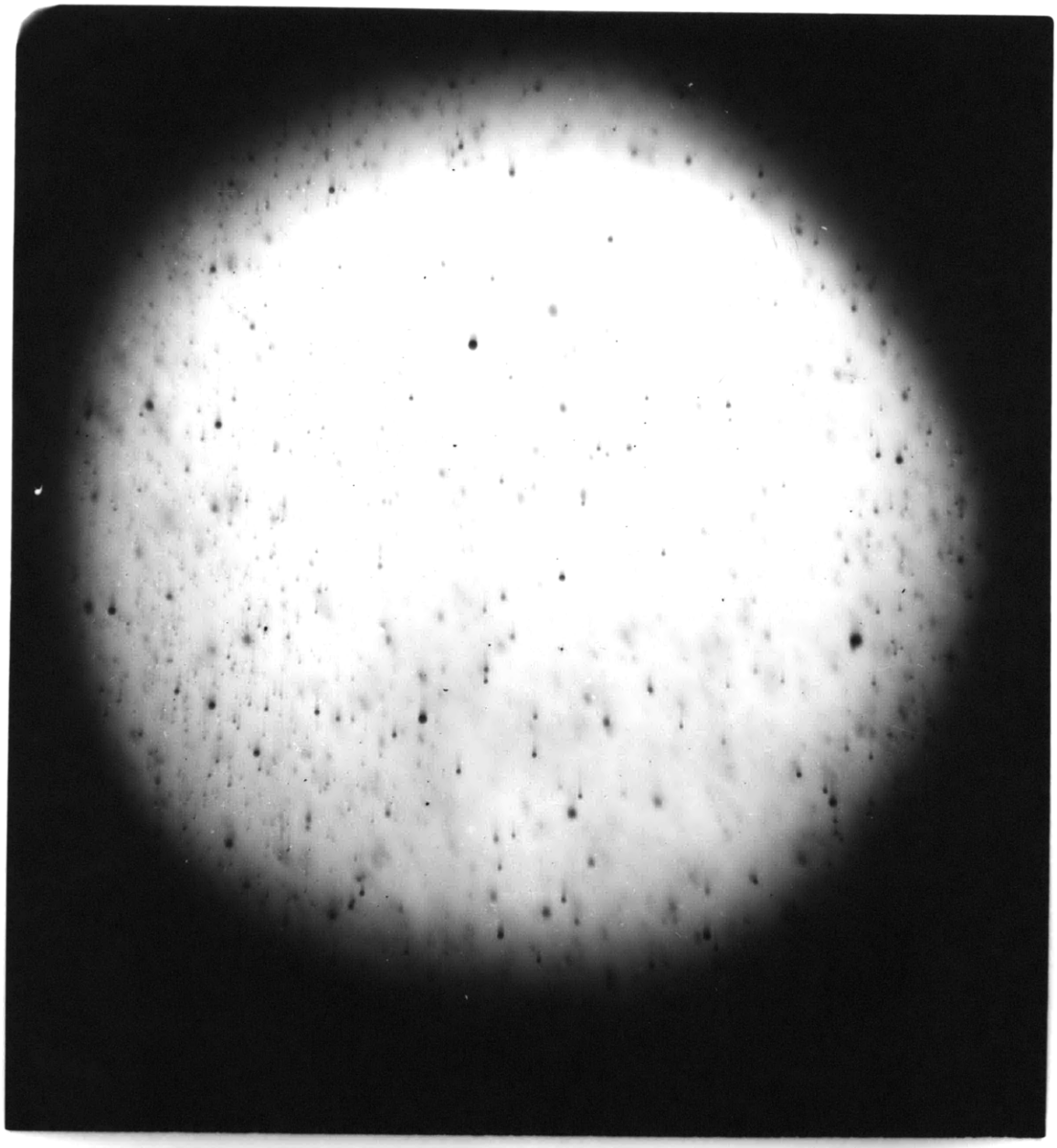


Figure 7. A shadowgraph of spray drops at center of tunnel cross section. (Original magnification 3.5X, enlarged approximately 2X).

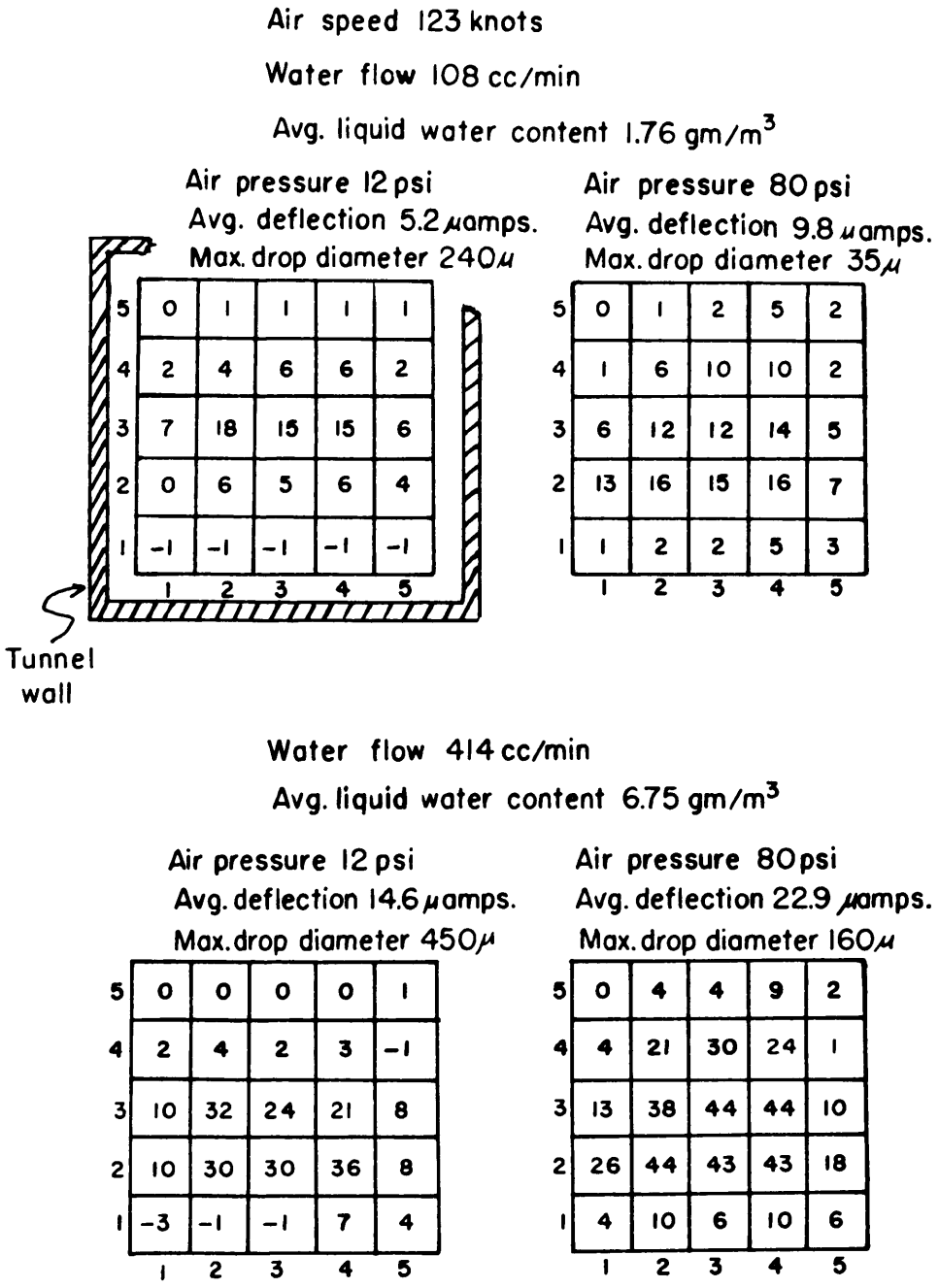


Figure 8. Examples of cloud instrument data obtained at the Hanscom Field spray tunnel. The numbers are bridge current readings in microamps at grid points in the tunnel test section for four different combinations of water flow and air pressure.

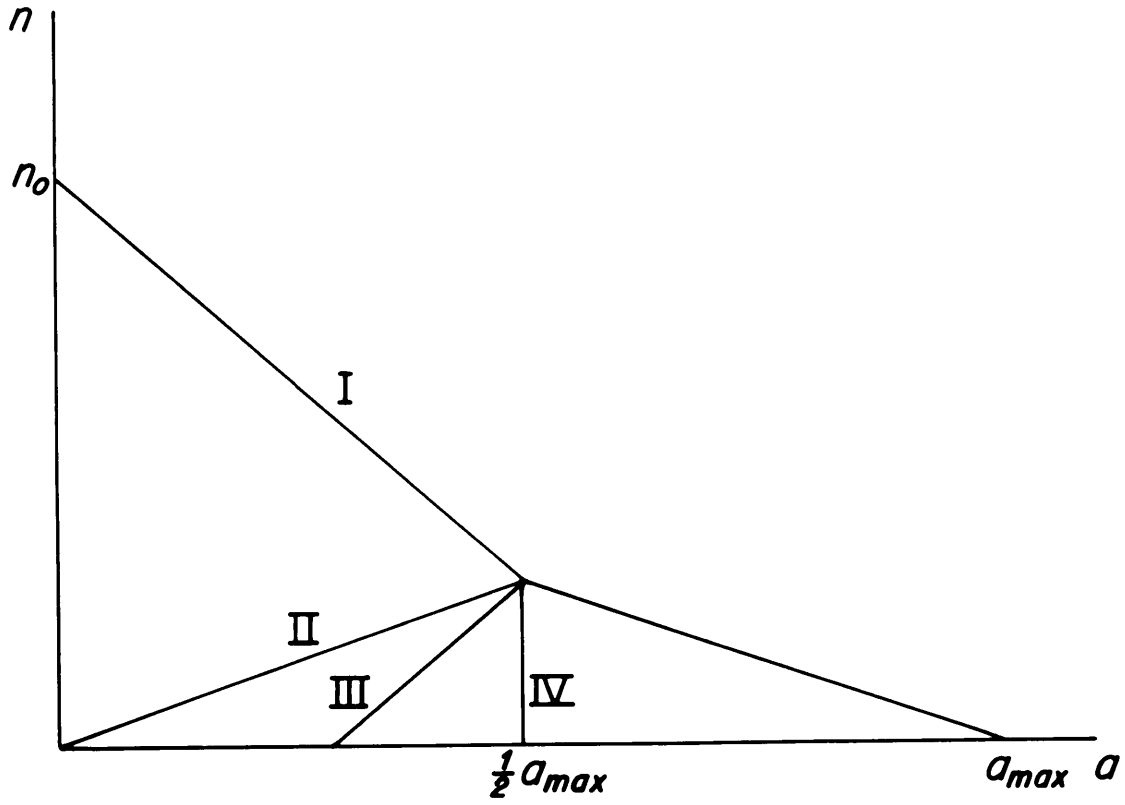


Figure 9. Model drop size distributions. Cases I, II, and III represent $N_1 >$, =, and $< N_2$, respectively. Case IV is $N_1 = 0$.

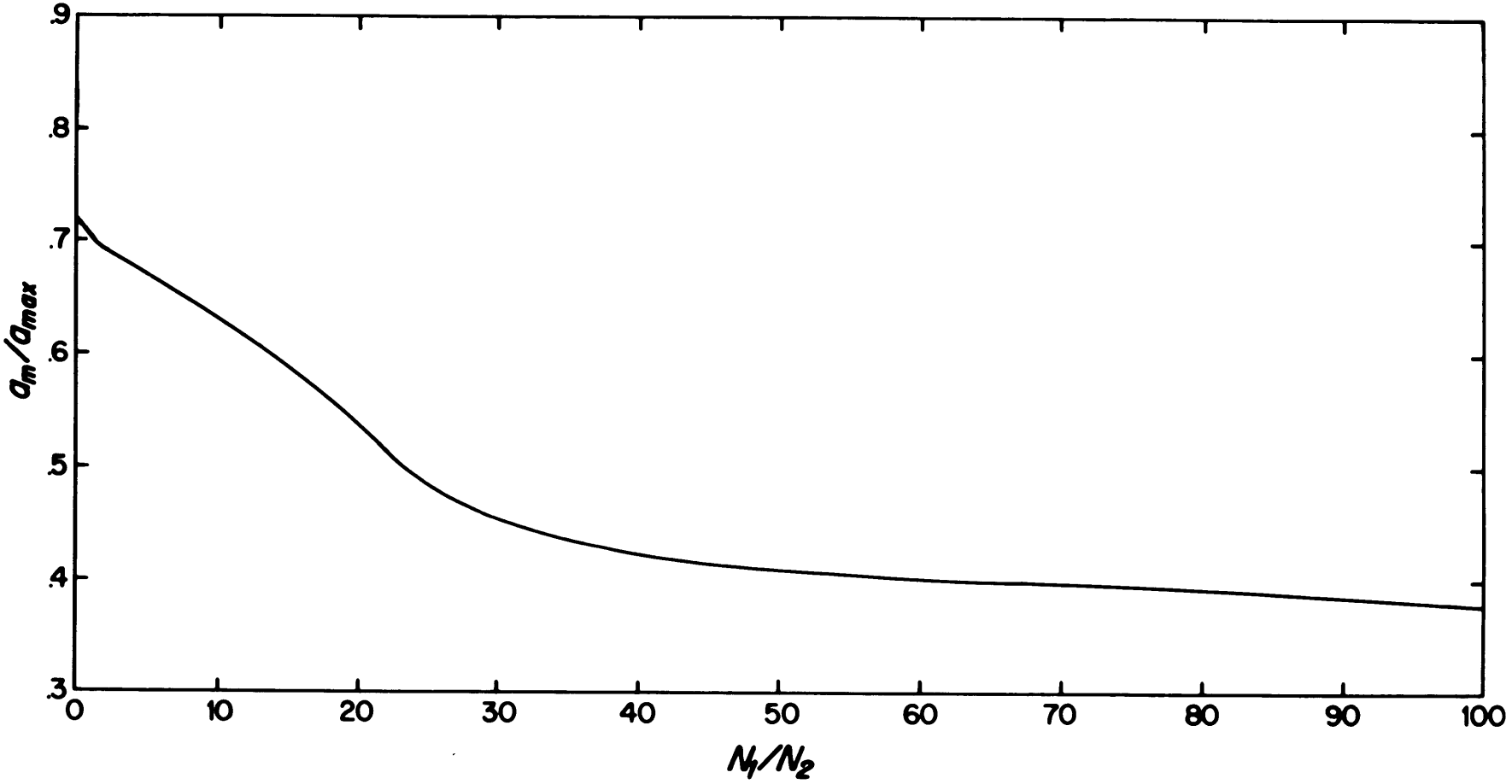


Figure 10. a_m/a_{max} as a function of N_1/N_2.

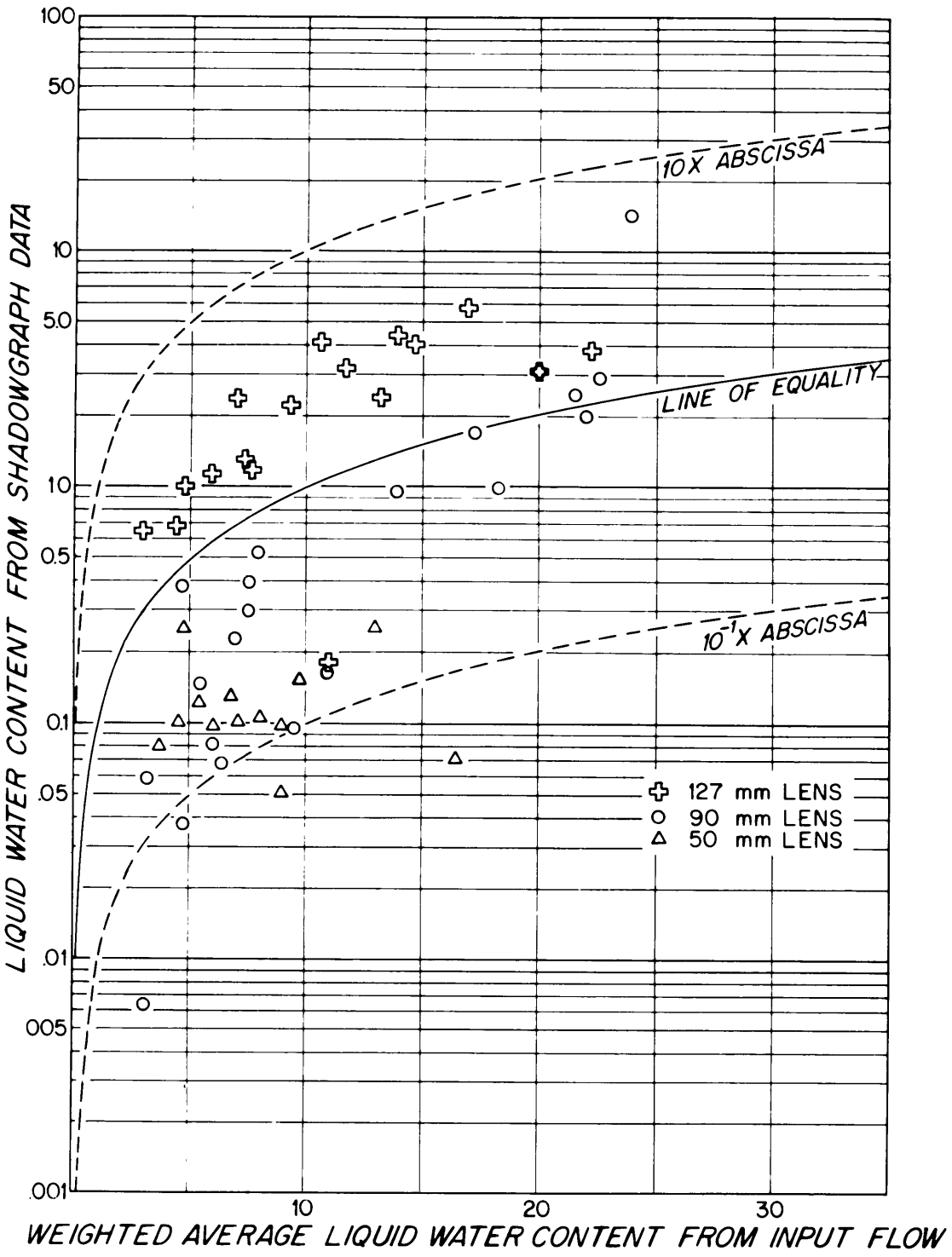


Figure 11. Comparison of weighted average liquid water content with values computed from shadowgraph drop counts.

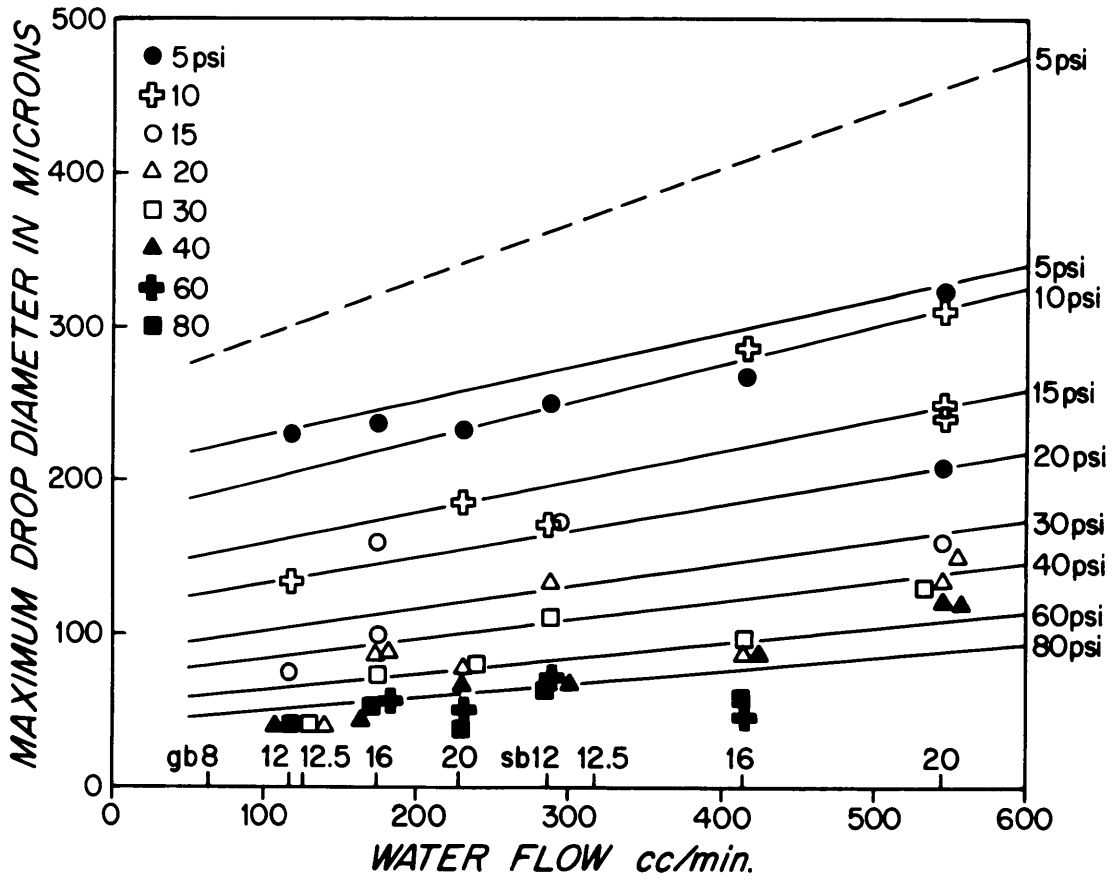


Fig. 12. Maximum drop diameter of tunnel spray from shadowgraph pictures as a function of water flow input and nozzle air pressure. Data fitted subjectively with equation

$$2a_{max} = \frac{.79W + 655}{\sqrt{P}} - 33$$

where W is water flow rate in cc/min and P is air pressure in lb/sq.in., except for pressure of 5lb/sq.in.

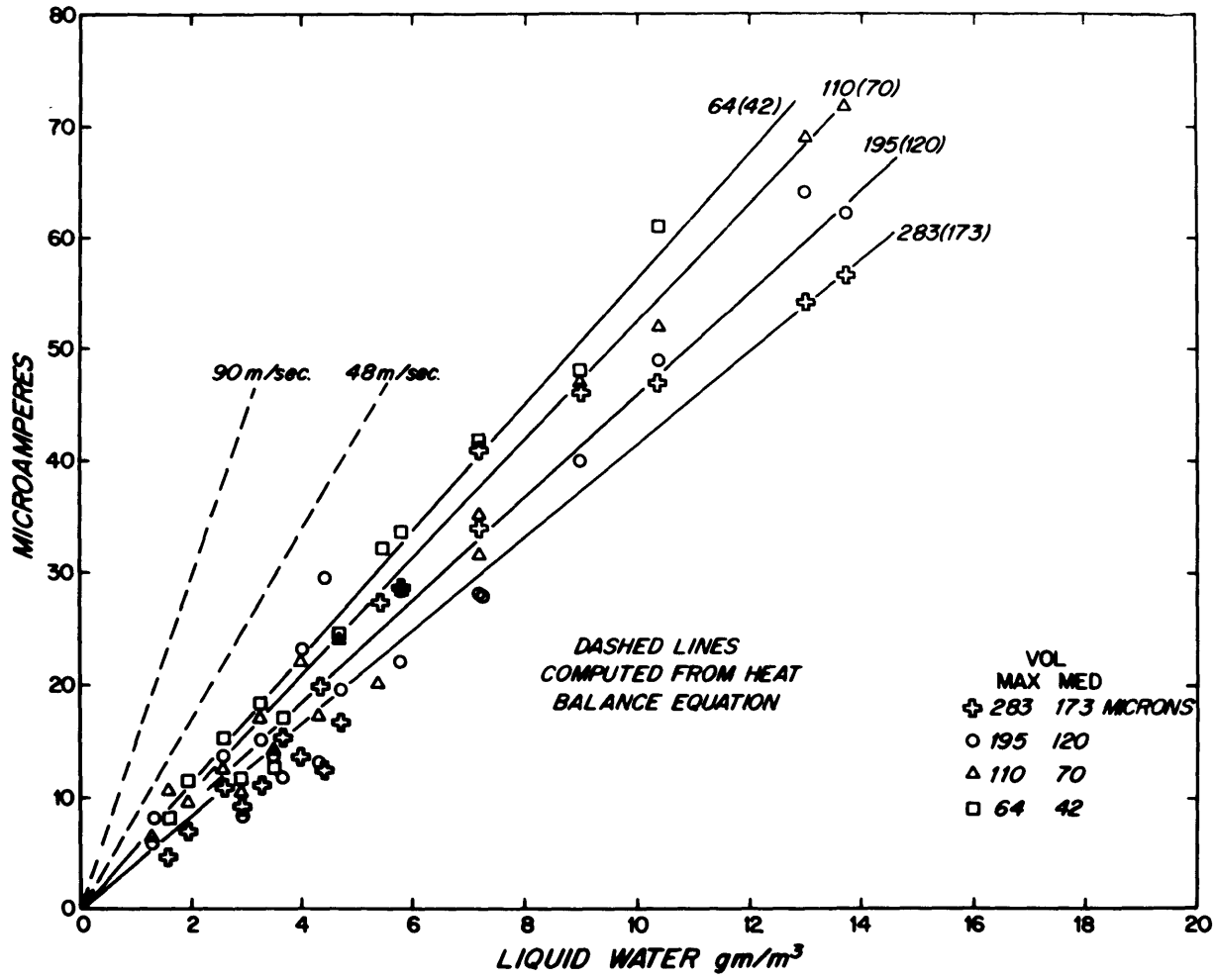


Figure 14. Calibration of cloud instrument over air speed range from 95 to 176 knots.

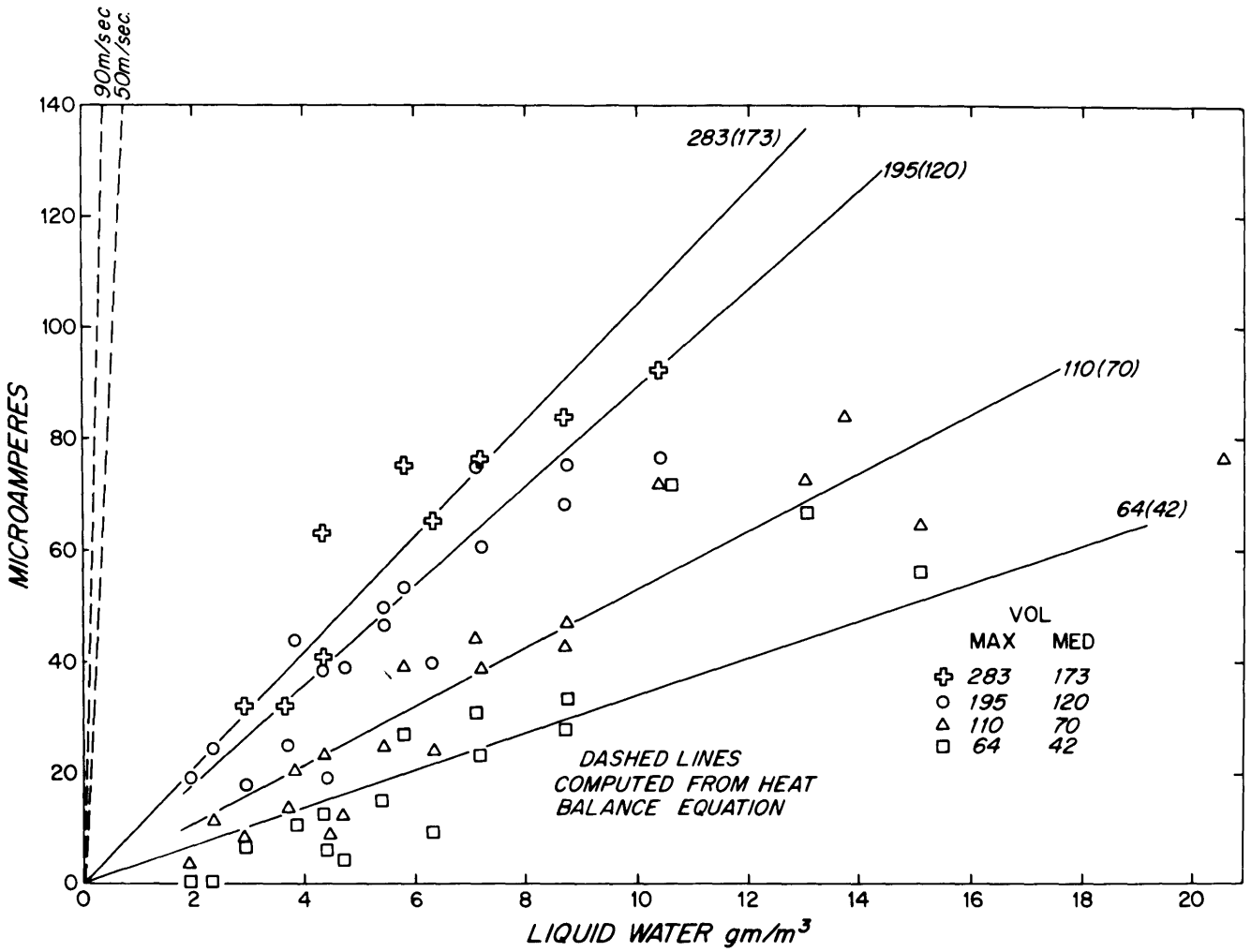


Figure 15. Calibration of precipitation instrument over air speed range from 95 to 176 knots.

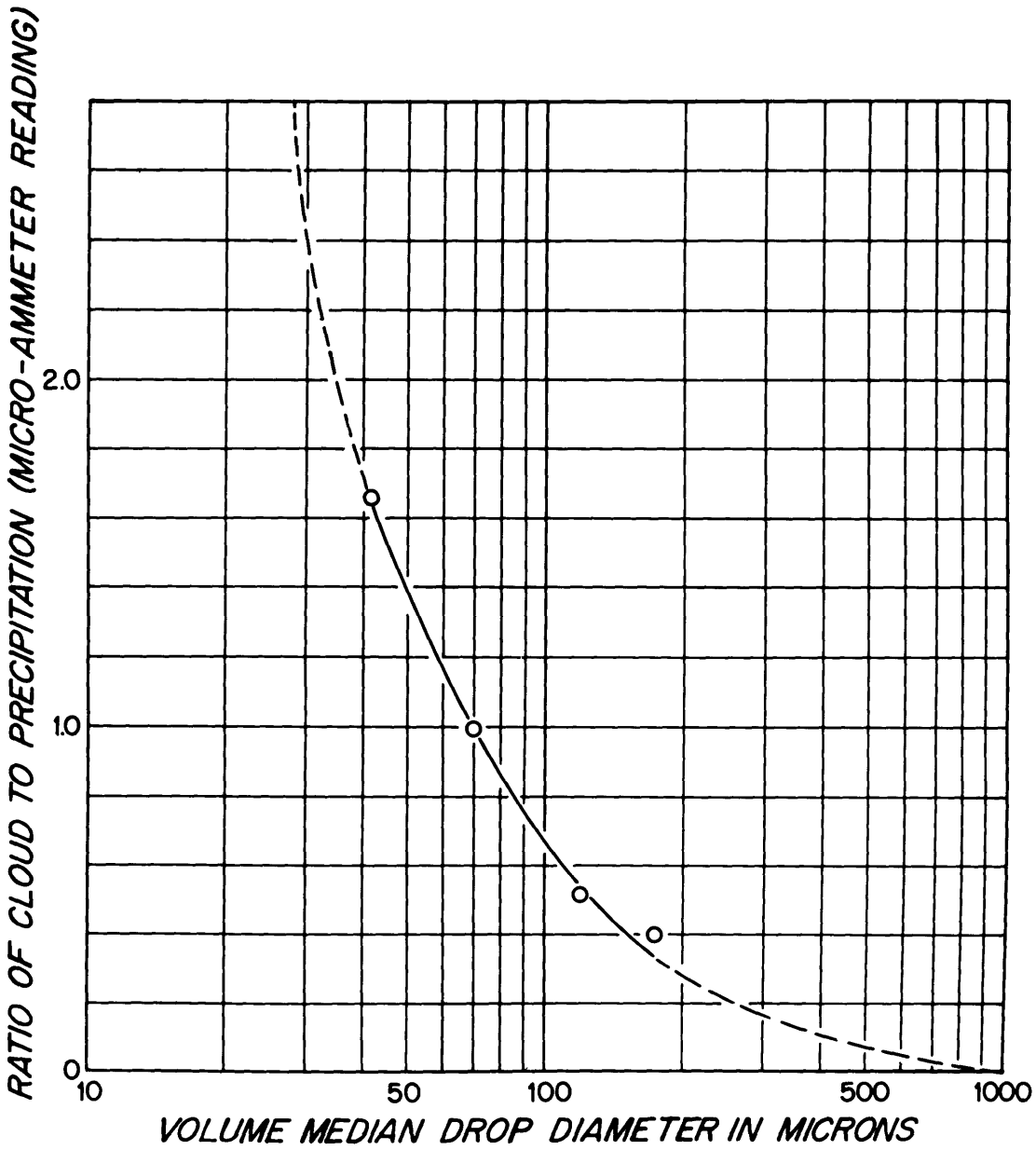


Figure 16. Ratio of cloud to precipitation instrument bridge current as function of volume median drop diameter.

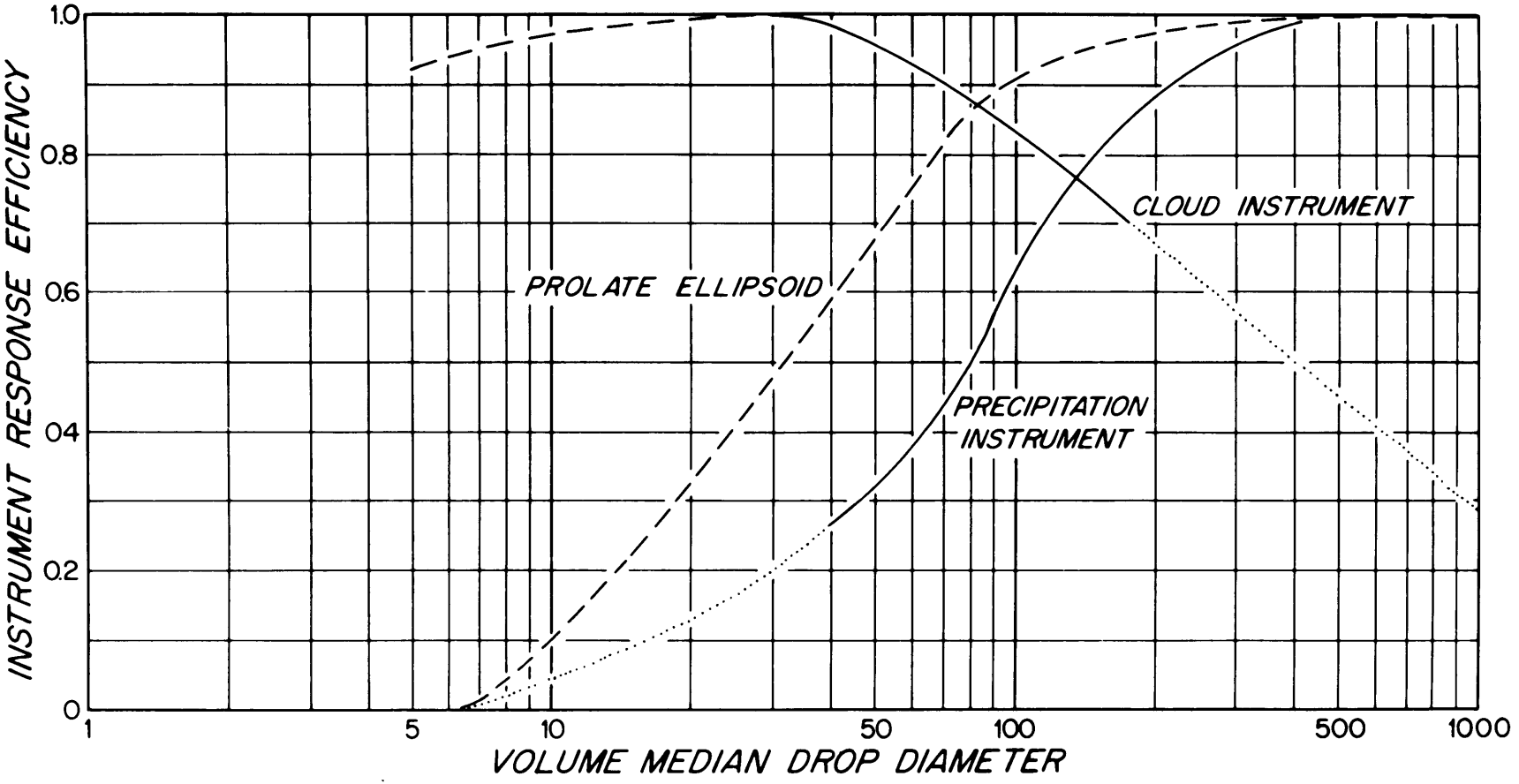


Figure 17. Instrument response efficiency as a function of volume median drop diameter.

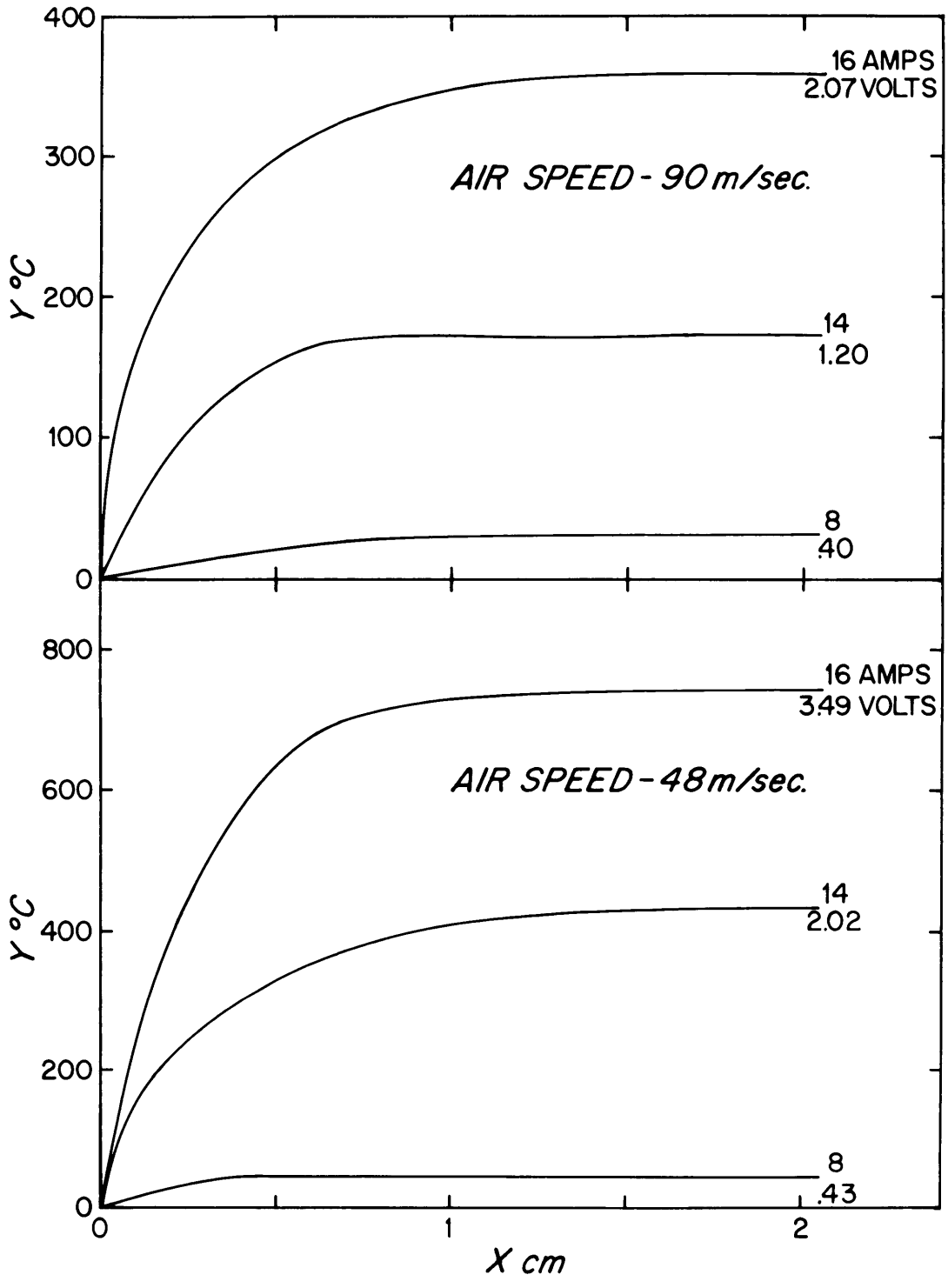


Figure 18. Theoretical temperature profiles of cloud instrument hot wire in dry air.

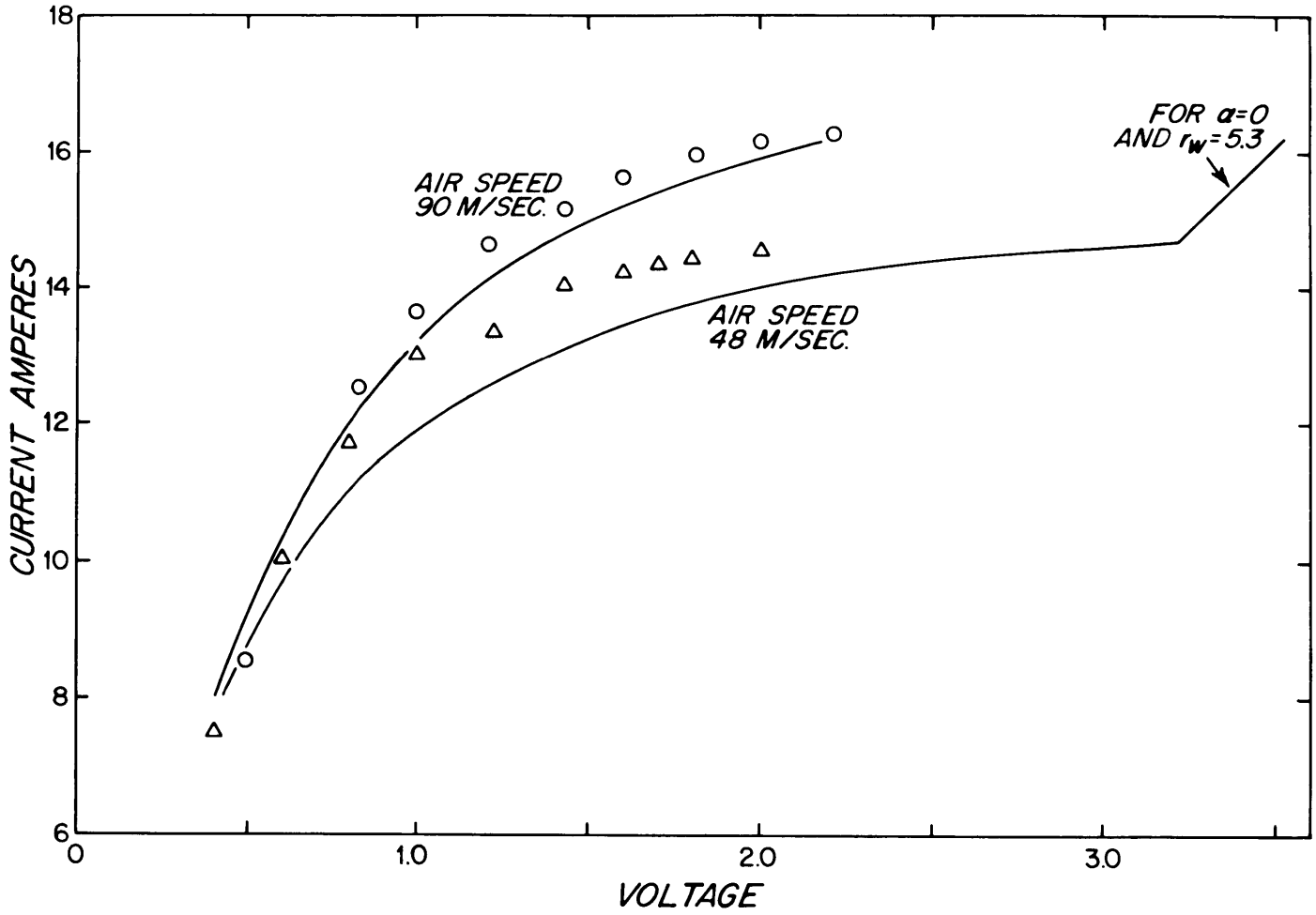


Figure 19. Comparison of computed and observed current-voltage relationship for dry cloud instrument.

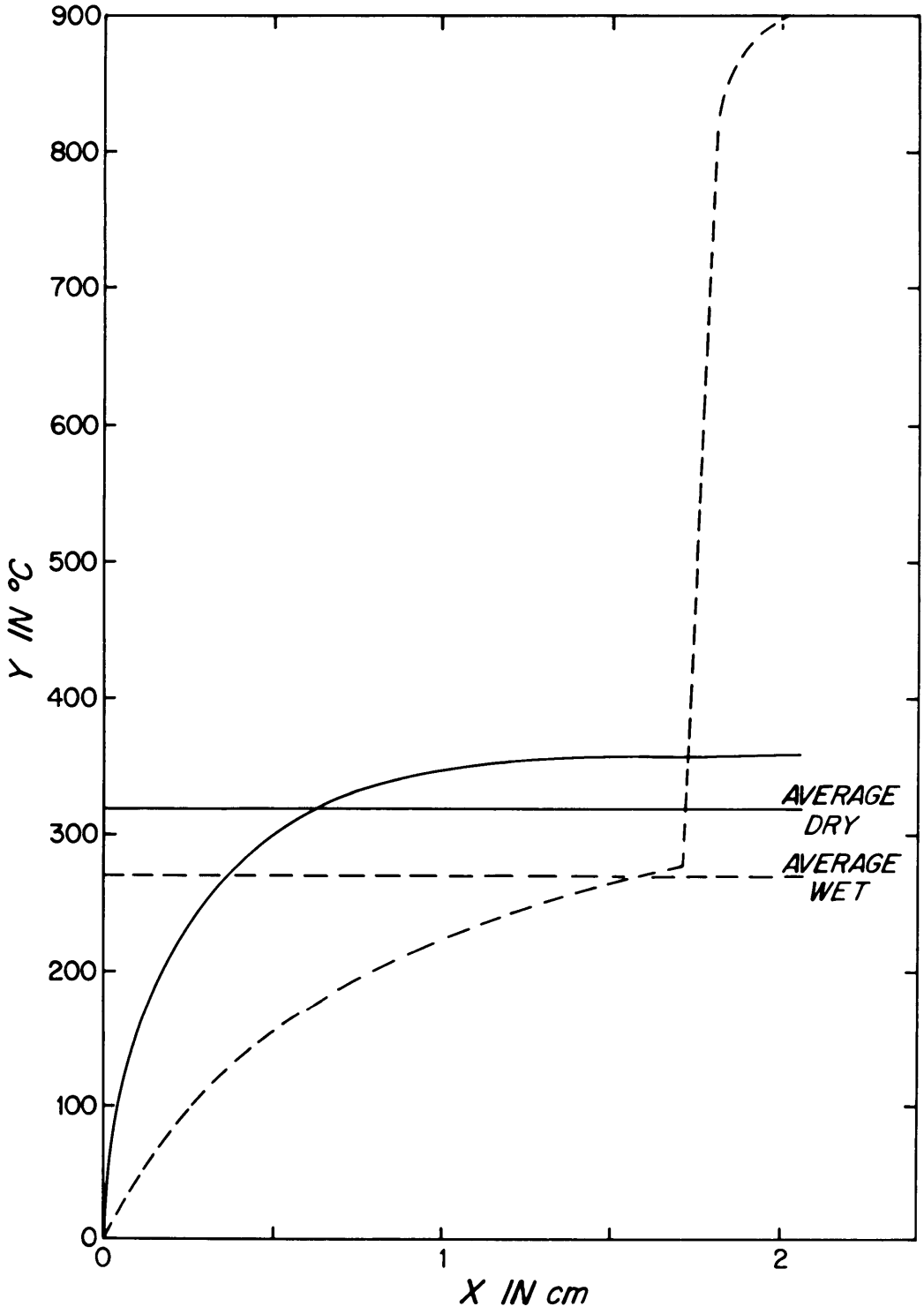


Figure 20. Hypothetical temperature profile of wet cloud instrument hot wire as compared with corresponding dry wire.

PART II

Dynamics of Cumulus Convection

1. Historical introduction.

Theoretical analysis of cumulus convection essentially started with the "parcel" concept, which is still very much with us in meteorological thermodynamic charts and in many textbooks on meteorology. More recent developments in cumulus convection have their origin in the work of Stommel (1947, 1951) and Houghton and Cramer (1951) on entrainment in cumulus clouds. The impetus for Stommel's work came from aircraft observations of trade-wind cumulus by McCasland and Woodcock during the 1946 Wyman Expedition to the Caribbean - summarized in a monograph by Bunker, Haurwitz, Malkus and Stommel (1949).

In Stommel's work and some of the later work, the cumulus cloud was modeled as a steady-state jet. In contrast, Scorer and Ludlam (1953), while accepting the entrainment notion, proposed a "bubble" model for convective elements. This was based on impressions gained from conversations with glider pilots. Scorer (1957) combined tank experiments and dimensional analysis to arrive at a rational development of the "bubble" or "thermal" model in a neutral environment. Both the steady-state jet and "bubble" models are essentially modified parcel theories, which allow for mixing of the parcel with environmental fluid.

Concurrently with and following Scorer's tank experiments, others performed more detailed experiments. In particular Woodward (1959) and Saunders (1962) used neutrally buoyant particles to demonstrate the detailed flow in and around a buoyant tank element. The flow was remarkably

like Hill's spherical vortex. Turner (1957, 1963) explored the behavior of buoyant vortex rings and in later experiments introduced the equivalent of latent heat release.

An additional variation on the experiment theme was introduced by Malkus and Witt (1959) in their numerical convection experiments, which was followed by similar and more carefully-done experiments by Ogura (1962, 1963) and Lilly (1962, 1964). All the numerical experiments had certain features in common, namely, (1) use of the equations of motion, continuity, and thermodynamics, (2) an assumed eddy coefficient of viscosity, and (3) assumptions concerning the initial conditions. In general the numerical experiments do not support the existence of bubble-like elements in a conditionally unstable atmosphere, but neither do they support the steady-state jet model. Ogura's experiment in particular appears to lean more towards an expanding jet with a mushroom-like structure.

An alternate form of numerical analysis has been based on the assumption of some sort of steady-state jet or "bubble" model circulation. For the steady-state jet model, computations have been made on the basis of continuity, thermodynamic, and buoyancy conditions averaged over the jet cross section. The prototype computation has been that of Houghton and Cramer followed by Haltiner (1959), and Squires and Turner (1962). In the case of the bubble model, a simple form such as a sphere has been assumed for an isolated element rising under the influence of buoyancy resulting from the effect of condensation and some assumed law of entrainment. Examples of such computations are

those by Ludlam (1958), Levine (1959), and Mason and Emig (1961). The above numerical analyses may be designated as parametric entrainment models.

In general all the theoretical work is based on the same basic equations of motion, continuity, and thermodynamics; but the complex interactions involved make the isolation of unique boundary value problems impossible. Therefore each school of thought has tended to develop approximate techniques and notations with only a superficial regard for each others' work. An attempt will be made in the following sections to bring some sort of unity into this work.

Possibly the tank experiments with the various forms of buoyant blobs and jets have been most helpful in giving physical insight into the forms of turbulent motion assumed by transient buoyant fluid impulses in a neutral or stable environment, but the problem of extrapolating laboratory experiments to extremely irregular cumulus convection is not at all a simple one.

The numerical experiments by Ogura (1962, 1963) appear to have been most effective so far in yielding some insight into the form that atmospheric convection elements tend to assume in neutral, stable, and unstable environments. Yet even in Ogura's numerical experiments the conclusiveness of the results is limited by the assumption of a constant eddy viscosity coefficient and the limited grid network dictated by the limitations of machine capacity. A feature of Ogura's work (1962), which makes his later results credible is his success in partially reproducing the detailed behavior of buoyant elements in tank experiments.

2. Comparative analysis of tank experiments in terms of the author's bubble model.

Instead of treating the various parametric entrainment models in chronological order of introduction, the simplest mathematical treatment is taken first. The analysis and notation advanced by Scorer (1957) has been adopted by others largely due to its simplicity and empirical success. By dimensional analysis Scorer deduced the equation

$$W^2 = C^2 gBr \qquad (1)$$

for the vertical velocity W of a thermal where C^2 is essentially a Froude number, g the acceleration of gravity, and r the radius of largest horizontal cross section. B is the average buoyancy defined as the ratio of average density excess to the environment density.

In tank experiments the outline of the model thermal was usually followed by the dye contained in it. Therefore, although the buoyancy decreased with time, the product of buoyancy and volume BV was conserved so that $BV = B_o V_o$, where B_o and V_o are the initial buoyancy and volume, respectively.

By setting $W = \frac{dZ}{dt}$ where W is now considered to be the vertical velocity of the center of mass of the thermal and Z its vertical coordinate, Scorer derived the equation

$$t = kZ^2 \qquad (2)$$

by integration of equation (1). The constant k is given by

$$k = m^{\frac{1}{2}}/2nC(gB_oV_o)^{\frac{1}{2}} \qquad (3)$$

where m and n are constants by virtue of the assumption of similarity. The constants m and n are constants of proportionality with the equations

$$n = \frac{Z}{r}$$

and

$$m = \frac{V}{r}$$

Obviously if m, n, and C are constants, then $k(B_oV_o)^{\frac{1}{2}}$ is a constant and the constant

$$C = \frac{m^{\frac{1}{2}}}{2nk(B_oV_o)^{\frac{1}{2}}} \qquad (4)$$

Thus the combination of Scorer's dimensional analysis and assumption of similarity defines the thermal's behavior entirely in terms of a simple constant parameter n.

Scorer's analysis may be very simply shown to be the equivalent of the writer's 1959 analysis in which he assumed rates of mass entrainment and detrainment, $K_e \frac{W}{r}$ and $K_d \frac{W}{r}$, respectively. From the conservation of mass constraint on a spherical thermal and these assumed mixing laws the writer derived the equation

$$\frac{dr}{dt} = \frac{K_e - K_d}{3} W. \qquad (5)$$

Integration of this equation yields the linear equation

$$r - r_o = \frac{K_e - K_d}{3} Z \qquad (6)$$

where k_e and k_d are coefficients of entrainment and detrainment, respectively. For the tank experiments in a neutral non-turbulent environment, the detrainment parameter is probably zero, and we can then relate k_e to Scorer's n

$$\frac{k_e}{3} = \frac{1}{n} \quad ,$$

considering $r >> r_o$.

(For a turbulent or stable environment the introduction of k_d may be appropriate, however.) Then an equation for the conservation of momentum was written essentially as

$$\frac{d(1+\alpha)MW}{dt} = Mg B - k_d \frac{MW^2}{r} , \tag{7}$$

where M is the mass of the thermal element and α is the apparent mass coefficient due to acceleration of the surrounding fluid. (Relative acceleration of the internal fluid is neglected.) The viscous drag on the thermal has been assumed entirely due to turbulent mass exchange between the thermal and static environment. Then since

$$\frac{dM}{dt} = (k_e - k_d) M \frac{W}{r} \tag{8}$$

equation (7) reduces to

$$(1+\alpha) \frac{dW}{dt} = g B - (1+\alpha) \frac{k_e}{r} W^2 + \alpha \frac{k_d}{r} W^2 \tag{9}$$

In the case of the tank thermals the equation for conservation of buoyancy may be written as

$$\frac{dMB}{dt} = - \frac{k_d}{r} WMB \tag{10}$$

which by equation (8) reduces to

$$\frac{dB}{dt} = -\frac{k_e}{r} WB \tag{11}$$

Then since $\frac{d}{dt} = W\frac{d}{dz}$,

equations (9) and (11) may be written as

$$\frac{dW^2}{dz} = \frac{2g}{1+\alpha} B - 2\frac{k_e}{r} W^2 + 2\alpha \frac{k_d}{r} W^2 \tag{12}$$

and

$$\frac{dB}{dz} = -\frac{k_e}{r} B. \tag{13}$$

In the case of a neutral environment ($k_d = 0$) the solution of equation (13) is by substitution from equation (6)

$$B = B_o \xi^{-3} \tag{14}$$

where

$$\xi = 1 + \frac{k_e}{3}\frac{z}{r_o}$$

Substitution of equations (14) and (6) in equation (12) makes possible its integration so that

$$W^2 = W_o^2 \xi^{-6} + \frac{3g B_o r_o}{2(1+\alpha)k_e} \xi^{-2}\left[1 - \xi^{-4}\right]. \tag{15}$$

Now to compare equation (15) with Scorer's equation (1), we set $W_o = 0$ and neglect the ξ^{-4} term, which is justified if $\frac{k_e}{3}\frac{z}{r_o} > 1$. Substitution from equation (14) for B_o in equation (15) results finally in

$$W^2 = \frac{3g Br}{2(1+\alpha)k_e} \tag{16}$$

This is of the same form as Scorer's equation (1).

For a sphere, α is $\frac{1}{2}$ (Menzel, 1960, pp.228 and 229), so that the coefficient C^2 of Scorer's equation (1) by comparison with equation (16) is $\gamma/k_e = \eta/3$. According to Scorer's (1957) experiments, η is approximately 4, which gives us the values $k_e = .75$ and $C = \sqrt{1.33} = 1.15$. This agrees well with Scorer's experimental evaluation, $C \simeq 1.2$. Therefore the tank experiments are consistent with the assumption of $\alpha = \frac{1}{2}$ and of a spherical shape. (A similar but not as detailed analysis was performed by Saunders (1962) in connection with his analysis of experiments on the penetration of a stable interface.)

Equations (6) and (15) may also be applied to the non-buoyant puff in the experiments described by Grigg and Stewart (1963) and Richards (1965). The buoyancy equation (14), of course, is dropped and equation (15) reduces to

$$W = W_o \xi^{-3} \qquad (15')$$

3. Internal circulation of a thermal.

The writer has derived considerable physical insight into the nature of the circulation developed in tank thermals from looking at many of the unpublished experiment photographs taken by Dr. P. Saunders and from some simple experiments of his own with potassium permanganate solutions in a neutral environment. All of the above experiments had gross features in common. The initial density distribution was rapidly

reformed into a bowl-like structure. In Dr. Saunders' streak photographs, the associated circulation appeared to be organized into a spherical vortex-like circulation with the dense bowl-shaped fluid concentrated at the leading surface of the thermal, as drawn by Scorer (1957). The streak photographs also indicated that the level of internal small-scale turbulent motion was at least an order of magnitude smaller than the vortex motion and the vertical translation of the thermal. In the later stage of development a ring of relatively dense material appeared to be concentrated at the ring vortex axis. Furthermore the vortex circulation appeared to be very rapidly organized just after release of the buoyant material and remained constant or increased slowly thereafter.

In the numerical experiments performed by Malkus and Witt (1959), Ogura (1961, 1962), and Lilly (1961, 1962), an eddy viscosity was introduced arbitrarily which was assumed constant except by the last author. Obviously the introduction of mixing parameters in the "bubble" models discussed in Section 2 must imply some sort of eddy viscosity. An approximate analysis can be performed to establish a relation of the mixing parameters k_e and k_d to an eddy viscosity. This may make possible a less arbitrary choice of eddy viscosity in future numerical experiments.

In tank experiments with a neutral environment the isolated thermal or puff is essentially a turbulent mass of fluid moving and spreading into a non-turbulent environment. Turner (1963) has provided us with a study of buoyant thermals moving into neutral turbulent

surroundings. This corresponds to the case of $k_d > 0$. In both cases there is an average internal gradient of velocity and buoyancy, but in a still neutral environment there is no average gradient outside the thermal or puff. In a turbulent environment an average external gradient of velocity and buoyancy is induced.

The average eddy fluxes of momentum and buoyancy out of a thermal or puff are related approximately to the average internal shear and buoyancy gradients by

$$\tau_e = -\mu_e \frac{W}{r} \tag{17}$$

and

$$F_e = -k_e \frac{B}{r} \tag{18}$$

respectively, where μ_e is the internal eddy viscosity coefficient and k_e the internal eddy diffusion coefficient. Since in a coordinate system moving with the thermal the average air velocity of the surrounding air past it is -W, the eddy flux of momentum into the thermal of mass

$$M = \frac{4}{3}\pi\rho r^3$$

may be written as

$$\tau_e = -\frac{MW}{4\pi r^2} k_e \frac{W}{r} = -\frac{1}{3} k_e \rho W^2 \tag{19}$$

where $k_e\frac{W}{r}$ represents the rate of entrainment. Similarly we obtain

$$F_e = -\frac{MB}{4\pi r^2} k_e \frac{W}{r} = -\frac{1}{3} k_e \rho B W. \tag{20}$$

By elimination of τ_e and F_e from equations (17) and (19) and equations (18) and (20)

$$\mu_e = \kappa_e = \tfrac{1}{3} k_e \rho r W \tag{21}$$

which is the internal eddy transfer coefficient.

Similarly the external eddy fluxes are

$$\tau_d = \mu_d \frac{fW}{r}, \tag{17'}$$

$$F_d = \kappa_d \frac{fW}{r}, \tag{18'}$$

$$\tau_d = \tfrac{1}{3} k_d \rho W^2, \tag{19'}$$

and

$$F_d = \tfrac{1}{3} k_d \rho B W \tag{20'}$$

where f represents some fraction less than one. fW and fB represent the average external velocity and buoyancy established by the external turbulence. The external eddy transfer coefficient is then

$$\mu_d = \kappa_d = \tfrac{1}{3} k_d \rho r W. \tag{21'}$$

The eddy transfer coefficients are also related to the Reynolds number of the flow defined as

$$Re = \frac{r \rho W}{\mu} \tag{22}$$

where μ is the molecular coefficient of viscosity. By elimination of W from equations (21) and (21') with equation (22) we obtain

$$\mu_e = \tfrac{1}{3} k_e \mu Re$$

and

$$\mu_d = \tfrac{1}{3} k_d \mu Re$$

4. Extension of the bubble model to cumulus convection.

The bubble-model as already described is very easily adapted to dry convection in an atmosphere of neutral stability and is equivalent to an analysis developed by Priestley (1957). However the problem of extending it to cumulus convection is complicated by the condensation, drop coalescence, and precipitation processes. Ludlam (1958) made an attempt to adapt Scorer's equations to a spherical bubble-model of a cloud element. Ludlam's treatment was essentially an estimate of the buoyancy of a bubble by interpolating between a saturated environment sounding and the behavior of an adiabatic parcel. The writer's previous treatment (1959) was an attempt to arrive at the buoyancy of a bubble more exactly as a consequence of the particular entrainment law assumed therein. A revised and corrected version of his development follows.

To simplify the analysis, the environment of the bubble is assumed to be saturated and to have a temperature lapse rate intermediate between a dry adiabat and a moist adiabat. This environment can be thought of as the residual cool cloud surrounding the bubble (see Figure 1). The difference between the environment potential temperature θ_e and the potential temperature θ_m of the moist pseudo-adiabat intersecting the environment sounding at cloud base is assumed to be a linear function of height:

$$\Delta\theta_m = \theta_m - \theta_e = \overline{\theta}_e \gamma_1 Z \qquad (23)$$

$\overline{\theta}_e$ is the average θ_e over the total depth of bubble penetration.

Equation (12) carries over into the atmospheric bubble model, but with

$$\mathcal{B} = \left(\frac{\Delta\theta}{\theta_e} - \Delta\ell\right) \qquad (24)$$

where $\Delta\theta = \theta - \theta_e$, θ is the average potential temperature inside the bubble, ℓ is the liquid water mixing ratio, and $\Delta\ell = \ell - \ell_e$. Equation (13) is replaced by a conservation of entropy equation

$$\frac{d\phi}{dz} = -\frac{k_e}{r}\Delta\phi \tag{25}$$

where ϕ is the average entropy of the bubble, $\Delta\phi = \phi - \phi_e$ and ϕ_e is the entropy of the environment.

The entropy of saturated moist air, neglecting the specific heat of liquid water, is related to the potential temperature θ and mixing ratio x by the equation

$$\phi - \phi_o = C_p \ln\frac{\theta}{\theta_o} + L\left(\frac{x}{T} - \frac{x_o}{T_o}\right) \tag{26}$$

where C_p is the specific heat of air at constant pressure, T the absolute temperature, L the latent heat of vaporization, and the subscript nought represents some arbitrary reference level of entropy such as its value at cloud base. We define the dimensionless variable Π as

$$\Pi = \left(\frac{p_e}{p_o}\right)^{R/c_p} \tag{27}$$

where p_e is the environment pressure, p_o the pressure at cloud base, and R the gas constant for air. Then the equation for potential temperature is

$$\theta = T/\Pi \,, \tag{28}$$

and the hydrostatic equation takes the form

$$\frac{d\Pi}{dz} = -\frac{g}{C_p\theta} . \tag{29}$$

Substitution from equation (28) in equation (26) and differentiation at constant Π leads to a formula for $\Delta\phi$:

$$\Delta\phi = \frac{C_p}{\theta}\Delta\theta + \frac{L\Delta x}{\theta\Pi} - \frac{Lx}{\theta^2\Pi}\Delta\theta \tag{30}$$

The derivative of equation (26) with respect to Z is by virtue of equations (28) and (29)

$$\frac{d\phi}{dz} = \frac{C_p}{\theta}\frac{d\theta}{dz} + \frac{L}{\theta\Pi}\frac{dx}{dz} + \frac{gLx}{C_p\theta^2\Pi^2} - \frac{Lx}{\theta^2\Pi}\frac{d\theta}{dz} \tag{31}$$

The integrated form of the Clapeyron-Clausius equation, which relates X to θ and Π may be written as

$$x = \frac{C'}{\Pi^{1/\kappa}} e^{-L/R_v\theta\Pi} \tag{32}$$

where C' is an arbitrary constant and R_v the gas constant for water vapor. Differentiation of this equation at constant Π results in

$$\Delta x = \frac{xL}{R_v\theta^2\Pi}\Delta\theta \tag{33}$$

and its derivative with respect to Z determines $\frac{dx}{dz}$ as a function of θ and Z.

$$\frac{dx}{dz} = \frac{gx}{C_p\kappa\theta\Pi} + \frac{xL}{R_v\theta^2\Pi}\frac{d\theta}{dz} - \frac{gxL}{R_vC_p\theta^2\Pi^2} \tag{34}$$

$$\kappa = R/C_p$$

Substitution of equation (33) into (30) and equation (34) into (31), followed by substitution of equations (30) and (31) into equation (25), produces the differential equation for potential temperature

difference $\Delta\theta$:

$$\frac{d\Delta\theta}{dz} = \frac{d\Delta\theta_m}{dz} - \frac{k_e}{r}\Delta\theta \tag{35}$$

$d\Delta\theta_m/dz$ signifies the quantity

$$\frac{d\Delta\theta_m}{dz} = \frac{\frac{L}{\eta C_p}\frac{q\chi_m}{\theta_m \Pi}\left(\frac{L}{R_v\theta_m\Pi} - \frac{1}{K} - 1\right)}{C_p + \frac{L^2\chi}{R_v\theta_m^2\Pi^2} - \frac{L\chi}{\theta_m\Pi}} \frac{d\theta_e}{dz} \tag{36}$$

where the subscript m represents values on the moist pseudo-adiabat.

A similar process leads to the mixing ratio differential equation:

$$\frac{d\Delta\chi}{dz} = \gamma_3 - \gamma_2 - \frac{k_e}{r}\Delta\chi, \tag{37}$$

where χ is the bubble mixing ratio, $\Delta\chi = \chi - \chi_e$, $\gamma_2 = -\frac{d\chi_m}{dz}$, $\gamma_3 = -\frac{d\chi_e}{dz}$, and

$$\frac{d\Delta\chi_m}{dz} = -\frac{\Pi C_p}{L}\frac{d\theta_m}{dz} - \frac{\frac{q\chi_m}{\theta_m\Pi}\left(1+\frac{L\chi_m}{C_pK\theta_m\Pi}\right)}{C_p + \frac{L^2\chi_m}{R_v\theta_m^2\Pi^2} - \frac{L\chi_m}{\theta_m\Pi}} - \frac{d\chi_e}{dz} \tag{38}$$

The liquid water conservation equation may be written as

$$\frac{dM\ell}{dz} = M\ell_e\frac{k_e}{r} - M\ell\frac{k_d}{r} - M\left(\frac{d\chi}{dz} + \gamma_p\right) \tag{39}$$

where γ_p represents the rate of loss or gain of liquid water through precipitation (positive for a loss and negative for a gain). Substitution of equations (37) and (8) into equation (39) results in

$$\frac{d\Delta\ell}{dz} = \frac{k_e}{r}\left(\Delta\chi - \Delta\ell\right) - \gamma_4 + \gamma_2 - \gamma_p \tag{40}$$

where $\gamma_4 = \frac{d\ell_e}{dz}$. The parameter γ_p is intertwined in a complicated fashion with the mechanism of drop growth by condensation and coalescence and the interaction of drops with the air motion.

The system of equations (35), (37), (40), and (12) may be integrated exactly by numerical methods with a computer for a given environment and a given γ_p. However approximate bubble model formulae for the behavior of $\Delta\theta$, ΔX, $\Delta\ell$, and W may be derived if the following assumptions are made:

(1) $k_d, k_e, \gamma_1, \gamma_2, \gamma_3, \gamma_4$ and γ_p are constant.

(2) Set $\theta_e = \bar{\theta}_e$ in formula (24) for B. In an environment for which γ_1 is a constant, γ_2 and γ_3 are not strictly speaking constants; and γ_p is even less likely to be constant. However, as will appear later the errors introduced by the above assumptions are probably well within the accuracy of the data with which the formulae are to be compared.

Subject to the above assumptions the solutions of the bubble-model differential equations have the following forms:

Case I $\quad k_d = 0$

$$\Delta\theta = \Delta\theta_o \xi^{-3} + \frac{3\gamma_o \bar{\theta}_e \gamma_1}{4 k_e}\left(\xi - \xi^{-3}\right) \tag{41}$$

$$\Delta X = \frac{3\gamma_o(\gamma_3 - \gamma_2)}{4 k_e}\left(\xi - \xi^{-3}\right) \tag{42}$$

$$\Delta\ell = \frac{3\gamma_o}{4 k_e}\left[(\gamma_3 - \gamma_2)(1 - \xi^{-3}) + (\gamma_2 - \gamma_4 - \gamma_p)(\xi - \xi^{-3})\right] \tag{43}$$

$$W^2 = \xi^{-6} W_0^2 + \frac{4 r_0 g}{k_e}\left\{\left[\frac{\Delta\theta_0}{\bar\theta_e} - \frac{3r_0}{16 k_2}(\gamma_1 - 2\gamma_2 + \gamma_4 + \gamma_p)\right](\xi^{-2} - \xi^{-6}) + \right.$$

$$\left. + \frac{3r_0}{32 k_e}(\gamma_1 - \gamma_2 + \gamma_4 + \gamma_p)(\xi^{-2} - \xi^{-6}) - \frac{3r_0}{28 k_e}(\gamma_3 - \gamma_2)(\xi - \xi^{-6})\right\} \qquad (44)$$

$$\xi = 1 + \frac{k_e}{3}\frac{z}{r_0}$$

The initial values of ΔX and $\Delta \ell$ have been assumed to be zero. For large ξ these solutions take the simpler forms (the values of ξ for which they have an accuracy of 5% are indicated):

$$\Delta\theta = \frac{3 r_0 \bar\theta_e \gamma_1}{4 k_e}\xi, \quad \xi \geq 2.7 \qquad (41')$$

$$\Delta X = \frac{3 r_0 (\gamma_3 - \gamma_2)}{4 k_e}\xi, \quad \xi \geq 2.7 \qquad (42')$$

$$\Delta \ell = \frac{3 r_0}{4 k_a}\left[\gamma_3 - \gamma_2 + (\gamma_2 - \gamma_4 - \gamma_p)\xi\right], \quad \xi \geq 2.7 \qquad (43')$$

$$W^2 = \frac{3 r_0^2 g}{k_e^2}\left[\frac{1}{8}(\gamma_1 - \gamma_2 + \gamma_4 + \gamma_p)\xi^2 - \frac{1}{7}(\gamma_3 - \gamma_2)\xi\right], \quad \xi \geq 2.1 \qquad (44')$$

Case II. $k_d = k_e$

$$\Delta\theta = \Delta\theta_0 e^{-\zeta} + \frac{r_0 \bar\theta_e \gamma_1}{k_e}(1 - e^{-\zeta}) \qquad (45)$$

$$\Delta X = \frac{r_0(\gamma_3 - \gamma_2)}{k_e}(1 - e^{-\zeta}) \qquad (46)$$

$$\Delta \ell = \frac{r_0}{k_e}\left[\gamma_2 \zeta e^{-\zeta} + \gamma_3(1 - e^{-\zeta} - \zeta e^{-\zeta}) - (\gamma_4 + \gamma_p)(1 - e^{-\zeta})\right] \qquad (47)$$

$$W^2 = \frac{4 r_0 g}{3 k_e}\left\{\frac{\Delta\theta_0}{\bar\theta_e}\zeta e^{-\zeta} + \frac{r_0 \gamma_1}{k_e}(1 - e^{-\zeta} - \zeta e^{-\zeta}) - \frac{r_0}{k_e}\left[\frac{\gamma_2}{2}\zeta^2 e^{-\zeta} + \right.\right.$$

$$\left.\left. + \gamma_3(1 - e^{-\zeta} - \zeta e^{-\zeta} - \frac{\zeta^2}{2}e^{-\zeta}) - (\gamma_4 + \gamma_p)(1 - e^{-\zeta} - \zeta e^{-\zeta})\right]\right\} \qquad (48)$$

$$\zeta = \frac{z}{r_0}.$$

As in Case I asymptotic forms of the above equations for ζ large may be written with approximately the same accuracy as follows:

$$\Delta\theta = \frac{\gamma_0 \bar{\theta}_e \gamma_1}{k_e}, \quad \zeta \geq 3 \tag{45'}$$

$$\Delta\chi = \frac{\gamma_0 (\gamma_3 - \gamma_2)}{k_e}, \quad \zeta \geq 3 \tag{46'}$$

$$\Delta\ell = \frac{\gamma_0}{k_e}(\gamma_3 - \gamma_4 - \gamma_p), \quad \zeta \geq 4.6 \tag{47'}$$

$$W = \sqrt{\frac{4\gamma_0^2 g}{3k_e^2}\left(\gamma_1 - \gamma_3 + \gamma_4 + \gamma_p\right)}, \quad \zeta \geq 4.6 \tag{48'}$$

Case III. The adiabatic parcel where $k_d = k_e = 0$.

$$\Delta\theta = \Delta\theta_0 + \theta_e \gamma_1 z \tag{49}$$

$$\Delta\chi = \Delta\chi_m \tag{50}$$

$$\Delta\ell = (\gamma_2 - \gamma_4) z \tag{51}$$

$$W^2 = \frac{4}{3} g \left[\frac{\Delta\theta_0}{\bar{\theta}_e} z + (\gamma_1 - \gamma_2 + \gamma_4)\frac{z^2}{2}\right] \tag{52}$$

The large scale physical context in which the foregoing formulae are to be viewed is essentially that described by Riehl (1954, pp. 63-70 and 150-153). The source of actively buoyant cloud masses is supposed to be the turbulent sub-cloud layer. The bubble model is intended to represent more or less the turbulent motion spectrum of the buoyant part of a trade wind cumulus cloud, at least in an average sense. The bubble environment is considered to be the turbulent relatively cool saturated residue left behind by buoyant bubbles that have lost their buoyancy by penetration into the

surrounding clear environment. The cool cloud environment has an unstable lapse rate compared to a pseudo-adiabat, but the clear environment has a stable lapse rate possibly slightly less than that of the cool air somewhere between the moist pseudo-adiabatic and the dry adiabatic. The maximum height of trade wind cumulus tops prevalent in a given area is inferred to be an index of the strength of large or meso-scale subsidence. Thus the cloud lines and clusters which occur in the trades and the so-called cloud layer may be looked upon as in a statistically steady state fed intermittently by buoyant masses ("bubbles"). The intermittent supply of buoyant rising air from the sub-cloud layer may be compensated by a less energetic intermittent descent of air from the cool cloud mass.

In the presence of large scale convergence the cloud layer probably extends to the tropopause and the conditional instability parameter γ_i approaches zero. For example at a zone of equatorial convergence or in tropical disturbances (easterly waves and hurricanes) the cloud layer has been found to have a moist adiabatic lapse rate within the accuracy of observation (Malkus 1958, 1960). Thus in tropical disturbances the vertical turbulent motions in the cloud layer may be dominated by initial impulses from the turbulence generated in the sub-cloud layer and therefore may, except in hurricanes, be less vigorous than the most vigorous buoyant motions generated in regions of large scale subsidence.

5. Discussion of the precipitation parameter.

The precipitation parameter γ_p lumps together a complex combination of interacting physical phenomena. First of all the initiation of condensation on nuclei is involved in the early stages of cloud development near cloud base where the initial drop size distribution is established. After the initial phase no new nuclei are activated (see Fletcher 1962, pp. 122-159). However, after a large percentage of cloud drops become larger than $40\,\mu$ in diameter, coalescence becomes an important factor. All three of the above stages of cloud formation have been dealt with quantitatively by various people whose theoretical and experimental work is summarized in the general texts on cloud physics by Mason (1957) and Fletcher (1962).

The interaction of droplets with turbulent motions within clouds has not been studied. However actual measurements of cloud drop size distributions appear to be broader in general than simple condensation computations indicate (Fletcher, 1962). Therefore turbulence may be an important influence on drop size distribution. The initial activation of nuclei may not be uniform in a cloud element generated by a turbulent impulse from below cloud base, since the number of nuclei activated depends on nucleus size distribution and vertical velocity.

In the body of a cloud the form of a positively buoyant element must also have an important bearing on the behaviour of γ_p. For example, a bubble-like element surrounded by air with a relatively low liquid water content must lose its liquid water by precipitation mainly through its lower surface, whereas a cross-sectional element of a

steady-state jet may gain liquid water from above, as well as lose it to the jet below. If the jet is bent over by wind shear, the loss of liquid water from the jet by precipitation may be much greater than in a vertical jet.

An approximately quantitative discussion of the behavior of r_p, may be made on the basis of the fall speed u of the volume median drop size. For a buoyant bubble the rate at which liquid water is being lost is $\pi r^2 \rho_a l u$ where $\rho_a l u$ is the average settling rate per unit area for a given volume median drop size and ρ_a is the air density. The effect of the environment liquid water is neglected, because it is generally relatively small. The rate of change per unit time of l due to precipitation is obtained by dividing by $\frac{4}{3}\pi\rho_a r^3$ which is

$$\left(\frac{dl}{dt}\right)_p = \frac{3lu}{4r} \tag{53}$$

and therefore

$$r_p = \left(\frac{dl}{dz}\right)_p = \frac{3lu}{4Wr} \tag{54}$$

Since in the observations to be described later only the liquid water content and volume median drop diameter can be derived from the hot wire instrument system, no information concerning the breadth or details of the drop size distribution is available. Therefore a very simple model drop-size distribution must be used to arrive at some rough estimate from the observed data of the collision efficiency and the value of the precipitation parameter.

A simple straight line drop-size distribution model like the one

used in the reduction of the shadowgraph pictures will be assumed, but without a kink in it (Figure 2). Let a_m represent the volume median radius, and let N_1 and N_2 be the number of drops per unit volume less than and greater than a_m, respectively. Also let a_{max} be the maximum drop radius. Then the linear drop size distribution function in terms of number/cm^4 may be written in the form

$$n = \frac{2(N_1 + N_2)}{a_{max}} \left(1 - \frac{a}{a_{max}}\right) \tag{55}$$

where a is the variable drop radius.

Then by multiplication of equation (55) by $\frac{4}{3}\pi a^3 da$ and proper integration, the liquid water is evaluated as

$$\rho_a \ell = \frac{8}{3}\pi\rho\left(\frac{N_1 + N_2}{a_{max}}\right)\frac{a_{max}^2}{20} \tag{56}$$

and

$$\rho_a \ell/2 = \frac{8}{3}\pi\rho\left(\frac{N_1 + N_2}{a_{max}}\right)\left(\frac{a_m^4}{4} - \frac{a_m^5}{5 a_{max}}\right) \tag{56'}$$

where ρ is the density of water.

Elimination of $\rho_a \ell$ from equations (56) and (56')finally results in

$$a_{max}^4 = 10 a_m^4 - 8\frac{a_m^5}{a_{max}} \tag{57}$$

The relevant solution of this equation is approximately

$$a_m = .68\, a_{max} \tag{58}$$

The ratio of N_2 to N_1 is determined by multiplying equation (55) by da and integrating it from 0 to a_m.

$$N_2 = .110\, N_1 \tag{59}$$

This broad drop-size distribution is consistent with what has been observed by others, and may now be applied to the bubble model to relate a coalescence efficiency parameter E to the observed volume median drop size and liquid water content. The coalescence process is now modeled by drops of volume quartile radius $a_2 = .84\ a_{max}$ falling through and collecting drops of volume quartile radius $a_1 = .55\ a_{max}$. We may also remark that the entrainment process, by introducing small drops from the environment, would tend to counteract their removal by the coalescence process, thereby keeping the distribution broad.

The equation for the rate of mass increase of the drops of size a_2 may be written as

$$(W-u_2)\frac{dm_2}{dz} = \frac{dm_2}{dt} = \pi a_2^2 E \rho_a l (u_2-u_1)/2 \ , \qquad (60)$$

where m_2 is the mass of a drop of radius a_2, E the collection efficiency of drops of size a_2 for drops of size a_1, ρ_a the air density, and u_2 and u_1 are the fall speeds of drops of size a_2 and a_1, respectively. An equation of the above form is given, for example, by Fletcher (1962, p.161). With the aid of the assumed model drop-size distribution and observed values of volume median drop size, numerical values may be given to all the quantities in equation (60) except E, for which it can be solved. Thus E may be estimated from the proper observational data.

6. Comparison of bubble model with steady state jet model.

Turner's (1962) starting plume experiment furnishes a laboratory analogue for the steady state jet model just as the isolated thermal experiments do for the bubble model. The starting plume in neutral surroundings has a linear law for r as a function of z as does the isolated thermal. According to Turner, the top of the starting plume has a circulation like an isolated thermal, but the resemblance is somewhat superficial as will become apparent from the following mathematical analysis. Let ΔM be the mass of a cross-sectional slab cut out of the plume (see Figure 3) by two horizontal planes a distance Δz apart. Then

$$\Delta M = \pi \rho r^2 \Delta z \tag{61}$$

where r is the radius of the slab. The conservation equations are written in a fashion analogous to the bubble model as follows:

the conservation of mass

$$\frac{1}{\Delta M} \frac{d\Delta M}{dz} = \frac{k_e}{r}, \tag{62}$$

the conservation of buoyancy

$$\frac{dB\Delta M}{dz} = 0, \tag{63}$$

the conservation of momentum

$$\frac{W}{\Delta M} \frac{dW\Delta M}{dz} = gB \tag{64}$$

The hydrodynamic mass coefficient α is omitted, because the plume is in a steady state except for the plume top.

Equations (61) and (62) may be readily converted to the form

$$\frac{1}{\Delta z}\frac{d\Delta z}{dz} + \frac{2}{r}\frac{dr}{dz} = \frac{k_e}{r} \tag{62'}$$

There is also a kinematic constraint on Δz, since each element of mass ΔM is constrained to be the bottom of the one above it. The vertical velocity of the top with respect to the bottom is $\frac{dW}{dz}\Delta z$ or

$$\frac{d\Delta z}{dt} = \frac{dW}{dz}dz$$

which by virtue of the relation $\frac{d}{dt} = W\frac{d}{dz}$ becomes

$$\frac{1}{\Delta z}\frac{d\Delta z}{dz} = \frac{1}{W}\frac{dW}{dz} \tag{65}$$

Substitution of equation (65) in equation (62') transforms it to

$$\frac{1}{W}\frac{dW}{dz} + \frac{2}{r}\frac{dr}{dz} = \frac{k_e}{r} \tag{62''}$$

the solution of which may be written as

$$Wr^2 = W_o r_o^2 \xi_p \tag{66}$$

where $\xi_p = \exp\int_0^z \frac{k_e}{r}dz$ and the subscript nought designates the values of variables when z is zero.

Equation (63) may be transformed by substitution from equation (62) to

$$\frac{dB}{dz} = -\frac{k_e}{r}B \tag{67}$$

which has the solution

$$B = B_o \xi_p^{-1} \tag{68}$$

The conservation of buoyancy in the plume may therefore also be stated as

$$W r^2 B = W_o r_o^2 B_o \tag{69}$$

(obtained by eliminating ξ_p from equations (68) and (66)). Equation (69) is one of the equations used by Turner in his discussion of the starting plume.

The conservation of momentum equation (64), upon substitution from equation (62), becomes

$$\frac{dW^2}{dz} = 2gB - 2\frac{k_e}{r} W^2 \tag{70}$$

The integration of this may be indicated as

$$W^2 = W_o^2 \xi_p^{-2} + 2g r_o B_o \xi_p^{-2} \int_o^z \xi_p \, dz \tag{71}$$

Now let the presumed linear relationship of r to z be written as

$$r = r_o + Cz \tag{72}$$

where, according to Turner (1962), C = .18 . We square (66) and substitute from equations (71) and (72) for W^2 and r^2 to get

$$\left(1 + C\frac{z}{r_o}\right)^4 = \frac{\xi_p^4}{1 + \frac{2gB_o}{W_o^2} \int_o^z \xi_p \, dz} \tag{73}$$

In the case of a plume without buoyancy (i.e. $B_o = 0$), this equation reduces to

$$\xi_p = 1 + C\frac{z}{r_o} \tag{74}$$

which implies $k_e = C$.

In general when B_o is not zero, equation (73) can be satisfied for all values of $\frac{B_o}{W_o^2}$ only if k_e is some unknown function of z. However, if k_e is assumed constant equation (73) reduces to

$$\left(1+C\frac{z}{r_o}\right)^4 = \frac{\left(1+C\frac{z}{r_o}\right)^{4S}}{1+\frac{2g r_o B_o}{W_o^2(S+1)}\left[\left(1+C\frac{z}{r_o}\right)^{S+1}-1\right]} \qquad (73')$$

where $S = \frac{k_e}{C}$. This is valid for all z only if $\frac{2g r_o B_o}{W_o^2(S+1)} = 1$ and $k_e = \frac{5}{3}C$. Thus k_e for the starting plume with buoyancy is much less (.30) than for the isolated thermal (.75). As stated by Turner the starting plume has a lower value of k_e, since it shields itself from mixing with the environment.

The main difference between the bubble model and the starting plume is the kinematic constraint placed on the motion by equation (65). Under conditions of decreasing buoyancy and vertical velocity as a function of z, the height Δz of an element of the jet tends to contract in spite of the broadening effect of entrainment. Hence there is a tendency to compress turbulent elements in the jet together vertically, and it is not readily possible to look upon the laboratory model jet as a system of bubble-like elements following each other in rapid succession. The starting plume model will not be extended to the atmosphere as the bubble model was in Section 4 because of the complications arising from the kinematic constraint expressed by equation (65). However numerical methods as used by others could be applied.

7. Extension of experience gained from tank and numerical experiments to cumulus convection.

In the trade wind cumulus the buoyancy and vertical velocity tend to increase for a considerable portion of the cloud depth whereas in most of the tank experiments the reverse is true - except for a brief interval just after release of the buoyant fluid when the vertical velocity is increasing. Turner (1963) did perform experiments in which the release of buoyancy was modeled by a chemical reaction accompanied by the release of gas bubbles and concluded that the release of buoyancy did not change the nature of the motion significantly. Yet Ogura (1963) in his numerical experiments, which took into account the effects of pressure and the release of latent heat in a way more closely resembling conditions in a cumulus cloud, obtained patterns favoring an elongated vertical jet-like configuration expanding horizontally and vertically rather than either the compact bubble-like thermal or the starting plume. Therefore the combined available evidence from laboratory and numerical experiments is inconclusive at present.

As already indicated in the analysis of the starting plume, the kinematics of the motion with decreasing buoyancy and vertical velocity makes it conceptually difficult to replace the starting plume by an equivalent rapid succession of bubble-like elements. However in the case of the trade-wind cumulus the increasing vertical velocity with height at least poses no kinematic difficulty in representing a cloud system such as a cloud line or cluster as an aggregate of buoyant bubble-like thermals immersed in a turbulent cool cloud matrix with a

relatively low liquid water content and volume median drop size. The more energetic intermittent impulses of buoyancy and vertical velocity in the sub-cloud layer may play the role of the cup of buoyant fluid in the isolated laboratory thermal.

If the bubble-like elements are sufficiently frequent and their spatial density sufficiently great, they can interact with each other and the relatively cool environment to force a jet-like circulation which contracts with increasing height in association with an increase of vertical velocity. A cloud system which has grown sufficiently in size and intensity may possibly form a contracting lower jet and break through into drier air aloft to form an upper expanding jet with decreasing vertical velocity. Such an upper jet may be more accurately modeled by the starting plume than by a conglomeration of isolated thermals. When an upper jet has reached the tropopause, the overall circulation may be similar to that assumed by Squires and Turner (1963) in their steady state jet model of a cumulonimbus cloud.

References

Bunker, A.F., B. Haurwitz, J.S.Malkus, and H.Stommel, 1949: Vertical distribution of temperature and humidity over the Caribbean Sea. Pap.Phys.Ocean.and Met.,Mass.Inst. of Tech. and Woods Hole Ocean.Inst., 11, 1, 82 pp.

Fletcher, N.H., 1962: The physics of rain clouds. Cambridge Univ. Press, Cambridge, 386 pp.

Grigg, H.R. and R.W.Stewart, 1963: Turbulent diffusion in a stratified fluid. J.Fluid Mech., 15, 174-186.

Haltiner, G.J., 1959: On the theory of convective currents. Tellus, 11, 5-15.

Houghton, H.G. and H.E.Cramer, 1951: A theory of entrainment in convective currents. J.Meteor., 8, 95-102.

Levine, J., 1959: Spherical vortex theory of bubble-like motion in cumulus clouds. J.Meteor. 16, 653-662.

Lilly, D.K., 1962: On the numerical simulation of buoyant convection. Tellus, 14, 148-172.

Lilly, D.K., 1964: Numerical solutions for the shape-preserving two-dimensional thermal convection element. J.atmos.Sci., 21, 83-98.

Ludlam, F.H., 1958: The hail problem. Nubila, 1, 12-96.

Malkus, J.S., 1958: On the structure of the trade wind moist layer. Pap.Pjys.Ocean.and Met., Mass.Inst.of Tech. and Woods Hole Ocean.Inst., 13, 2, 47 pp.

Malkus, J.S., and G.Witt, 1959: The evolution of a convective element: a numerical calculation. The Rossby memorial volume, Rockefeller Inst.Press and Oxford Univ.Press, New York, 425-439.

Malkus, J.S., 1960: Recent developments in studies of penetrative convection and an application to hurricane cumulonimbus towers. Cumulus Dynamics. Pergamon Press, London, 65-84.

Mason, B.J., 1957: The physics of clouds. Oxford University Press, London, 481 pp.

Mason, B.J. and R.Emig, 1961: Calculations of the ascent of a saturated buoyant parcel with mixing. Quart.J.R.meteor.Soc., 87, 212-222.

Menzel, D.H., 1960: Fundamental formulas of physics, Vol.1. Dover, New York, 364 pp.

References (continued)

Ogura, Y., 1962: Convection of isolated masses of a buoyant fluid: a numerical calculation. J.atmos.Sci., 19, 492-502.

Ogura, Y., 1963: The evolution of a moist convective element in a shallow, conditionally unstable atmosphere: a numerical calculation. J.atmos.Sci., 20, 407-424.

Priestley, C.H.B., 1953: Buoyant motion in a turbulent environment. Aust.J.Phys., 6, 279-290.

Richards, J.M., 1965: Puff motions in unstratified surroundings. J.Fluid Mech., 21, 97-106.

Riehl, H., 1954: Tropical meteorology. McGraw-Hill, New York, 392 pp.

Saunders, P.M., 1962: Penetrative convection in stably stratified fluids. Tellus, 14, 177-194.

Scorer, R.S., 1957: Experiments on convection of isolated masses of buoyant fluid. J.Fluid Mech., 2, 583-594.

Scorer, R.S. and F.H.Ludlam, 1953: Convection in the atmosphere. Quart.J.R.meteor.Soc., 79, 317-341.

Squires, P. and J.S.Turner, 1962: An entraining jet model for cumulo-nimbus updraughts. Tellus, 14, 422-434.

Stommel, H., 1947: Entrainment of air into a cumulus cloud. J.Meteor., 4, 91-94.

Stommel, H., 1951: Entrainment of air into a cumulus cloud II. J.Meteor., 8, 127-129.

Turner, J.S., 1957: Buoyant vortex rings. Proc.R.Soc., A 239, 61-75.

Turner, J.S., 1963: The motion of buoyant elements in turbulent surroundings. J.Fluid Mech., 16, 1-16.

Turner, J.S., 1963: Model experiments relating to thermals with increasing buoyancy. Quart.J.R.meteor.Soc., 89, 62-74.

Woodward, B , 1959: The motion in and around isolated thermals. Quart.J.R.meteor.Soc., 85, 144-151.

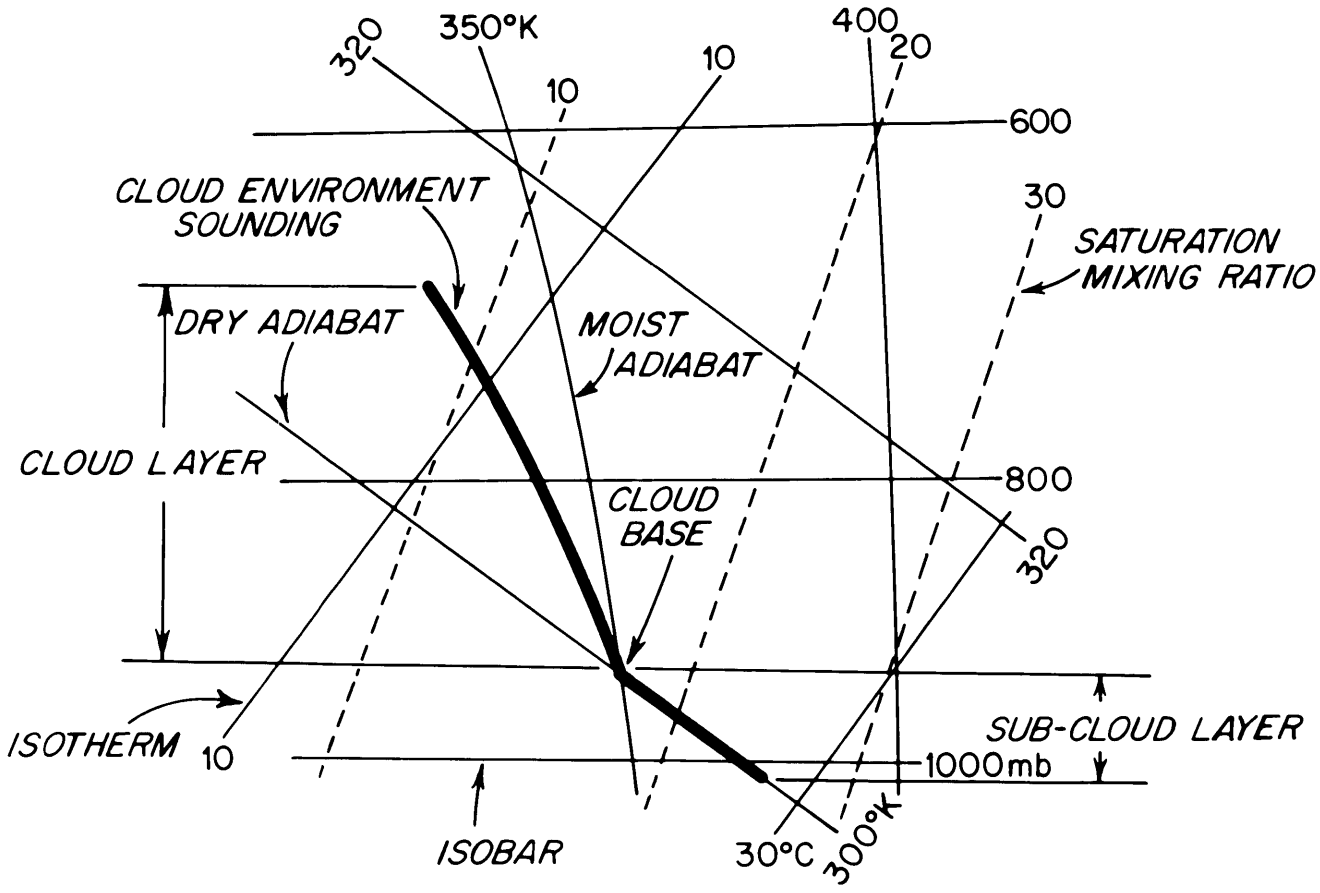


Figure 1. Schematic representation of environment sounding plotted on tephigram.

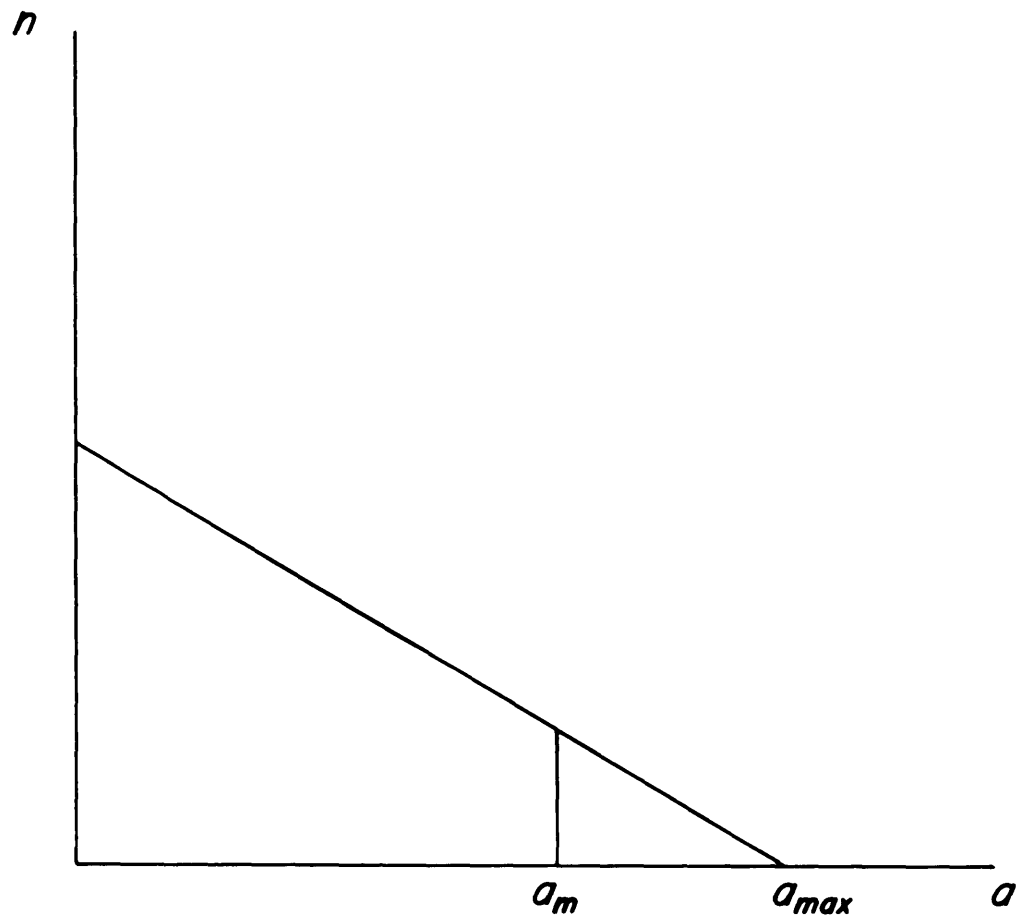


Figure 2. Model drop size distribution for collection efficiency computation.

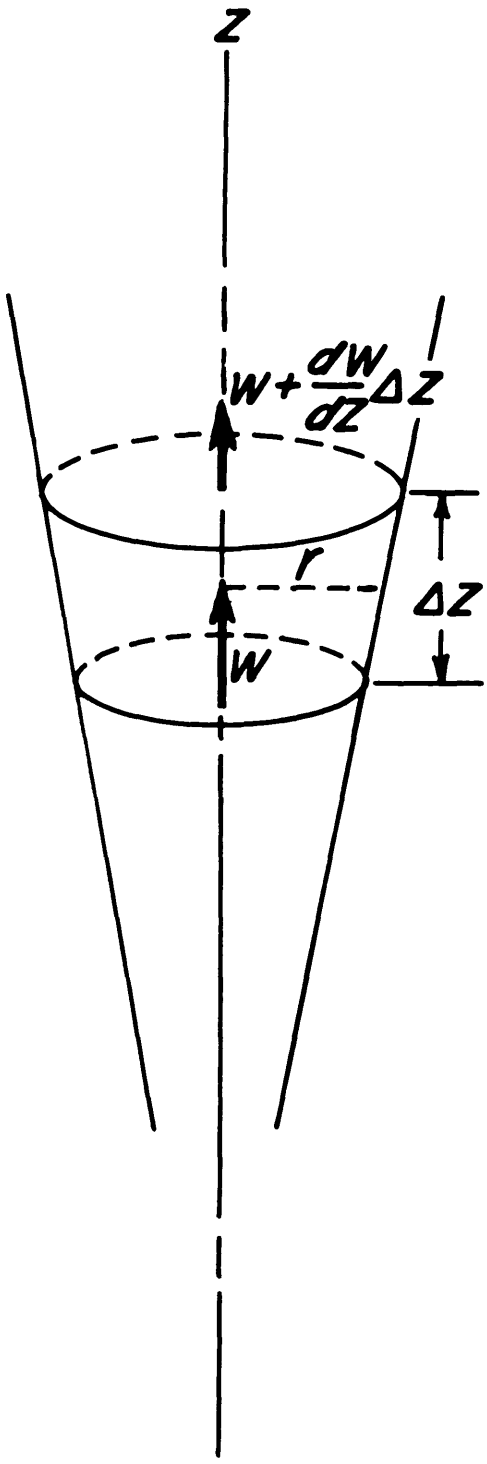


Figure 3. Diagram of starting plume showing cross-sectional element.
Arrows represent vertical velocity vectors of top and bottom surfaces.

PART III

AIRCRAFT OBSERVATIONS OF TRADE WIND CUMULUS AND THEIR INTERPRETATION

"It is probably undesirable to adopt the philosophy of one workman who was assigned the job of measuring a cable used in an underwater experiment. When asked if he had repeated the measurement as a check, he replied, 'Naw, if you measure it once, you know what you've got. If you measure it again and don't get the same answer, you don't know where you are.' " (E.Bright Wilson, Jr., 1952).

I. General description of aircraft instrumentation

The detailed observation of clouds from aircraft requires an elaborate instrument complex. During the years since the spring 1946 Wyman-Woodcock Expedition, the Woods Hole Oceanographic aircraft instrument system has undergone a gradual evolution from simple observation of dry- and wet-bulb temperature to its present capability of measuring vertical air velocity and liquid water content and time-lapse cloud photography. The addition of fast-response temperature and humidity instrumentation has also made possible observation of fine temperature and humidity detail in and around clouds.

The psychrograph, which records dry- and wet-bulb temperature on a Leeds and Northrup recorder, has thermistors with a response time of several seconds as the sensing elements. During field trips the psychrograph is operated almost continuously, since the paper speed is rather slow.

For resolution of detail on a smaller scale, for example during cloud runs, a recording oscillograph has been used. The oscillograph

has been used to record temperature, liquid water content, vertical acceleration, attitude, and air speed. (The last three are needed for computing vertical velocity.) The vertical velocity instrument system and reduction method is that developed by Bunker (1955) and is essentially the same as that used by Malkus (1954), except for addition of the attitude gyro.

2. The observational procedures and descriptive comments

There are two basic observational procedures, which may be followed in observing clouds from aircraft. One procedure developed by Malkus (1954) was dependent for its effectiveness largely on the degree to which a cloud could be characterized as a steady state jet. This consisted of picking a persistent reasonably well-isolated cloud while cruising at cloud-top height and then making passes through it at successively lower altitudes at intervals of 2000 feet. In addition Malkus used photographs from different angles to arrive at some sort of profile of the cloud shape.

The other procedure used in obtaining liquid water content data, summarized by Ackerman (1959), consisted of passes at various altitudes through a cloud field. The second technique is better adapted to a statistical study of transient cloud characteristics than the first.

The writer has used both modes of operation but has not succeeded in getting as exhaustive a study of one cloud as Malkus did. Nevertheless, all the data accumulated by the writer and his collaborators in the Caribbean is homogeneous in the sense that the observations were

made over a sub-tropical oceanic area. However, the data are not homogeneous in quality, since the aircraft instrument system, particularly the part for measuring cloud liquid water content, was being developed and modified between field trips. The liquid water content measurements were at least corrected for differences in instrument exposure. (See discussion of instrument exposure in Part I (pp.7 and 8.)) Therefore, although considerable information is contained in the data, the control of the data quality is not as good as one might desire.

The problem then becomes one of interpreting many observations from a single aircraft along straight lines through many clouds to arrive at the essential characteristics of the distribution of liquid water, temperature, and turbulent motion in space and time. To begin with, there are some general descriptive properties of these clouds that have become apparent to the author after seeing many records. Cloud base generally was confined to an altitude in the neighborhood of 600 m, which is consistent with the rather uniform sea surface temperature and saturation vapor pressure characteristic of sub-tropical oceanic areas. The temperature and liquid water content records at heights about two-thirds of the interval from cloud base to cloud top occasionally showed maximum values which were warm and rather flat-topped in profile (Figure 1). These temperature records usually showed fine-scale indentations in the flat-topped region, but the liquid water content records were usually flat-topped and smooth. This difference in detail between the temperature and liquid water content records is

undoubtedly due to the slower instrument response time of the latter. Intermediate between flat-topped and utterly irregular profiles (Figure 5) were some with "a hole in the middle", similar to those described by Ackerman (1959). (See Figures 2, 3 and 4). The flat-topped profiles and those with a "hole" were often embedded in very irregular regions of low liquid water content. (See Figures 3 and 4.) Also the irregular regions of low water content were generally cool compared to the clear air whereas the flat-topped regions were at least as warm as the clear air and certainly warmer than the cool cloud air.

The flat-topped profiles usually had sharp edges too, as also noted by Warner (1955). These profiles may have been the result of penetrations just below the cap of a bubble-like thermal. The sharp edges were probably due to sharp temperature gradients that tend to develop kinematically in the flow field at the cap of the thermal. The holes may be penetrations far enough below the cap to have indications of a hollow intrusion from below of environment air. However the one-dimensional nature of a cloud pass makes it practically impossible to draw conclusions concerning the vertical structure and extent of such thermals.

3. Statistical analysis of cloud records

Since it is impossible to penetrate the same thermal at different altitudes with only one aircraft, the performance of an atmospheric experiment analogous to a tank experiment is impossible.

Furthermore, it has been found difficult to define a unique environment sounding for a given cloud. Therefore a more statistical approach to the problem has been adopted.

Two examples of cloud-line observations were selected for lag autocorrelation and correlation analysis of the physical variables such as temperature, vertical velocity, and liquid water content. Only five records were selected for such analysis because of the large amount of labor involved in transferring the analogue record information to punched cards. The lag autocorrelation was intended to show if any dominant scale of lumpiness existed and how it compared with the sub-cloud layer depth. The correlation analysis was meant to show the cross-correlation of the physical variables as objective evidence that the more energetic and denser parts of the cloud were indeed driven by buoyancy forces.

The two cases selected for analysis were penetrations of cloud lines on two different field trips. The first case was a series of three passes through the top, middle, and just above cloud base across a cloud line. The passes were made by Mr. Bunker, who was kind enough to take an early model of the hot wire cloud instrument on his field trip. This series was selected because Mr. Bunker's turbulence equipment was working well along with the cloud instrument. However, the temperature records were not too good since they were made with a thermopile instrument that seemed to be affected excessively by wetting from the cloud. During the next field trip made by Mr. Bunker, on which the writer also came along, an early model of the precipitation instrument

as well as the cloud instrument was used. Also a new fast-response platinum resistance thermometer was used for the first time, but unfortunately a modified version of the turbulence system did not work. However, two passes were made along the cloud line at two levels, one near cloud top and the other somewhat lower. Although made during a different field trip, they supplemented the first case very nicely.

The deviations from clear environment temperature in Run #3349 at 10,000 feet were generally negative. One of the cloud elements had a square-topped liquid water content record about 180 meters in diameter with an irregular temperature record low relative to its environment, which indicated inertial overshoot of the element and also possibly mixing with dry air. (See Figure 5 for run with indication of inertial overshoot.) The deviations from clear environment temperature on Run #3350 at 7000 feet were in general positive and positively correlated with the liquid water records. Run #2940 at 7000 feet had a broad updraft about 800 meters wide with a peak vertical velocity of 12.2 m/sec. Part of the updraft was cool and most of the record was irregular (not square-topped). Near the entrance edge of the updraft there was a square-topped segment of temperature and liquid water content record about 200 meters wide. Thus the foregoing updraft was not itself an example of a square-topped feature but appeared to have one embedded in it.

Run #2942 at 4000 feet did not have any outstanding features. Run #2943 at 2500 feet just above cloud base had an extensive weak cloud on one side of the main cloud body and two small outlying clouds on the

other side with distinctly square-topped record profiles. A schematic diagram of the structure of the above cloud line runs showing distinctive features is given in Figure 6. The relative positions of the cloud runs are extremely uncertain, but the writer has placed them subjectively in reasonable positions.

In general the small clouds (about 100 to 300 meters in diameter near cloud-base level) have been found to have square-topped record profiles more often than those at higher levels. The higher frequency of square-topped cloud features at lower levels may be a combined consequence of greater density of buoyant elements near cloud base and the smaller probability of aircraft penetration of faster-moving elements at higher levels.

The lag autocorrelation analyses presented in Figures 7, 8, 9, 10, 11, and 12 were meant to show objectively the horizontal scale of structure in cumulus convection. These analyses were made of time series extending from first cloud penetration to last exit into clear air as shown in Figure 6.

Some feeling for the relation of scale and shape to the autocorrelation coefficient as a function of lag time may be obtained from Figure 13 in which the results of analysis of an artificial periodic square wave function with a period of 5 seconds and with square tops of 2½ seconds' duration are shown. If several square tops of 2½ seconds' duration - equivalent to a 150 meter space scale - were spaced irregularly, then the autocorrelation function would probably go in

roughly a straight line from 1 to near zero at about 5 seconds. The residual larger scale would probably be related to the over-all size of the group of square tops.

The autocorrelation analyses of the runs along a cloud line, shown in Figures 11 and 12, have the most distinct evidence of a dominant scale size. Their oscillatory character is nearly periodic in nature. The distance from the zero point to the first minimum in Figure 12 corresponding to a run at 7000 feet, is obviously smaller than in Figure 11 corresponding to a run at 10,000 feet. Therefore there is obvious evidence of an increase of scale with altitude in these two analyses. The distances from the zero point to the first minimum or first distinct change in slope are plotted in Figure 18 superimposed on the theoretical graph of bubble radius versus altitude. There is an obvious trend toward larger scale size with increasing altitude, starting with the smallest scale found in the sub-cloud layer. The cross cloud line runs represented by triangles have a systematically larger scale than the runs along the cloud line represented by circles. This difference may possibly be due to the greater probability of encountering active compact thermals in runs along than across a cloud line. The features encountered in the cross cloud line run therefore may have been somewhat diffused in scale.

The cross-correlation analyses are given in Table 1 with other pertinent information. The cloud-temperature and cloud-vertical velocity correlations are all positive up to the 7000-foot level. The cloud-temperature correlation at 10,000 feet is decidedly negative, indicating

either inertial overshoot or mixing with dry air. If vertical velocity data had been available for this run, it would undoubtedly have been positively correlated with vertical velocity (see Figure 5, for example).

In addition a histogram analysis of all the available Caribbean cloud data was made. The analysis is an extension of Ackerman's (1959) method of statistical summary of liquid water content data gathered with the U.S.Weather Bureau aircraft. The horizontal extent of unbroken cloud and average and maximum values of cloud liquid water over each unbroken cloud interval along with corresponding values of the volume median drop diameter were read from each cloud record. The average and maximum deviation from the cloud environment temperature and vertical velocity were also read.

The class interval structure of the histogram analysis is as follows. First, a rough classification was made of the cloud runs based on the approximate maximum cloud top height observed in the area of operation (roughly within a radius of 20 km). Four maximum cloud-top height intervals were chosen to split the data into reasonably large samples. Classification in this way presumably stratifies the data according to a criterion possibly related to large-scale subsidence (Riehl, 1954, p.378). The horizontal unbroken cloud extent and corresponding average and maximum values of deviation from clear environment temperature and vertical velocity were tabulated for each run. The same procedure was followed for the average and maximum cloud liquid water and corresponding volume median drop diameters. (Table 2 is

a sample from this tabulation corresponding to the cloud lines discussed earlier.) All this information was put on punched cards, and a computer was used to construct frequency tables according to a convenient grouping scheme. Bar graphs of the medians, 80th percentiles, and extremes as a function of altitude were derived from the frequency tables and are given in Figures 13, 14, and 15. The numbered altitudes in these figures represent the class limits of cloud run heights.

The writer intended that the cloud extent statistics, as given in Figures 14, 15, and 16, yield objective information concerning the prevalent dimensions of the residual cool cloud of a cloud system. Cloud lines and clusters give a subjective impression of relatively large flat bases and small tops. Also the maximum horizontal dimensions of clouds appear to vary directly as the maximum prevalent cloud top height. The cloud extent statistics of Figure 14 as compared with those of Figures 15 and 16 certainly confirm the latter impression, and there is even some slight indication of trend toward larger size in going from Figure 15 to 16. The large extremes in these two figures are probably the consequence of including a few runs along cloud lines. Their medians and 80th percentiles do not show any distinct trend with altitude. However, large flat bases may be obscured by inability to define cloud boundaries exactly at low liquid water contents prevalent near cloud base, or they may be more apparent than real because of the superposition of a large number of smaller cloud masses on each other in the line of sight.

The statistical distributions of average and maximum values

of the physical cloud variables given in Figures 14, 15, and 16 were intended to demonstrate the applicability of the bubble model to compact buoyant cloud masses and the existence of the relatively less energetic more extensive turbulent cool cloud matrix. The relatively low values of the medians as compared to the 80th percentiles and the extremes are indicative of the higher probability of encountering relatively cool and low density cloud material with relatively low levels of turbulent kinetic energy. The higher probability is in turn indicative of the greater extent in space and time of cool cloud matrix.

If individual thermals whether they are transient jet- or bubble-like buoyant elements grow and lose their buoyancy shortly after breaking into clear air and then diffuse in the cloud layer, the average and maximum values of the physical variables provide a measure of the buoyant activity of the cloud. Also if a given cloud segment is in its most active state in a given cloud pass at a given level, the average and maximum values of the physical variables should be larger than those of any other cloud pass at that level. Therefore the largest values of the average and maximum at a given level provides an estimate of the upper and lower bound of the temperature excess, vertical velocity excess, or liquid water content of the most active buoyant element. The maximum average and maximum values as a function of altitude can be compared to the values predicted by a model of an active thermal. The motivation for the above analysis is not the literal detailed verification of the validity of a given model, but the investigation of how well a simple model can reproduce the statistical behavior of clouds

and what mixing parameter values are appropriate.

4. Fitting of the bubble model to the cloud data

If maximum cloud top height is an index of subsidence intensity (Riehl, 1954, p.378), then the occurrence of small shallow clouds may be inferred to be a consequence of strong local subsidence. Some of the shallow clouds penetrated by Bunker in February, 1958, appeared to have square-topped and warm records about 100 to 300 meters in diameter. Most of the shallow clouds, however, were cool and irregular and penetrated to a height about 600 meters above cloud-base level. Therefore in what may be called suppressed conditions, the individual clouds are usually either bubble-like elements or their larger dissipating residues. The larger cloud systems such as cloud lines or cloud clusters, which may penetrate to levels as high as 20,000 feet, may be more appropriately represented as groups of buoyant elements immersed in a relatively cool dissipating cloud matrix containing less liquid water.

In terms of the large scale features or average soundings, the cloud layer has been viewed as a static conditionally unstable layer capped by an inversion with drier air above (Bunker, Haurwitz, Malkus and Stommel, 1949). Actually in August, 1963, particularly in the neighborhood of Barbados the trade-wind inversion was absent and the cloud layer was merely capped by very dry air. Wexler and Malkus (1958) noted that individual aircraft soundings of temperature and dewpoint do not indicate any clear relation to the type of cloud regime, whether it is relatively suppressed or disturbed. The writer also has found

that the stability evaluated from a single aircraft sounding varies greatly from place to place in a given area and from time to time during a given day. Therefore the soundings made in August 29, 1963 (one by the Woods Hole aircraft, two by the CRAWFORD, and one by Seawell airport on one day over a period from 8:00 A.M. to 8:00 P.M.) were plotted on the same chart. The envelope of all the observations for the one day are given in Figure 17, as the shaded area between two zig-zag lines connecting the observations at the edges of the fluctuation band. For purposes of comparison average soundings are also given in Figure 17. (Jordan, 1957, and Garstang, 1965, private communication.)

Cloud base was at about 600 m, and maximum cloud top on this day was about 3000 m. The separation of temperature and dewpoint shows that apparently none of the soundings went through cloud. The breadth of the cloud-layer temperature fluctuation band is considerably greater than that of the sub-cloud layer. The band of the dewpoint is considerably wider than that of the temperature. The fluctuation bands are about 1^{o} wide, 3^{o} wide, and 10^{o} wide for the sub-cloud layer temperature and dewpoint, the cloud layer temperature, and cloud layer dewpoint, respectively. The width of the sub-cloud layer band may possibly be due to instrumental error but the fluctuation bands of the cloud layer are well beyond any conceivable error. These fluctuations must be due to mesoscale circulations or gravitational waves. Thus the cloud layer is by no means the static environment postulated in cloud models or numerical experiments.

Since the cloud statistics given in Figures 14, 15 and 16 are a composite derived from several field trips and individual soundings are so variable, the August San Juan average sounding which in the cloud layer lies well within the fluctuation band was selected as typical of the area to compute bubble-model constants. The average values of these constants were found to be $\gamma_1 = 4.7 \times 10^{-8}$, $\gamma_2 = 2.3 \times 10^{-8}$, and $\gamma_3 = 3.3 \times 10^{-8}$ cm^{-1}. The microphysical parameter γ_p was computed by equation (54) of Part II from the 80th percentile values of liquid water content, volume median drop size, and vertical velocity summarized in Figures 15 and 16. The maximum value of γ_p with $r_o = 100$ m and for $k_e = k_d = .5$ was $1.3 \times 10^{-8} cm^{-1}$. The maximum value of γ_p found for $k_d = 0$ and $k_e = .5$ with $r_o = 100$ m was $4.7 \times 10^{-9} cm^{-1}$. These values of γ_p were used in bubble model computations and compared with computations for $\gamma_p = 0$. The results differed appreciably. The extremes of the bubble model computations for $k_e = .75$ with upper and lower limits of $r_o = 100$ and 300 m, respectively, including the above extremes of γ_p are given in Figure 18.

The means of average and maximum values of the extremes presented in Figures 14, 15, and 16 are superimposed on the theoretical bubble model curves given in Figure 18 with the exception of one extremely large value of the liquid water. This one point, which is way out of line with the others, is the direct result of one cloud run made off the northwestern tip of the island of Puerto Rico on the way home from the August 1963 field trip to Barbados. This one anomalous

observation can make physical sense only in terms of a large storage of water by repeated updrafts in the same region combined with the effect of precipitation from above. We may be justified in excluding this one point, because the observation was made in the lee of a large land mass.

In interpreting the results summarized in Figure 18 we must keep in mind the uncertainties introduced by the limited control of accuracy in the data. The volume median drop size determination is uncertain by $\pm$ 29%. The corresponding uncertainty in liquid water content read from the cloud instrument calibration for a size of 100 microns is $\pm$ 12 %. The uncertainty in the calibration itself is $\pm$ 12 % so that we may estimate the total uncertainty as $\pm$ 24 %. The uncertainty in the temperature is largely due to the unmeasured altitude fluctuation, which can be as much as $\pm$ 100 m in a cloud run. The corresponding temperature fluctuation is approximately $\pm$ .6^{o}C. The accuracy of the vertical velocity determination as estimated by Bunker (1953) is $\pm$ 16 cm sec^{-1}. Telford and Warner (1962) have considered this estimate to be unduly optimistic, because of the uncertainty introduced by the attitude gyroscope's drift correction mechanism. Bunker estimated the gyroscope attitude accuracy at $\pm$ .11 degree. A more realistic estimate under flight conditions might be $\pm$ .4 degree. The vertical velocity determination might then be at most accurate to $\pm$ 50 cm sec^{-1}.

The scale sizes from the autocorrelation analyses, as given in Figure 18, appear to favor an expanding scale with altitude. The superadiabatic values of liquid water near cloud base altitude may reasonably be attributed to precipitation. The liquid water at higher

altitudes favors within the accuracy estimated above the bubble model with k_d much less than k_e. The temperature data is at least not inconsistent with the evidence so far presented. The vertical velocity, however, is much too large to be consistent with the other data. The excess value can only be accounted for if buoyant masses rise through the cool cloud matrix frequently enough to impart an average upward velocity to it as high as 4 or 5 m sec^{-1} near cloud top.

5. Estimate of collection efficiency parameter.

The extreme values of volume median drop size and vertical velocity given in Figures 15 and 16 may be used to make a rough estimate of collection efficiency E. The values of u_2 , u_1 , and m_2 may be computed from the above drop size with the simple model drop size distribution given in Part II. The value of $\frac{dm_2}{dz}$ was estimated by dividing m_2 by its corresponding altitude above cloud base. The values of E corresponding to the data contained in Figures 15 and 16 obtained by substitution in equation (60) of the computed numbers yielded values of 1.1 and .7, respectively.

6. Summation

The above observational study has yielded definite evidence that parts of a cloud system such as a line or a cluster are indeed driven by buoyancy forces. The existence of inertial over-shoot at maximum cloud top height has also been established. The accumulated observational

experience has furthermore yielded descriptive information, which suggests the existence of bubble-like thermals with sharp temperature and liquid water gradients possibly associated with the kinematics of the flow field at the top of the thermal. The cool cloud regions have been correlated with relatively low liquid water content.

The autocorrelation analyses have yielded evidence of increasing scale with altitude, which coupled with evidence derived from the histogram analyses implies that the laboratory value of the entrainment parameter may be extended to cumulus clouds. The observed vertical velocities, which are large compared to the theoretical values, suggest that the buoyant portions may induce upward motions in the cool cloud matrix.

In addition to the above factual information, apparently profitable statistical approaches to the problem of rationalizing the dynamics of cumulus convection have been suggested. The use of autocorrelation analysis to establish scale implies logically the application of spectrum analysis. The comparison of the sub-cloud layer spectrum with that of the cloud layer could possibly yield objective information concerning the scale range which is transferred to and amplified in cumulus clouds. Histogram analysis of large amounts of data with better and more accurate instruments may be used to refine the bubble-model representation and to study the large scale heat, water, and momentum balance of the cloud layer. The possibility of relating cloud microphysics to dynamics has been explored.

The results of the above observational pilot study and its relation to existing theoretical analysis constitute, in the author's eyes, sufficient motivation for improving aircraft instrumentation and conducting more extensive observational aircraft operations. The possibility of parametric representation of the effect of clouds on the large-scale wind field should appeal to individuals interested in the dynamics of the trades and hurricanes. For people with more practical and operational inclinations, the use of aircraft in observations over the oceans combined with satellite observations should have considerable appeal.

References

Ackerman, B., 1959: The variability of the water contents of tropical cumuli. J.Meteor., 16, 191-198.

Bunker, A.F., 1953: Investigations into a method of shearing stress determinations from an airplane in flight. Woods Hole Oceanographic Institution, unpublished manuscript, reference number 53-52.

Bunker, A.F., 1955: Turbulence and shearing stresses measured over the North Atlantic Ocean by an airplane-acceleration technique. J.Meteor., 12, 445-455.

Bunker, A.F., B. Haurwitz, J.S.Malkus, and H.Stommel, 1949: Vertical distribution of temperature and humidity over the Caribbean Sea. Pap.phys.Ocean.and Meteor., Mass.Inst.Tech. and Woods Hole Ocean.Inst., 11, 1, 82 pp.

Jordan, C.L., 1957: A mean atmosphere for the West Indies area. National Hurricane Research Project, preprint series number 6.

Malkus, J.S., 1954: Some results of a trade-cumulus cloud investigation. J.Meteor., 11, 220-237.

Riehl, H., 1954: Tropical meteorology. McGraw Hill, New York, 392 pp.

Telford, J.W. and J.Warner, 1962: On the measurement from an aircraft of buoyancy and vertical air velocity in cloud. J.atmos.Sci., 19, 415-423.

Wexler, R. and J.S.Malkus, 1958: Tropical meteorology. Observational studies of tropical clouds: results of 1956 Caribbean aircraft expedition. Woods Hole Ocean.Inst.,Woods Hole, Mass. Unpublished manuscript, reference number 58-46.

Wilson, E.B.,Jr., 1952: An introduction to scientific research. McGraw-Hill, New York, 375 pp.

Table 1

Cloud line data

Date	Record number	Altitude feet	Correlation coefficient cloud-liq. water vert.vel.	cloud-liq. water temp.
2/24/58	2940	7,000	.730	
	2942	4,000	.184	
	2943	2,500	.320	
11/16/59	3349	10,000		-.455
	3350	7,000		.434

Table 2

Date	Record number	Cloud dist. km.	Altitude feet	Type of statistic	Cloud liquid water gm/m^3	Vol. median drop diam. microns	Temp. diff. from env. °C	Vert. vel. m/sec.	
2/24/58	2940	1.4	7000	Avg.	0.3	-	-	-0.3	
				Max.	0.7	-	-	+4.8	
		2.3		Avg.	0.7	-	-	+3.7	
				Max.	1.2	-	-	+12.2	
2/24/58	2942	4.7	4000	Avg.	0.3	-	-	-0.4	
				Max.	0.8	-	-	+3.0	
2/24/58	2943	2.1	2500	Avg.	0.3	≤ 30	-	+0.7	
				Max.	0.4	≤ 30	-	+2.4	
		.2		Avg.			-	+0.7	
				Max.			-	+1.6	
		.3		Avg.			-	+1.5	
				Max.			-	+2.8	
2/24/58		3.2	1600	Avg.	Probably		-	-0.2	Under cloud
				Max.	precipitation		-	+1.7	base
11/16/59	3349	.2	10,000	Avg.	1.0	117	-.7	-	
				Max.	1.2	97	-.4	-	
				Avg.	1.1	150	-.8	-	
				Max.	1.9	92	-.1	-	
				Avg.			-.4	-	
				Max.			-.15	-	
	3350	.4	7000	Avg.	0.1?	84	0	-	
				Max.	0.1?	84	-.15	-	
		3.1		Avg.	0.3?	238	+.1	-	
				Max.	0.3?	230	+.4	-	
		.1		Avg.	0.5	92	+.2	-	
				Max.	0.7	81	+.8	-	
		.1		Avg.	0.1	84	+.1	-	
				Max.	0.2	84	+.25	-	
		.3		Avg.	0.1	60	+.1	-	
				Max.	0.1	72	+.25	-	
		.3		Avg.	1.3	199	+.2	-	
				Max.	1.7	74	+.65	-	
		.1		Avg.	0.8	88	+.4	-	
				Max.	1.4	78	+1.0	-	
		.3		Avg.	1.1	70	+.5	-	
				Max.	2.2	58	+1.1	-	
		1.0	~~7000~~	Avg.	0.7	100	0	-	
				Max.	1.5	76	0.6	-	

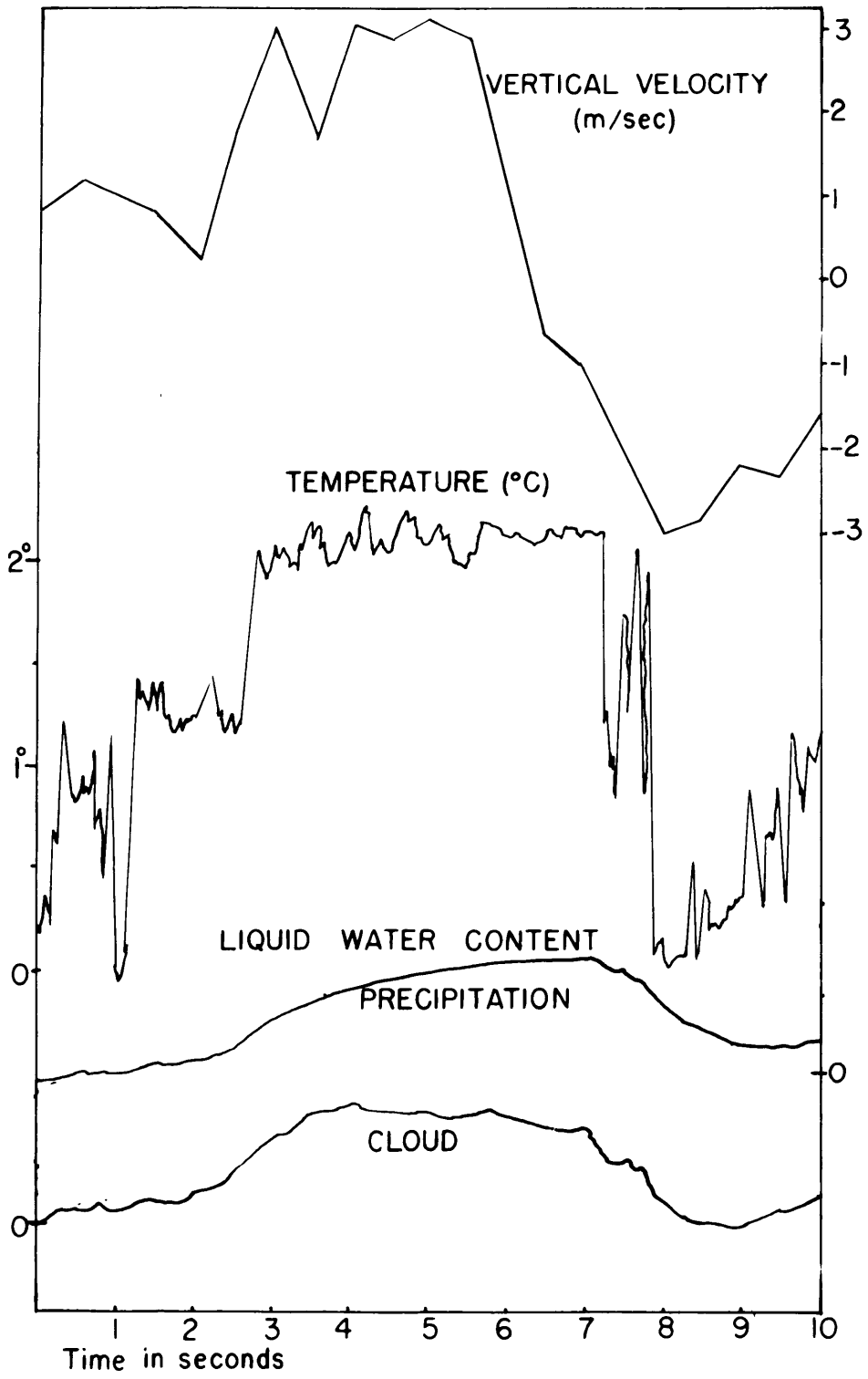


Figure 1. Example of flat-topped temperature and liquid water record profiles. Run number 4123, May 28, 1962, at 6100 feet.

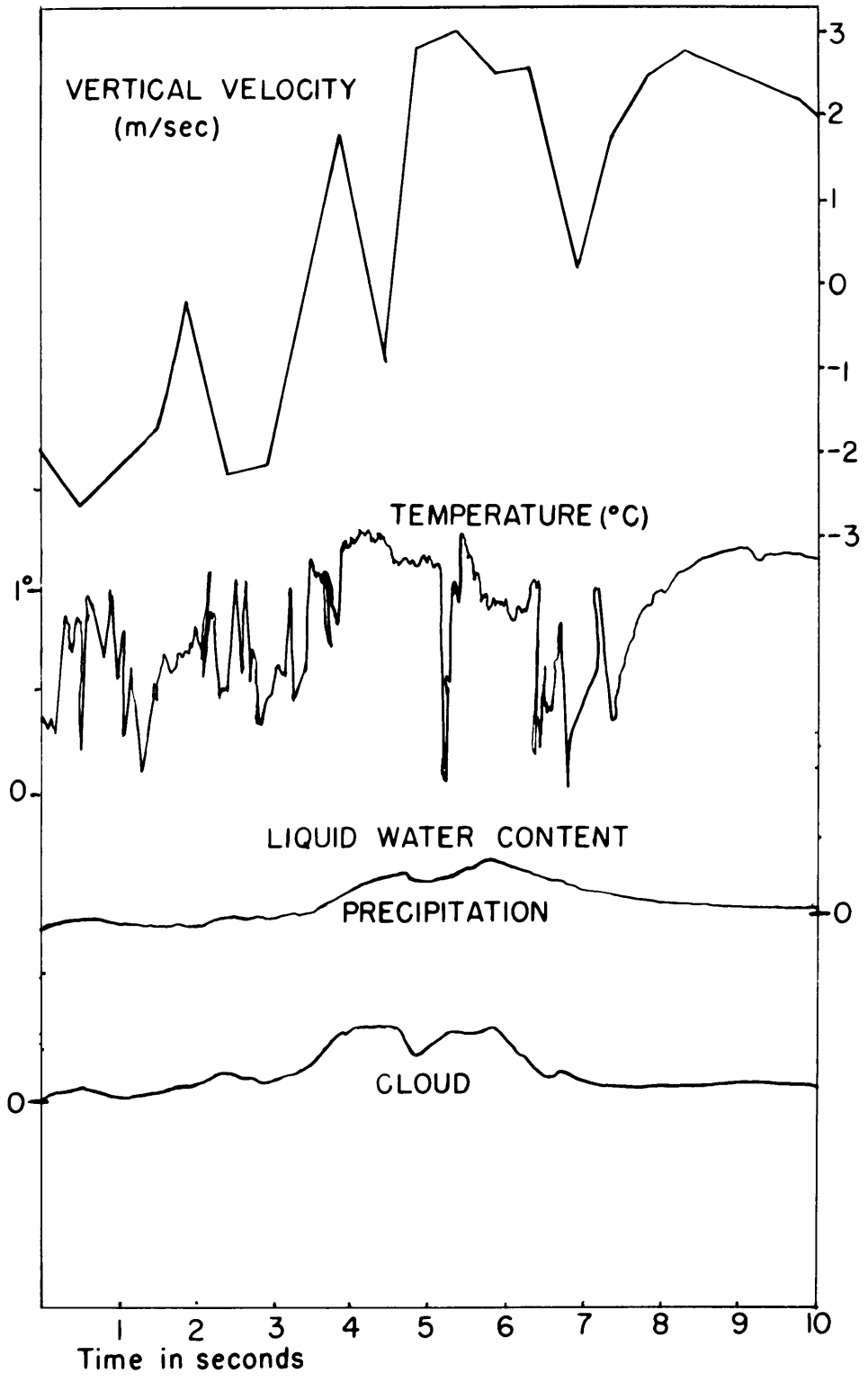


Figure 2. Example of temperature and liquid water record profiles with "hole in the middle". Run number 4107, May 27, 1962, at 6200 feet.

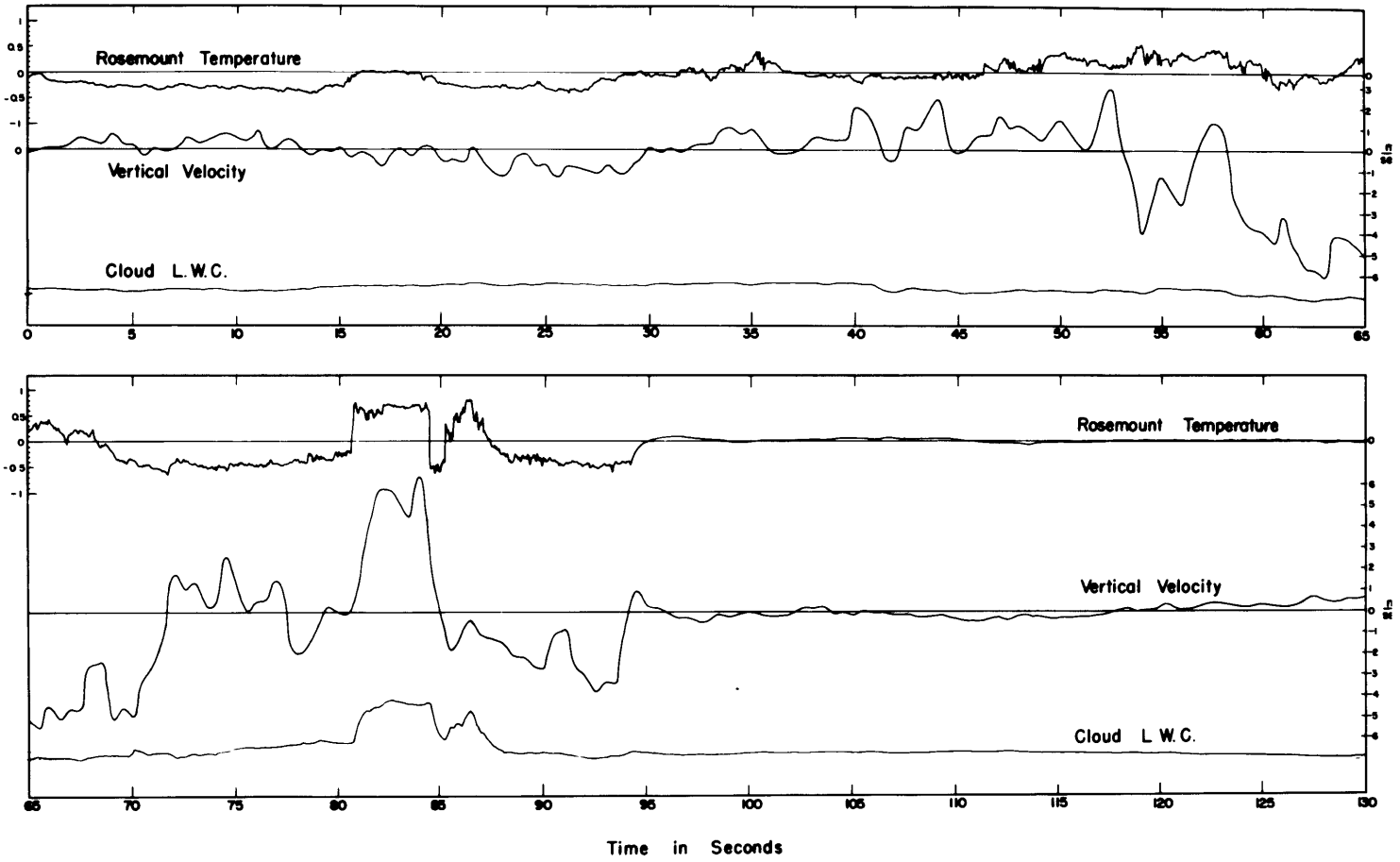


Figure 3. A complete cloud run which contains a relatively warm flat-topped record of relatively high liquid water content with "hole on the side" immersed in less dense cool cloud at 6000 feet.

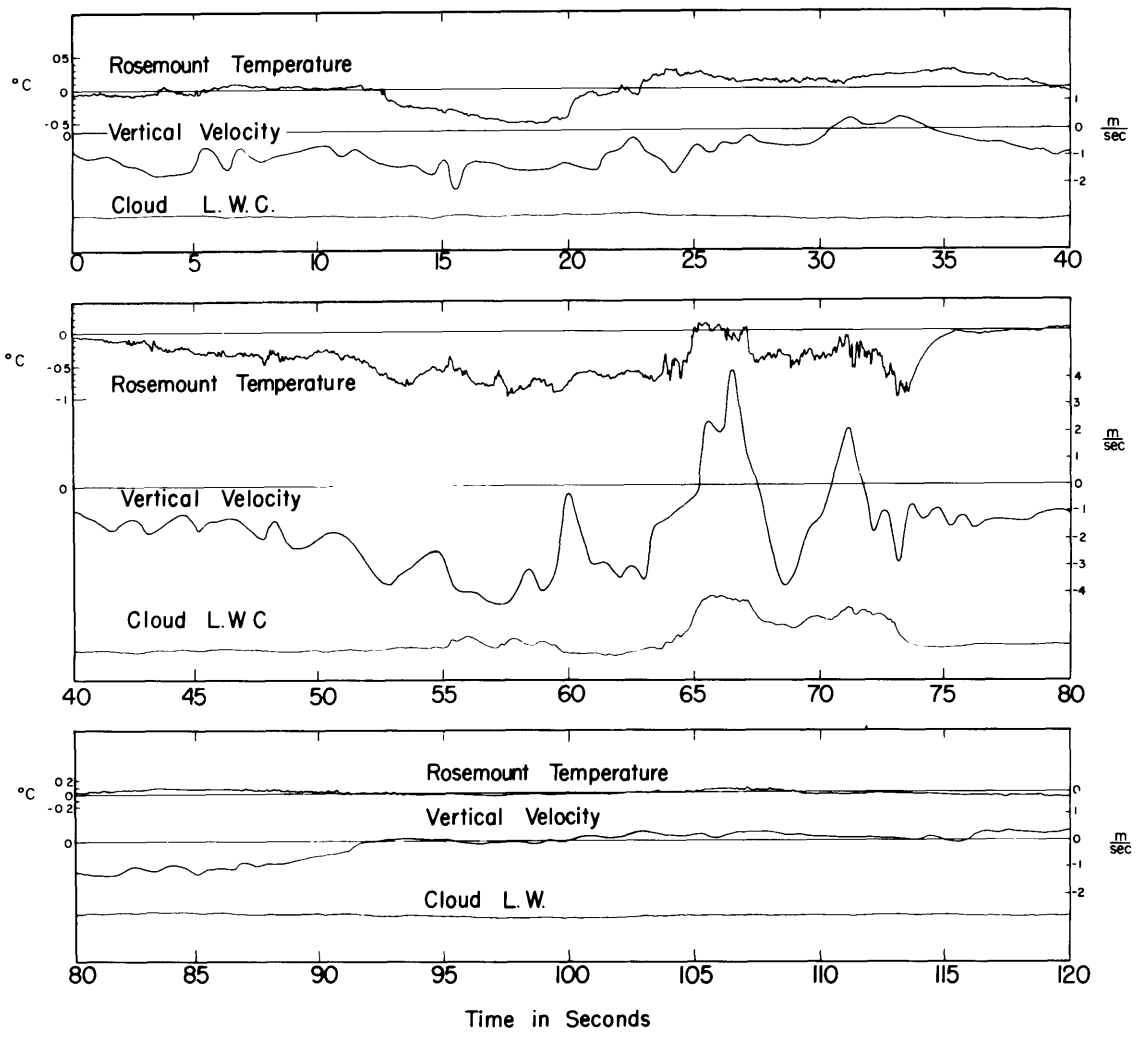


Figure 4. A complete cloud run which contains a relatively warm, somewhat irregular flat-topped record with a large "hole in the middle" and two vertical velocity peaks immersed in less dense cool cloud at 7400 feet. The double velocity peak might be indicative of two separate thermals near each other.

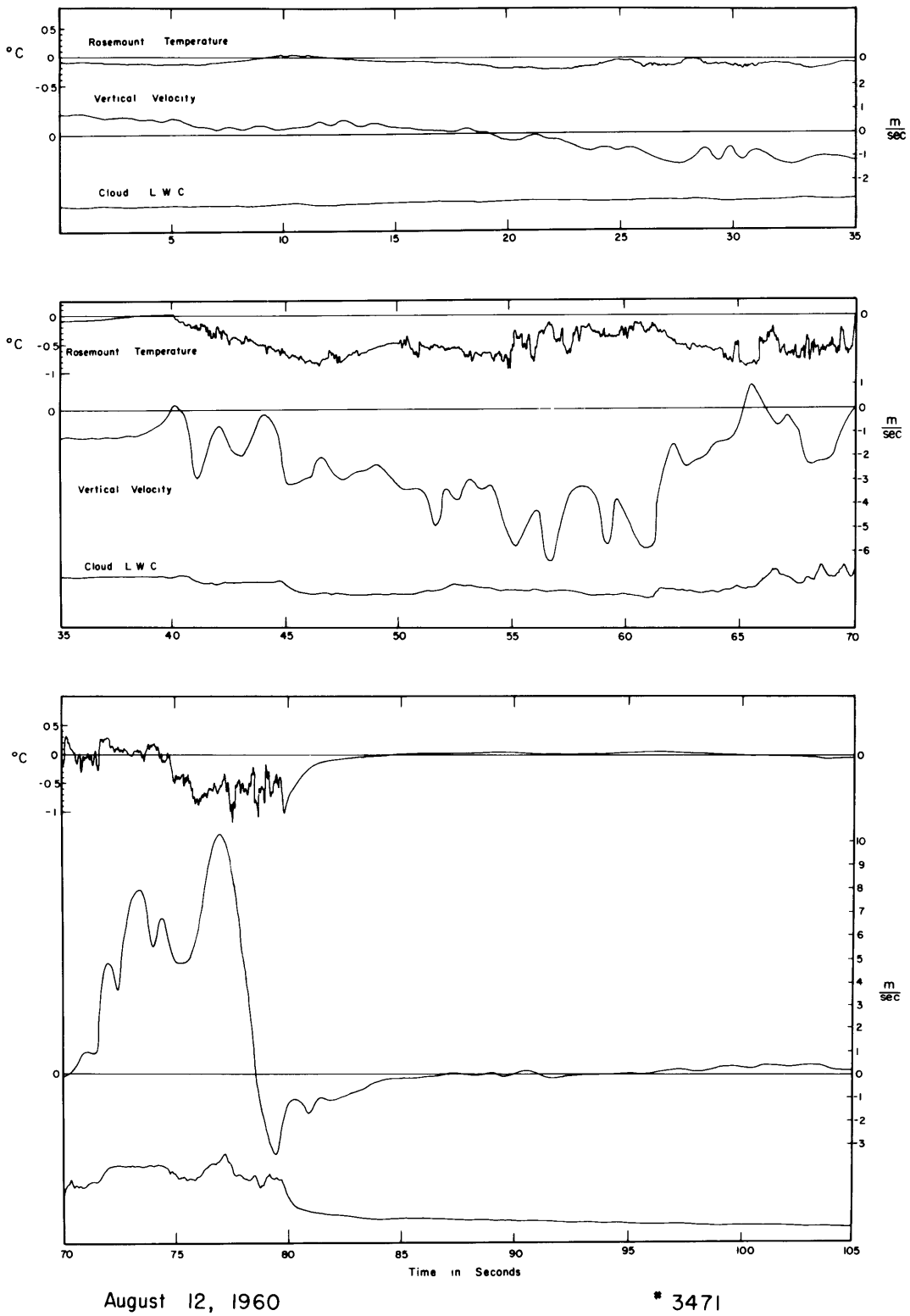


Figure 5. A complete cloud run containing an irregular cool updraft indicative of inertial overshoot made at 9900 feet.

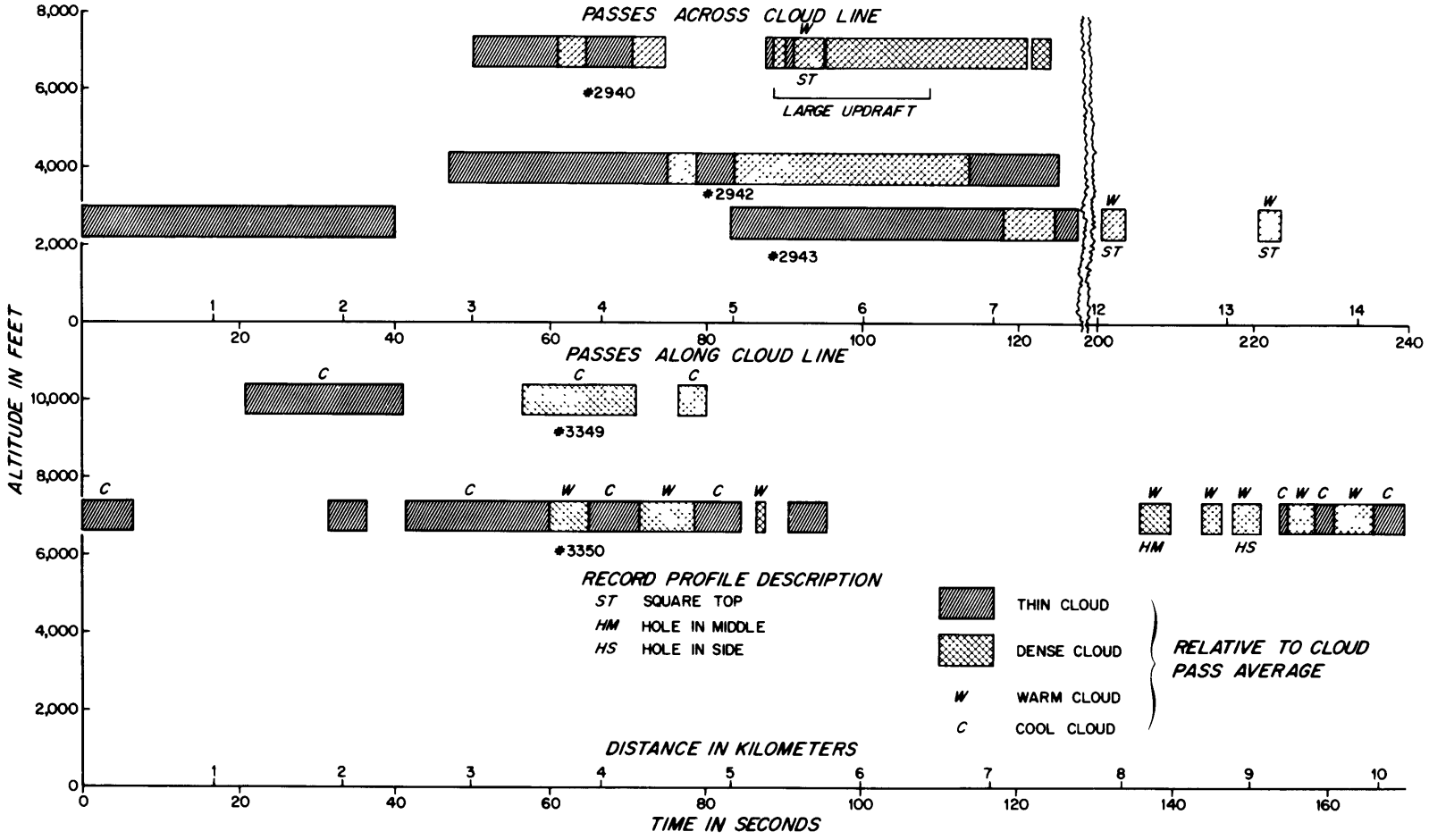


Figure 6. Diagram of principal features of cloud line runs selected for autocorrelation and correlation analysis. Relative horizontal positions of runs are very inexact.

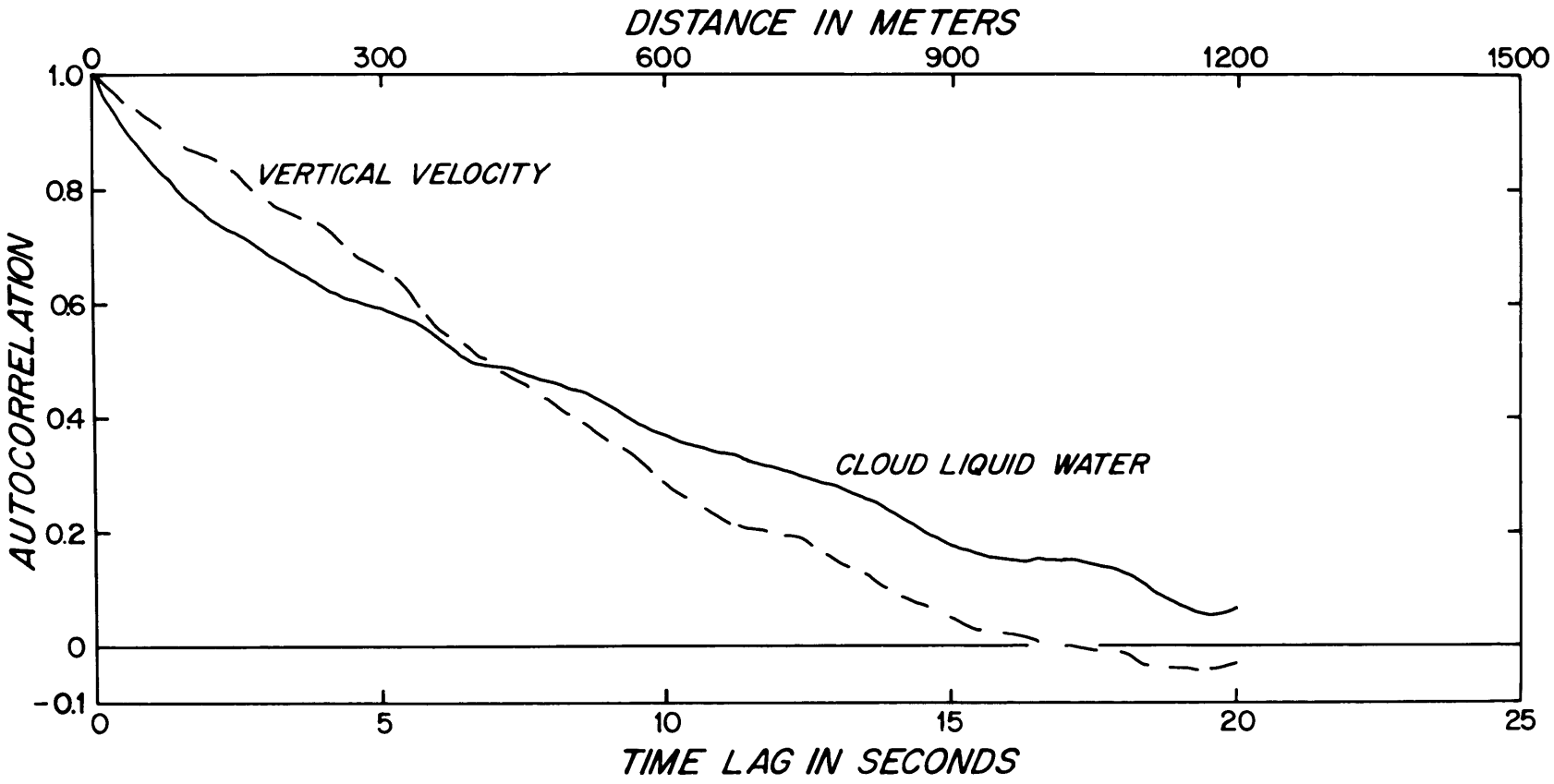


Figure 7. Autocorrelation analysis of cloud run #2940 across a cloud line, February 24, 1958, at 7000 feet.

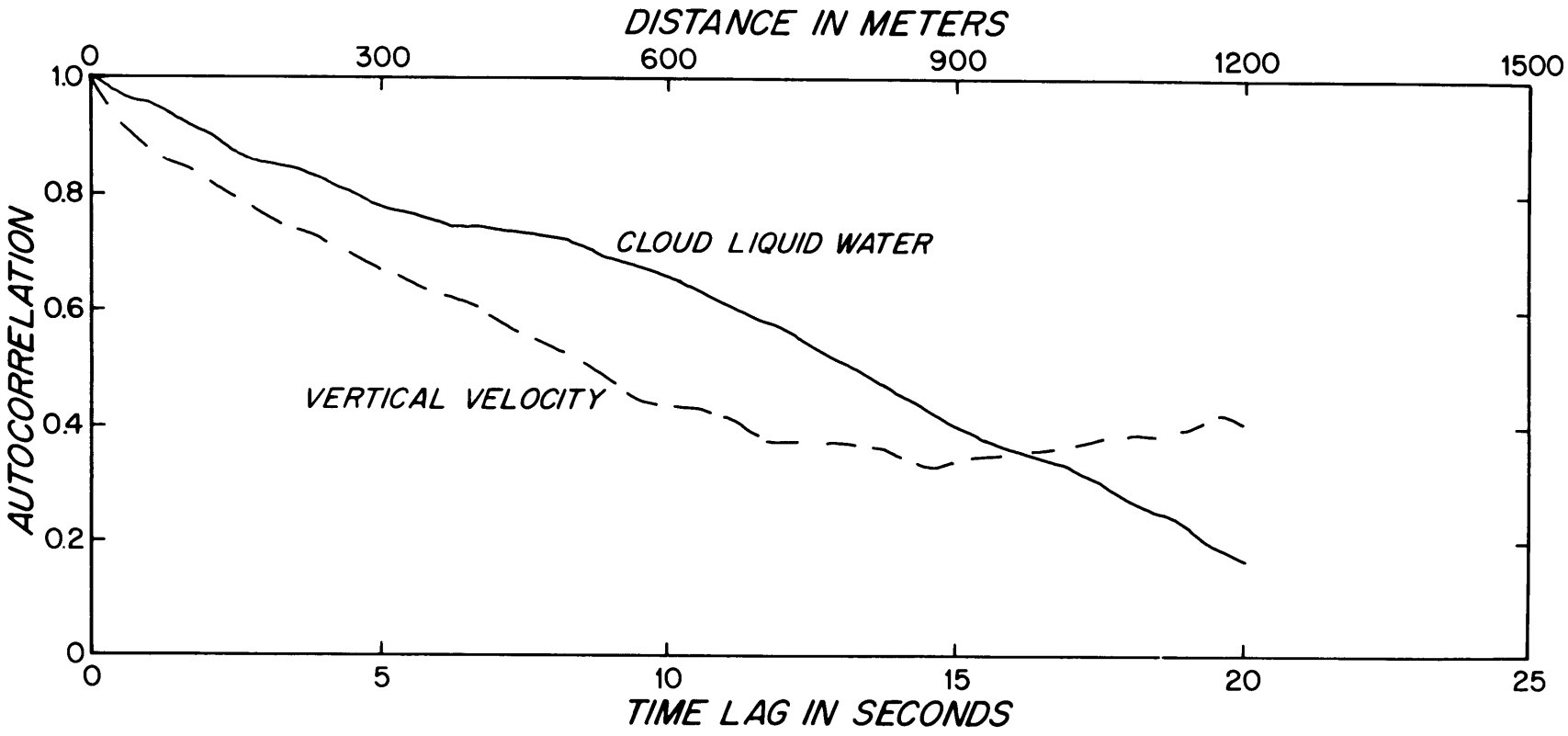


Figure 8. Autocorrelation analysis of cloud run #2942 across same cloud line as in Figure 7, February 24, 1958, at 4000 feet.

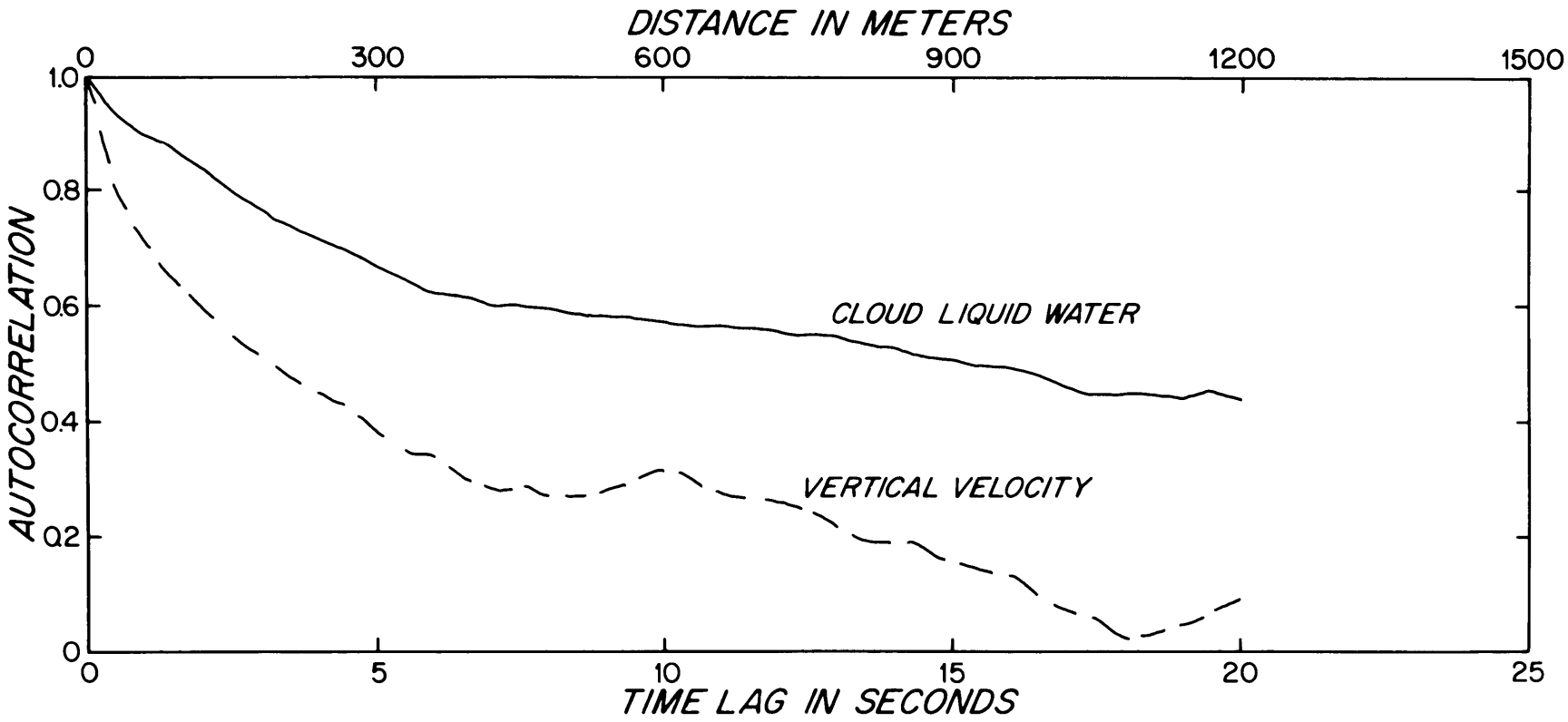


Figure 9. Autocorrelation analysis of cloud run #2943 across same cloud line as in Figure 7, February 24, 1958, at 2500 feet.

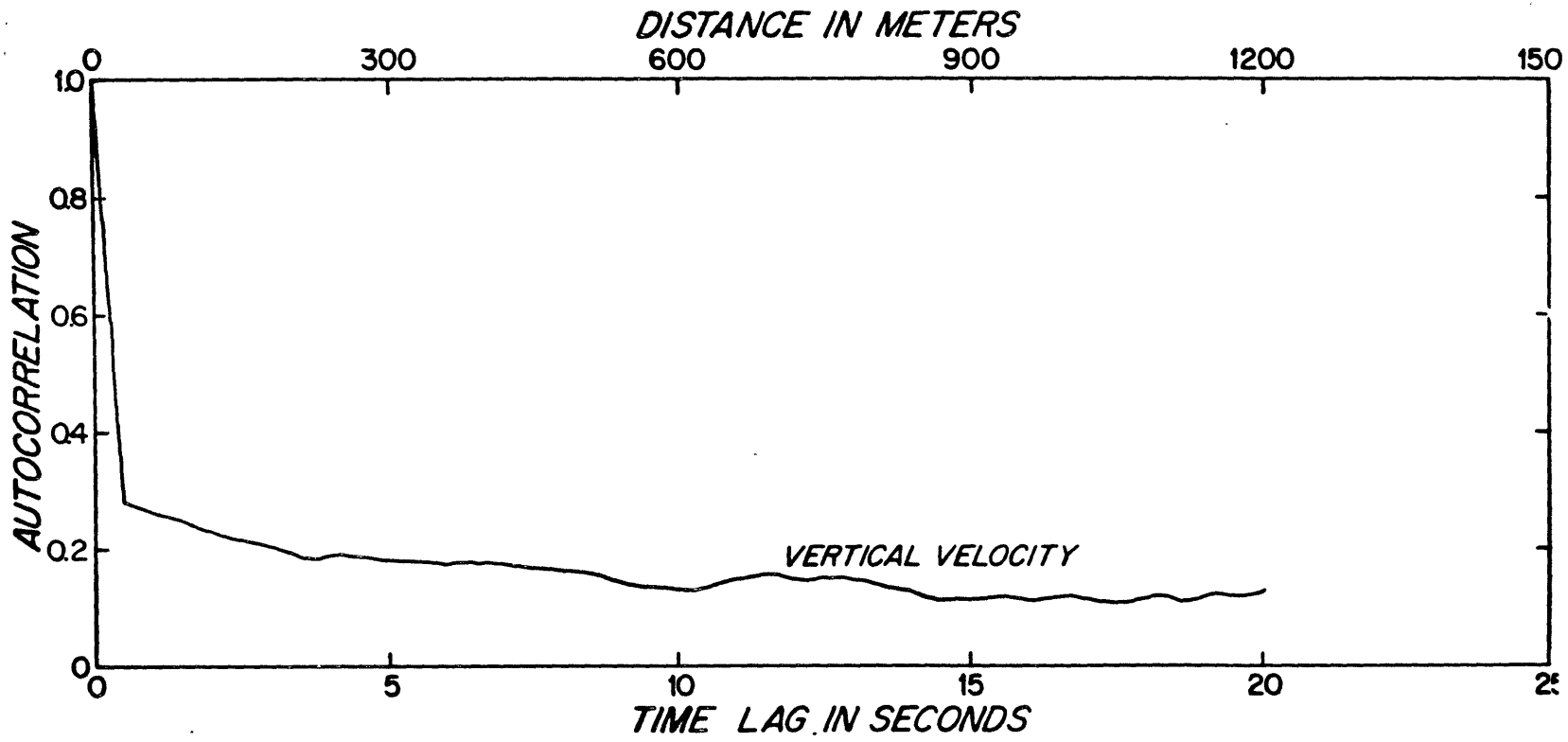


Figure 10. Autocorrelation analysis of run #2944 below cloud base across same cloud line as in Figure 7, February 24, 1958, at 1600 feet.

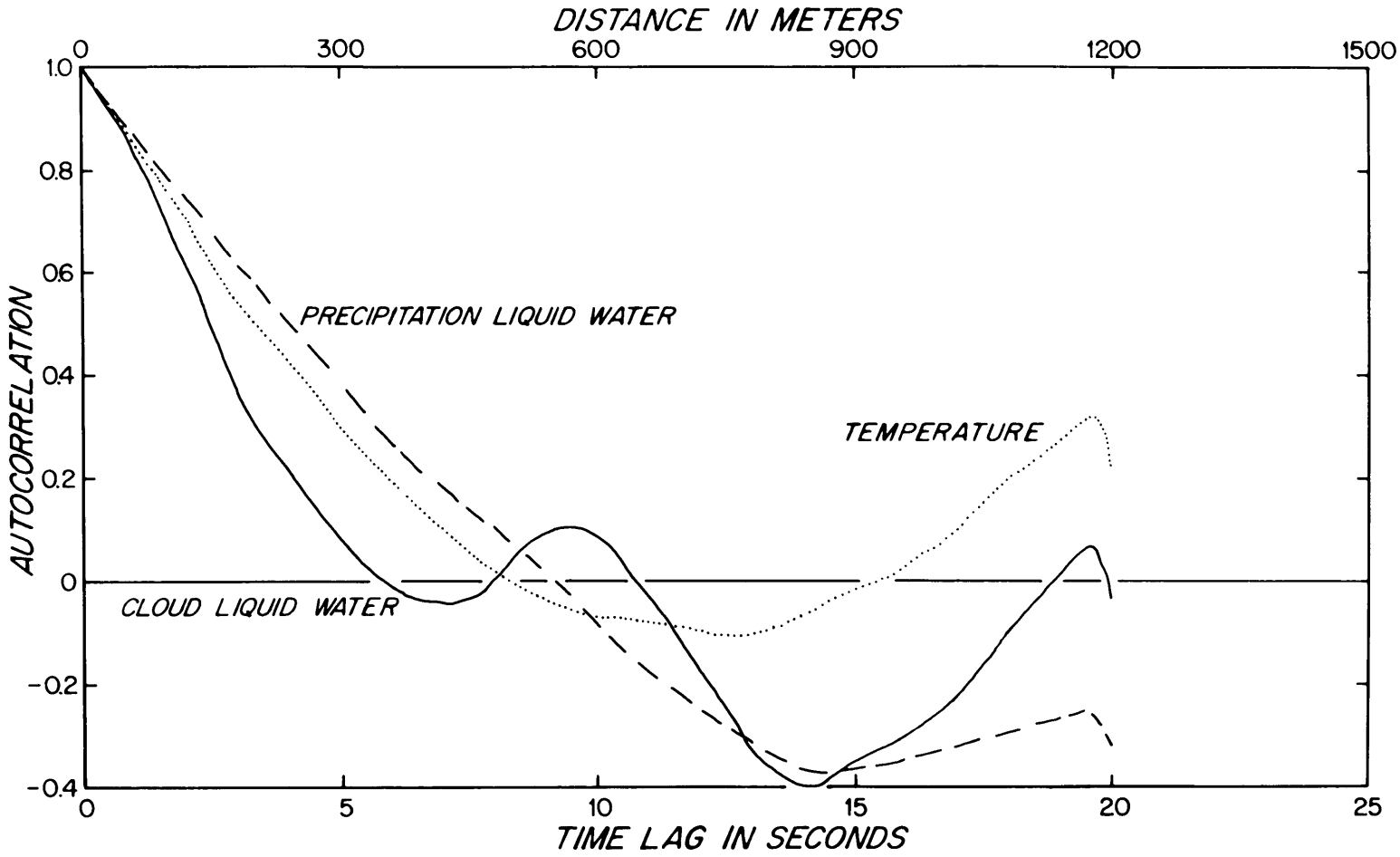


Figure 11. Autocorrelation analysis of cloud run #3349 along a cloud line, November 16, 1959, at 10,000 feet.

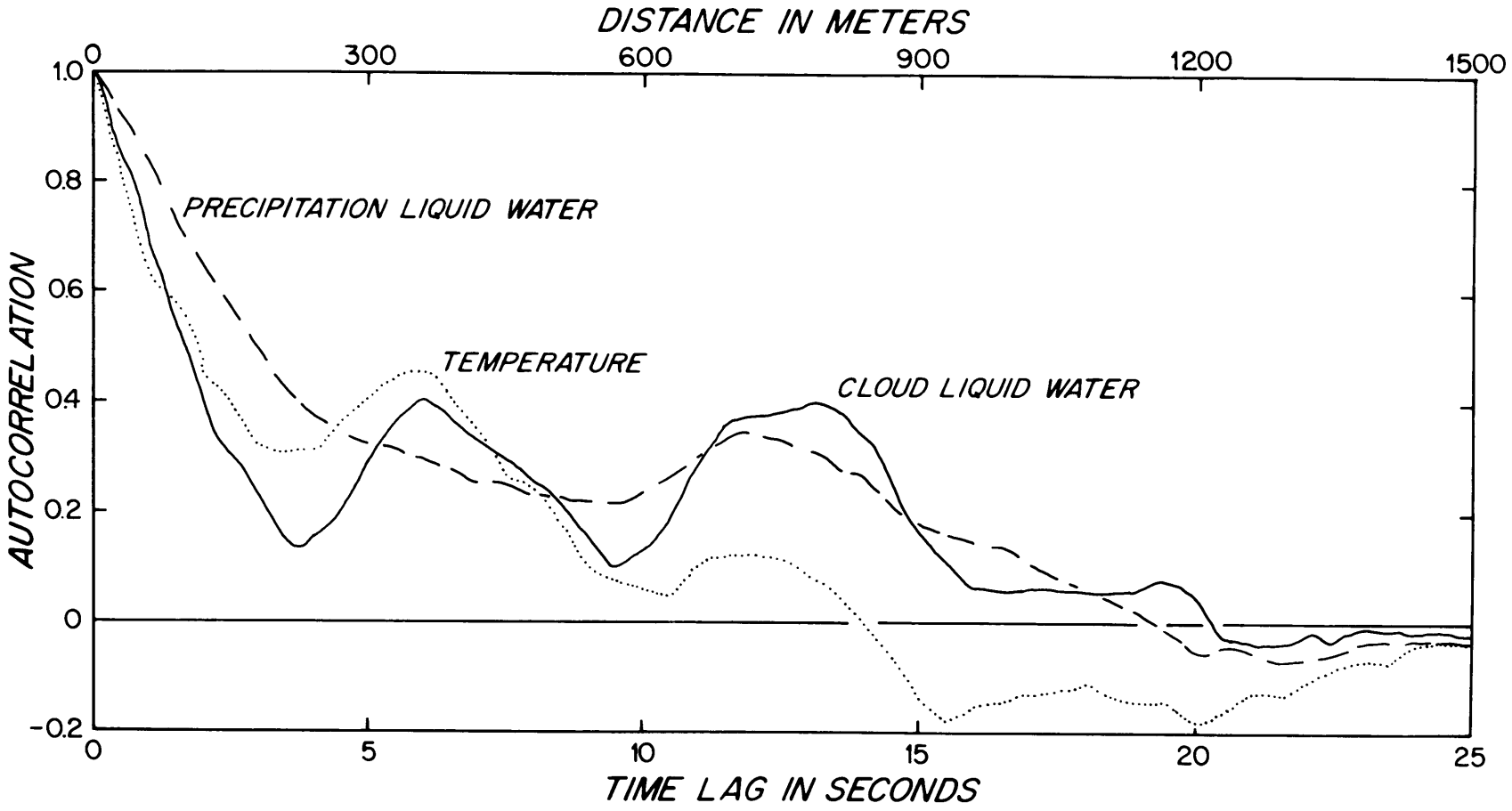


Figure 12. Autocorrelation analysis of cloud run #3350 along same cloud line as in Figure 11, November 16, 1959, at 7000 feet.

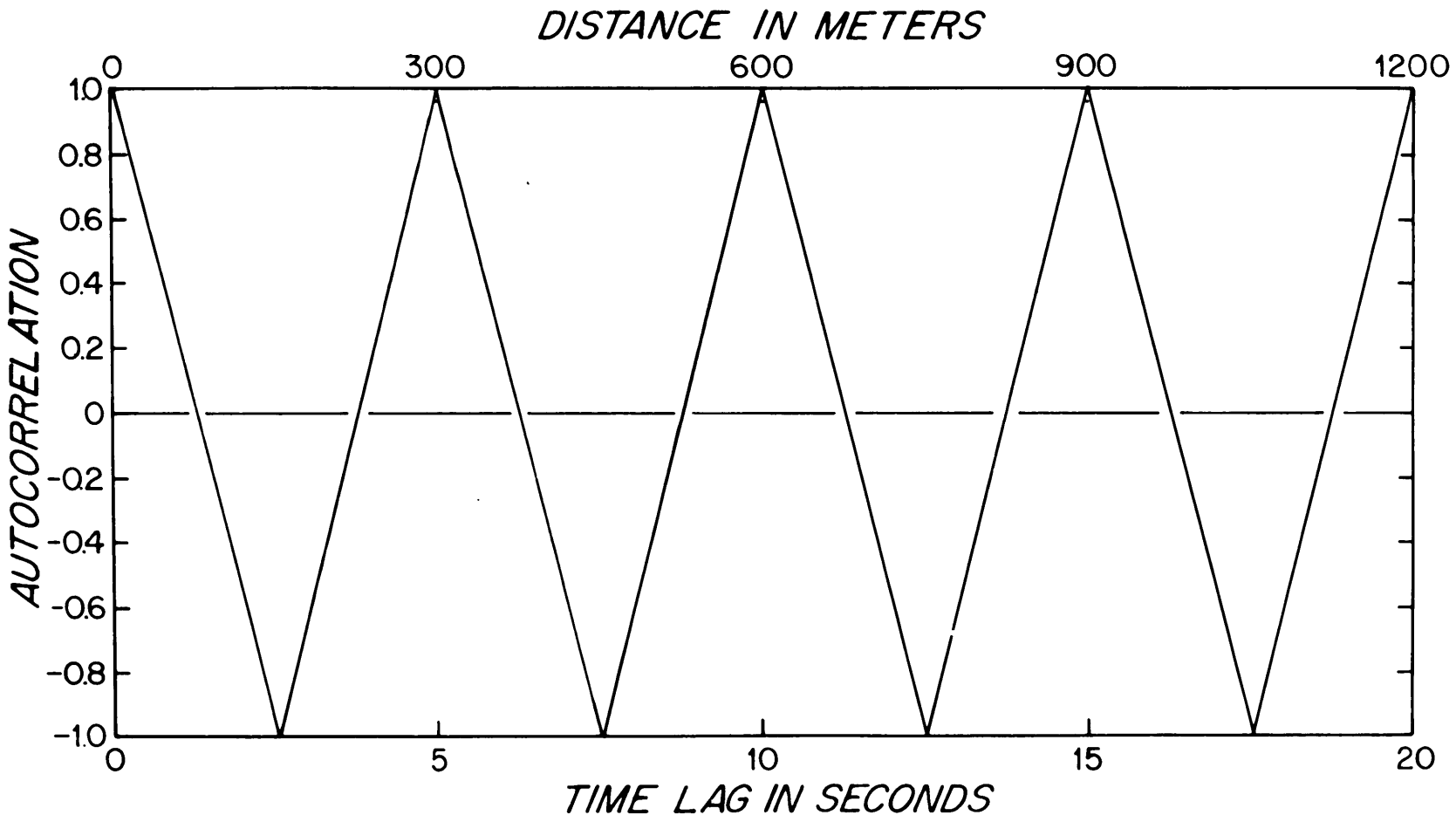


Figure 13. Autocorrelation analysis of square wave with 5-second period and square tops of 2½ seconds duration.

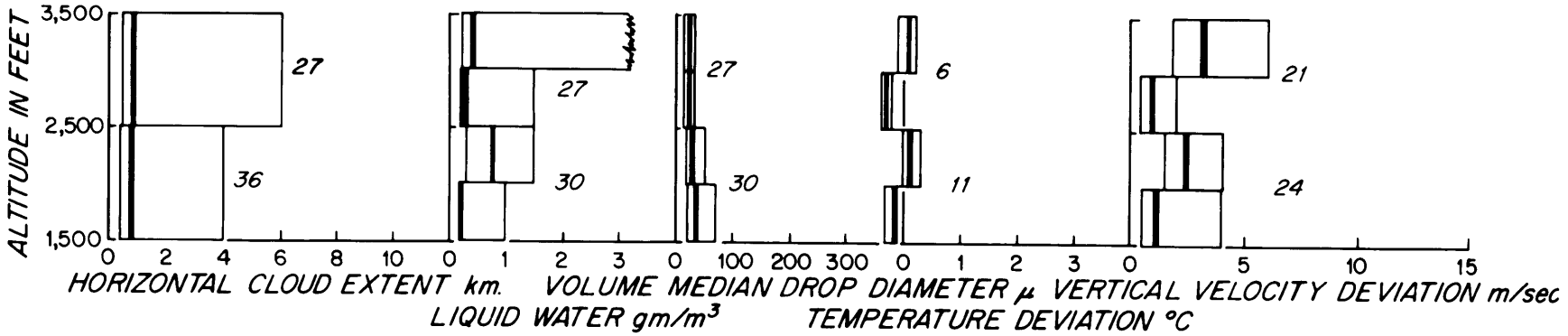


Figure 14. Bar graphs from cloud data frequency tables for classification according to maximum cloud top < 5000 feet in area of operation. The numbered altitudes represent statistical cloud run altitude class limits. The bars represent statistics of unbroken cloud intervals in the cloud runs. The ends of the bar represent the median and extreme, and the heavy line represents the eightieth percentile for the corresponding cloud run altitude class. The upper and lower bars represent the statistics for the average and maximum in unbroken cloud intervals. The number of observations is entered to the right or in each bar.

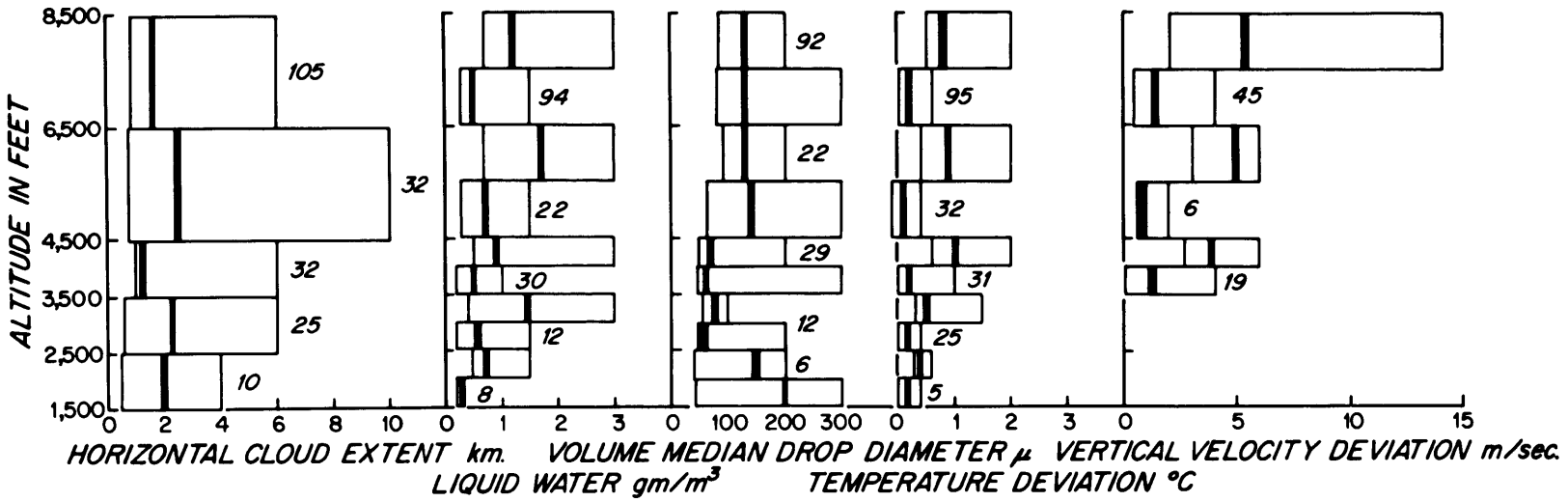


Figure 15. Same as in Figure 14, but maximum cloud top altitude is $\geq$ 7000 feet and $<$ 10,000 feet.

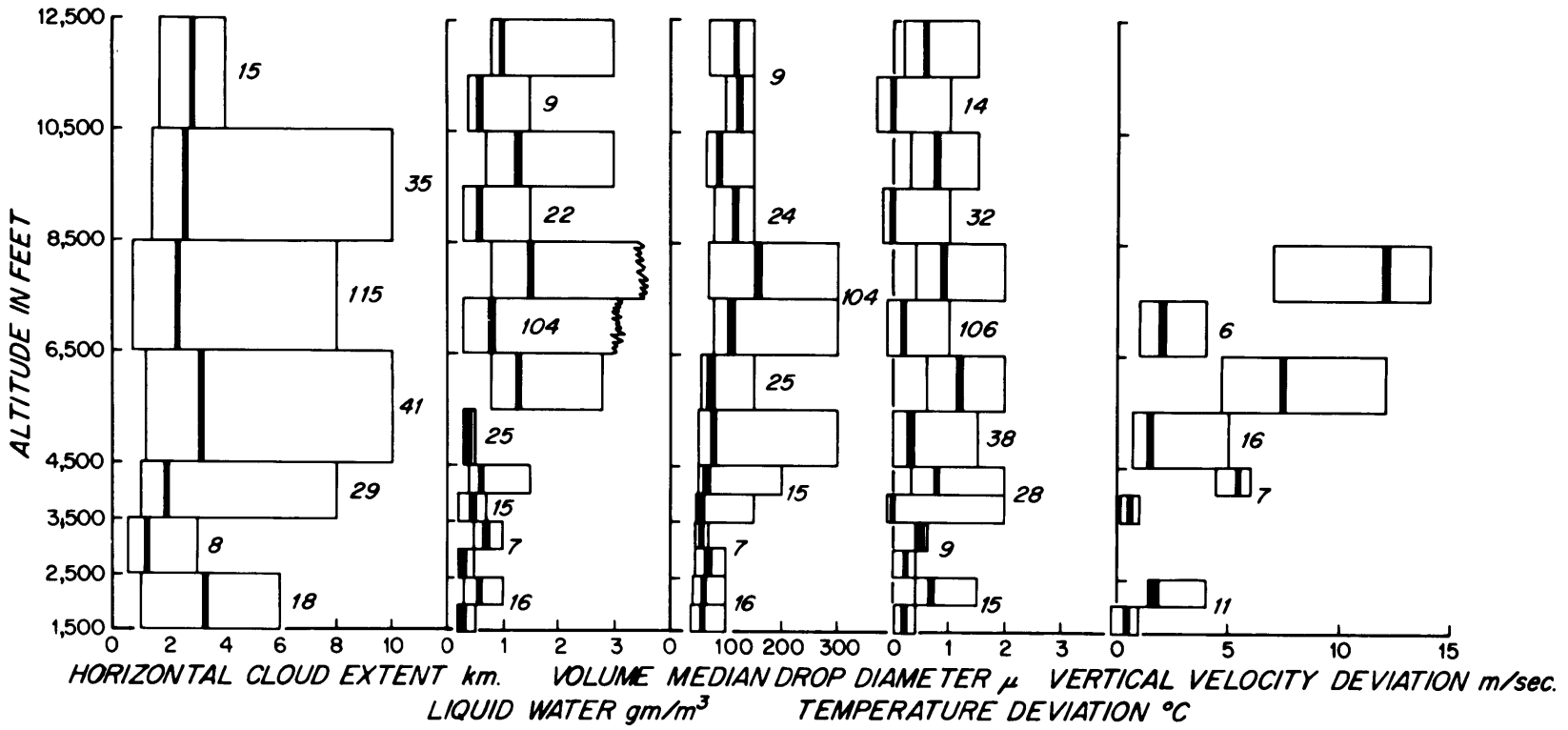


Figure 16. Same as in Figure 14, but maximum cloud top altitude is $\geq$ 10,000 feet and $<$ 16,000 feet.

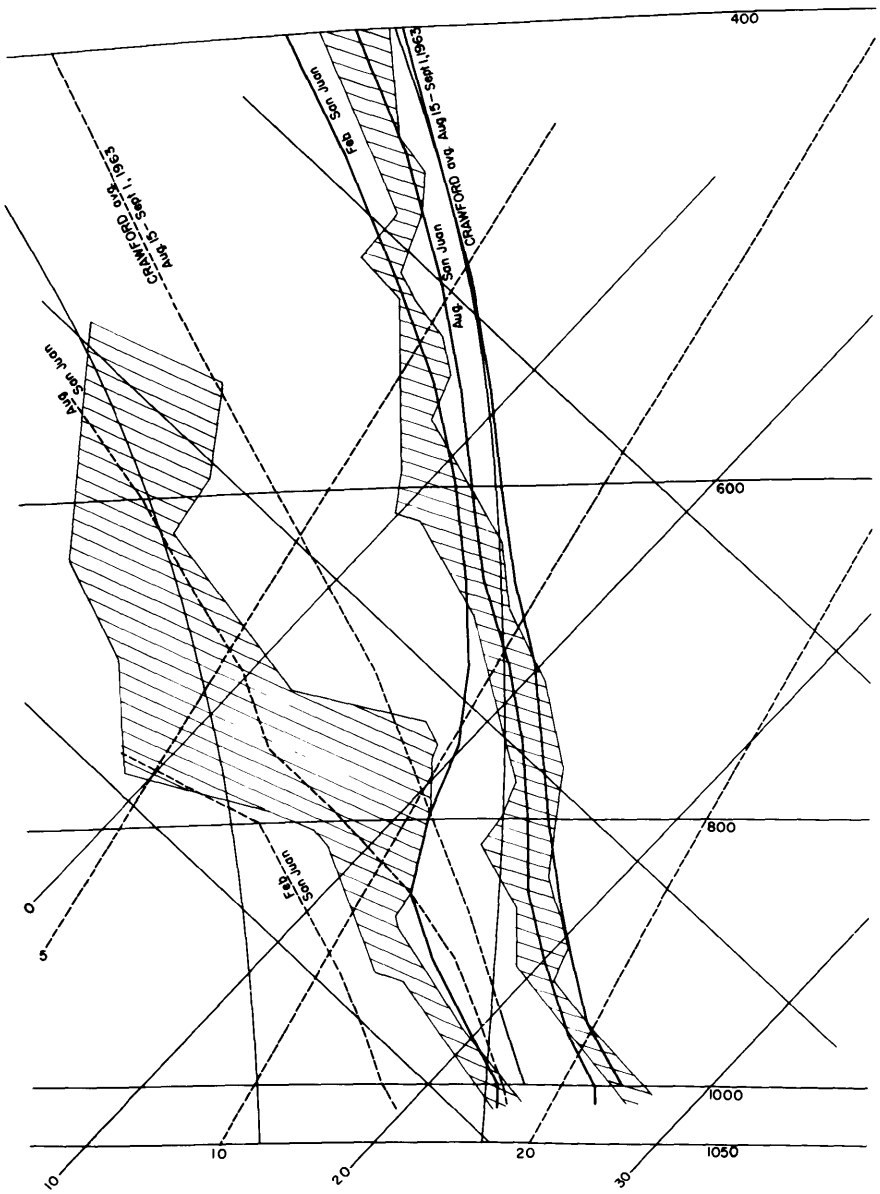


Figure 17. Composite of four soundings made in the Barbados area on August 29, 1963, from 8:00 A.M. to 8:00 P.M. (one by the Woods Hole aircraft, two by the CRAWFORD, and one by Seawell Airport). The envelopes of these soundings are the cross-hatched areas. The areas on the right and left are the temperature and dew-point fluctuation bands, respectively. Average soundings for San Juan and Barbados are superimposed. The soundings are plotted on a tephigram. (See Figure 1, Part II for description of tephigram.)

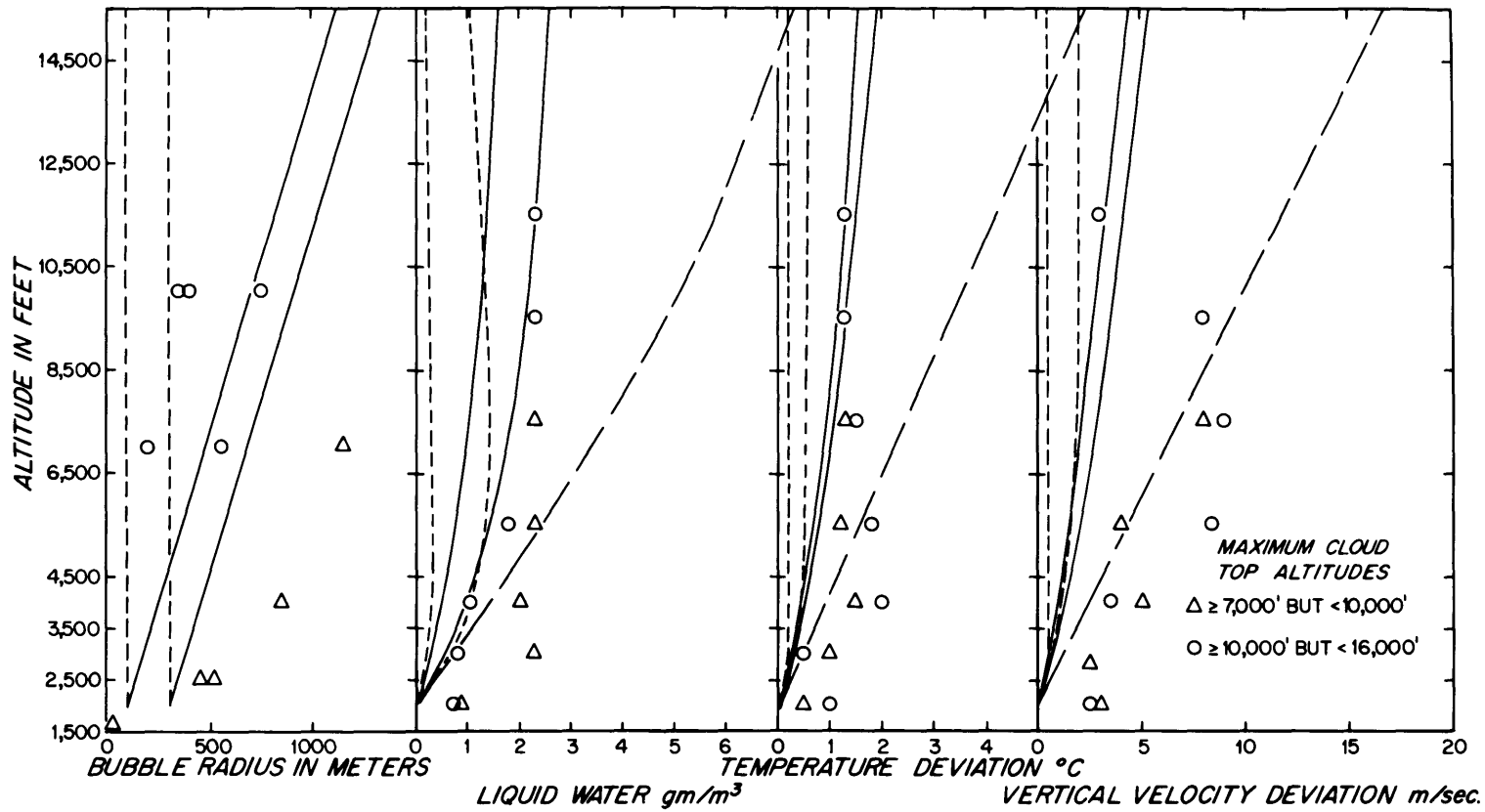


Figure 18. Means of extremes of average and maximum values observed in segments of unbroken cloud superimposed on theoretical curves. Long dashes are the adiabats, solid curves represent case $k_e = .75$ and $k_d = 0$, and short dashes the case $k_d = k_e = .75$. Extremes in these curves represent the extremes assumed for r_o and r_p .

PART IV

A FINAL ASSESSMENT AND SUGGESTED FUTURE WORK

1. The nature and extent of the author's contribution.

The work of the author to date stems directly from the pioneer effort of Malkus (1954) to relate the observed virtual temperature excess in cumulus clouds to observed vertical velocity in terms of Stommel's (1949, 1950) steady state jet model. Since then the author has added a hot wire liquid water content instrument system to the other aircraft instrumentation in order to obtain more detailed observational information concerning clouds.

A key problem in the observation of clouds has been the measurement of liquid water content and drop size distribution. The simple direct methods, such as impaction of cloud drops on coated slides, do not lend themselves readily to continuous cloud observation. Also the labor of sizing and counting drop impressions is a discouraging factor. Continuous recording total liquid water content instruments of various types have been developed in the past, but adequate attention to their calibration has been lacking. The author's interest in theory and observational verification coupled with previous experience in cloud instrument work motivated his intensive hot wire instrument development and calibration program. The simplicity of the hot wire principle was particularly attractive because of the ease with which its output could be recorded and the possibility of obtaining accurate observations in a relatively short time. The short development time turned out longer than expected because of calibration difficulties.

The author was forced to devise a companion precipitation instrument for the simple cloud instrument to compensate for its lack of sensitivity to large drops. Consequently the unexpected extra instrument work led to a bonus in the form of drop size information. The calibration problem, which also was more difficult than anticipated, was also solved by the author. The solution was arrived at by a judicious combination of old techniques and departure from the procedures established by Neel and Steinmetz (1950) and Neel (1951).

The author (1959) also combined entrainment and condensation in a bubble model. Numerical entrainment model computations have been made by others including allowance for the effect of liquid water content as well as temperature on buoyancy. Here the author's earlier bubble model has been corrected and revised to include the effects of liquid water and precipitation on buoyancy. Also the logic of all entrainment model calculations has been summarized and clarified.

On the observational side, a pilot statistical summary of data, gathered by the author and his collaborators has been made and a method suggested for comparing the data with entrainment models. Rather than try to verify the detailed structure of a model - bubble versus jet - an attempt to see how well a simple cloud model can reproduce the statistical behavior of clouds is suggested. A reasonable cloud model may then possibly be extended to the assessment of the relative importance of cloud microphysics and to the study of the dynamics of the trade wind circulation.

2. The role of microphysical phenomena in clouds

The effect of coalescence has been here introduced into the bubble model by way of the precipitation parameter γ_p . A rough calculation of collection efficiency of large drops for small drops has been made from the cloud observations too.

In the future initial drop size distributions and concentrations as computed by Howell (1949), Squires (1952), Twomey (1959), and Mordy (1959) may be introduced into model calculations and numerical experiments. As cloud observations improve, the effect of condensation nuclei on drop size spectrum may be studied. Also clouds over land and sea may be compared to evaluate the influence of condensation nucleus population differences.

A reasonable cloud model may be used to estimate the effects of cloud seeding as attempted by Malkus and Simpson (1964). The combination of better instrumentation, observation, and theory should eventually lead to definitive answers to questions concerning the effectiveness of cloud seeding.

3. Details of internal cloud motion

The increasing capacity of digital computers will undoubtedly make possible more elaborate numerical experiments in cumulus convection. The relation of mixing parameters to eddy transport coefficients already suggested here may make possible a more intimate interaction between numerical experiments, laboratory tank experiments, and observation. In particular realistic eddy viscosity coefficients may be established for use in numerical experiments.

An alternate approach to the numerical experiment may be made with truncated polynomial series. O'Brien (1961) has found exact solutions to the Navier-Stokes equations in the form of oblate and prolate spheroidal vortices to complement Hill's spherical vortex. The principal scale of motion may be represented by a spheroidal vortex while the smaller scales of motion are represented by polynomials of higher order.

4. Improvement of instrument system

A great obstacle to maximum use of the data in the present analogue type of recording system is the tremendous amount of labor required in data reduction. Introduction of a digital voltmeter and digital tape recording equipment would make it possible to do the data reduction by digital computer. Thus the lag between observation and interpretation of data would decrease. Also a much more complete statistical analysis of the data could be made, and more thought might then be given to interpretation of the results.

The instrument system could be made more complete and more effective by adding observational components or improving existing ones. In the past a particularly important component was missing, namely, a continuous record of altitude during a cloud pass, which is needed for evaluation of relative buoyancy. Vanes to study small-scale turbulence in clouds might be a valuable addition to the present turbulence system. The existing hot-wire instrument system may be modified to give more drop-size spectrum information. As supplements to the hot-wire

system a shadowgraph camera and impactor might be added. A variation of the vortex thermometer might be useful in minimizing temperature element wetting along with the dynamic correction. A 3-cm radar may be useful in supplementing the detailed one-dimensional observation of a cloud in an aircraft pass with a three-dimensional picture.

The accuracy of the author's calibration procedure can also be improved, perhaps to the point where liquid water mixing ratios are comparable in absolute accuracy to water vapor mixing ratios. For example, the water flow to the individual nozzles could be metered so that the liquid water distribution over the tunnel's cross section would be more uniform. If the nozzles were turned in more towards the tunnel axis, the intersecting spray plumes might, due to better turbulent mixing, contribute further to the uniformity of the cross sectional water distribution.

If the scientific motivation for meteorological observation from aircraft continues, there appears to be no reason why an adequate instrument system should not eventually evolve.

5. Relevance of the cumulus scale to larger scales of motion

Just as small-scale turbulence exerts an apparent eddy viscous drag on the horizontal motion of the sub-cloud layer, so does the cumulus scale on the larger scale motion in the cloud layer. Furthermore, the larger scale vertical motion essentially establishes the cumulus cloud environment. Therefore there is a complex interaction of cumulus scale and large scale motion of a type often loosely called a feed-back mechanism.

The stability of the trades is very likely bound up with such an interaction, which may in turn be involved with the formation of tropical disturbances.

If a reasonable parametric representation of cumulus convection is established, then the path is relatively clear towards evaluating eddy stresses and transports into the cloud layer from the sub-cloud layer for various cloud distributions and large scale vertical velocities. Mass exchanges may be related to observations of water vapor distribution and salt particle distribution in the clear air above the sub-cloud layer.

References

Howell, W.E., 1949: The growth of cloud drops in uniformly cooled air. J.Meteor.,6, 134-149.

Levine, J., 1959: Spherical vortex theory of bubble-like motion in cumulus clouds. J.Meteor.,16, 653-662.

Malkus, J.S., 1954: Some results of a trade-cumulus cloud investigation. J.Meteor., 11, 220-237.

Malkus, J.S. and R.H.Simpson, 1964: Modification experiments on tropical cumulus clouds. Science, 145, 541-548.

Mordy, W.A., 1959: Computations of the growth by condensation of a population of cloud droplets. Tellus, 11, 16-44.

Neel, C.B., 1955: A heated-wire liquid-water-content instrument and results of initial flight tests in icing conditions. NACA RM A54123, 33 pp.

Neel, C.B., and C.P.Steinmetz, 1952: The calculated and measured performance characteristics of a heated-wire liquid-water-content meter for measuring icing severity. NACA TN 2615, 59 pp.

O'Brien, Vivian, 1961: Steady spheroidal vortices - more exact solutions to the Navier-Stokes equation. Quart.J.appl.Math., 19, 163-168.

Squires, P., 1952a: The growth of cloud drops by condensation. I. General characteristics. Aust.J.Sci.Res. A, 5, 59-86.

Squires, P., 1952b: The growth of cloud drops by condensation. II. The formation of large cloud drops. Aust.J.Sci.Res. A, 5, 473-499.

Stommel, H., 1947: Entrainment of air into a cumulus cloud. J.Meteor., 4, 91-94.

Stommel, H., 1951: Entrainment of air into a cumulus cloud II. J.Meteor., 8, 127-129.

Twomey, S., 1959a: The nuclei of natural cloud formation. I. The chemical diffusion method and its application to atmospheric nuclei. Geofis.Pur.Appl., 43, 227-242.

Twomey, S., 1959b: The nuclei of natural cloud formation. II. The supersaturation in natural clouds and the variation of cloud droplet concentration. Geofis.Pur.Appl., 43, 243-249.

ACKNOWLEDGEMENTS

The author is indebted to Professor Norman A. Phillips for his constant interest, encouragement, keen critical insight, and many helpful suggestions, without which the writer's work would never have assumed its present form.

Doctor Joanne Simpson, who furnished the opportunity and initial impetus for the author's work, has been a constant source of interest and encouragement even though away from Woods Hole most of the time.

The author's colleagues at Woods Hole have been a constant source of inspiration in stimulating conversations. For example, Dr. Peter M. Saunders has helped the author clarify the relation of his work to that of the Imperial College school of thought. Also Mr. Andrew F. Bunker has been extremely helpful in aircraft instrumentation problems and in loaning his aircraft turbulence instrument system.

Dr. Robert M. Cunningham has been very kind in making available the spray tunnel and associated facilities of Hanscom Field for the calibration of liquid water content instruments.

Mr. Robert H. Pearson contributed considerable assistance in the instrument development.

Miss Margaret A. Chaffee contributed to the reduction of data and to the success of some of the aircraft observations.

Mrs. Mary C. Thayer has done considerable excellent work on data reduction and a particularly heroic job in preparing the final manuscript on time.

To the many others who have made valuable suggestions and assisted the author from time to time, he is also greatly indebted.

Biographical Note

The author was born in Boston, Massachusetts, on 16 July, 1915.

Education:

A.B. cum laude in astronomy at Harvard University, 1939

M.S. in meteorology at Massachusetts Institute of Technology, 1941

Graduate work in physics at Purdue University 1946-1948

M.S. in physics at University of New Mexico, 1956

Work toward Ph.D. in meteorology at Massachusetts Institute of Technology now being completed. Thesis sponsor Professor N. A. Phillips.

Experience:

Work during war at Eatontown Signal Laboratory (1941-1943), Radio Research Laboratory (1943-1944), and Applied Physics Laboratory (1944-1946).

Assistant instructor in Physics, Purdue University 1946-1948.

Aeronautical Research Scientist in cloud physics at Lewis Flight Propulsion Laboratory of NACA 1948-1951.

Lecturer in meteorology and teaching assistant in physics at University of New Mexico 1951-1956.

Research A sociate and assistant scientist in cloud physics at Woods Hole Oceanographic Institution 1956 to present.

My work at the NACA was concerned with the microphysics of clouds. A large part of my effort in this field was devoted to aircraft instrumentation for the observation of cloud liquid water and drop-size distribution. I also did some theoretical and laboratory work on supercooling of cloud drops.

At Woods Hole I have become interested in relating cloud microphysics to the study of cumulus convection. More recently my interest has expanded to the interaction of clouds with larger-scale atmospheric motions.

Biographical Note (continued)

List of publications:

1942: Bull.Amer.Meteor.Soc., 23, pp.52-61.

1950: NACA TN 2234, 27 pp.

1951: NACA TN 2458, 53 pp.

1951: NACA RM E51G05, 28 pp.

1952: NACA RM E51L17, 29 pp.

1959: J.Meteor., 16, 653-662.

1961: Aero-Revue, 36, 100-101.